IMPERIAL COLLEGE OF SCIENCE, TECHNOLOGY AND MEDICINE

Faculty of Engineering

Department of Chemical Engineering and Chemical Technology

Multifunctional Inorganic Hollow Fibre Membranes for Chemical Reactions

By

Ejiro oghene Patrick Gbenedio

A thesis submitted for the degree of Doctor of Philosophy and for the Diploma of Imperial College London

October 2010

Abstract

Over the last few decades, the availability of inorganic membranes which can withstand high temperatures and harsh chemical environments has resulted in a wide range of opportunities for the application of membranes in chemical reactions. In particular, the combination of membrane separation and catalytic reaction in a single operating unit is an attractive way to increase conversions, to achieve better yields and to make more efficient use of natural resources in many reactions.

In this work, a highly compact multifunctional Pd and Pd-Ag/alumina hollow fibre membrane reactor (HFMR) have been developed and applied to catalytic chemical reactions. The developed HFMR consists of a thin and defect free Pd-based membrane coated onto the outer surface of an alumina hollow fibre substrate with a unique asymmetric pore structure, i.e. a sponge-like outer layer and a finger-like inner layer where catalyst is deposited.

In one study, a Pd-Ag layer was coated onto the outer surface of the substrate followed by deposition of sub-micron sized Pt(0.5wt.%)/γ-alumina catalysts into the finger-like voids of the substrates. This design achieved propane conversion as high as 42 % at the initial stage of the reaction at 723 K and space-time yields (STY) of the HFMR were approximately 60 times higher than that of a fixed bed reactor (FBR). In order to further increase catalytic surface area in the reaction zone, a sol-gel method was used to deposit Pt(1 wt.%)/SBA-15 catalysts into the finger-like voids of a substrate to develop a Pd/alumina HFMR. Benefiting from this novel design, the functionalized alumina hollow fibre substrates with surface area/volume values of up to 1918.4 m^2/m^3 possess a specific surface area of about 31.8 m^2/g for catalysts. It was observed that in comparison with a conventional FBR, greater propene selectivity and propene yield was achieved by using the

HFMR for propane dehydrogenation. The generic advantages of the design of these compact HFMR systems can be applied to further applications such as the water-gas shift reaction, which was also carried out in this study.

Acknowledgements

I would like to express my sincere gratitude to my supervisor Prof. Kang Li for giving me the unique opportunity to work with him at Imperial. It has been a privilege to be part of his team, and I am grateful for sharing his knowledge in the membrane field. His support, patience and trust, especially in hard times, made me feel secure and helped me overcome any difficulties I faced.

I am forever indebted to my post-doc Dr. Zhentao Wu, who gave me a lot of help with experiments, insights and encouragement from day one. You continue to amaze me with your drive and hard work with every member in the membrane group.

Many thanks to my past and present colleagues at the Department of Chemical Engineering including, Sirichai Koonaphapdeelert, Chiao-Chien Wei, Benjamin Kingsbury, Irfan Mohd Mohamed Dzahir, Mohd Othman, Nur Hashim, Barbara Zydorczak, Krzysztof Kanawka, Hasrinah Hasbullah, Mukhlis Rahman, Renato Campos Vasconcelos, Ioannis Vyrides, Iwona Soroko; undergraduate students, Jason Sharp and Oluwaseyi Osiyemi; the laboratory technicians and store managers, Keith Walker, Tawanda Nyanbago, Nam Ly and to everyone else who has made my experience at Imperial memorable.

I am also grateful to EPSRC for providing the research grant for this work

Finally, I would like to thank to my parents, family and friends for the emotional support and prayers. You guys have been my inspiration during this academic journey. This work is dedicated to you all.

Table of Contents

Abstract 2
Acknowledgements 4
Table of Contents 5
List of Tables 9
List of Figures 10

CHAPTER 1
Introduction 14
1.1 Background 14
1.2 Objectives 20
1.3 Thesis structure and presentation 20

CHAPTER 2
Literature Review 23
Abstract 23
2.1 CHARACTERISTICS OF CERAMIC MEMBRANES 24
2.2 PALLADIUM COMPOSITE MEMBRANES 28
2.2.1 Permeation of hydrogen through Pd membranes 29
2.2.2 Permeation of gases through porous supports 34
2.3 FABRICATION OF PALLADIUM COMPOSITE MEMBRANES 36
2.3.1 Membrane Supports 36
2.3.2 Palladium Membranes 43
2.3.3 Palladium/silver Composite Membranes 54
2.3.3.1 Coating and Diffusion method 55
2.3.3.2 Co-deposition method 60
2.4 MEMBRANE APPLICATIONS 61
2.4.1 Palladium Membrane Reactors 61
2.4.1.1 Membrane reactor configurations 62
2.4.1.2 Catalyst deposition techniques 64
2.4.2 Catalytic Membrane Reaction Processes 71
2.4.2.1 Dehydrogenation Reaction 71
2.4.2.2 Water-Gas Shift (WGS) Reaction 72
2.4.2.3 Economic Feasibility of Pd-based Membrane Reactors 74

CHAPTER 3
Fabrication of Composite Pd/Alumina Asymmetric Hollow Fibre Membranes: A New Approach to Compact Multifunctional Membrane Reactors 80
Abstract 80
3.1 Introduction 81
3.2 Experimental 83
3.2.1 Materials 83
3.2.2 Fabrication of asymmetric inorganic hollow fibre membranes 84
3.2.3 Fabrication of Pd/Al_2O_3 hollow fibre composite membranes 86
3.2.4 Membrane characterization 87
3.3 Results and Discussion 89
3.3.1 Microstructure of Al_2O_3 hollow fibre substrates 89
3.3.2 Morphology of Pd/Al_2O_3 hollow fibre composite membranes 94
3.3.3 Performance of Pd/Al_2O_3 hollow fibre composite membranes 96
3.4 Conclusions 99

CHAPTER 4
A Novel Inorganic Hollow Fibre Membrane Reactor for Catalytic Dehydrogenation of Propane 100
Abstract 100
4.1 Introduction 101
4.2 Experimental 103
4.2.1 Materials 103
4.2.2 Preparation of multifunctional membranes 104
4.2.3 Characterization of multifunctional hollow fibre membranes 107
4.2.4 Dehydrogenation of propane to propene 108
4.3 Results and Discussion 109
4.3.1 Microstructure of asymmetric Al_2O_3 hollow fibre substrates 109
4.3.2 Catalyst preparation and deposition 111
4.3.3 Gas permeation of Al_2O_3 hollow fibre substrates 113
4.3.4 Sequential electroless plating of Pd/Ag membranes 114
4.3.5 Gas permeation of $Pd/Ag\text{-}Al_2O_3$ composite hollow fibre membranes 119
4.3.6 Dehydrogenation of propane to propene 121
4.4 Conclusions 127

CHAPTER 5
A Multifunctional Pd/Alumina Hollow Fibre Membrane Reactor for Propane Dehydrogenation 128
Abstract 128
5.1 Introduction 129
5.2 Experimental 131
5.2.1 Materials 131
5.2.2 Fabrication of multifunctional HFMR-II 132
5.2.3 Characterization of HFMR-II 134
5.2.4 Dehydrogenation of propane to propene using HFMR-II 134
5.3 Results and Discussion 135
5.3.1 Microstructure of asymmetric alumina hollow fibre substrates 135
5.3.2 Microstructure of the functionalized alumina hollow fibre substrates 137
5.3.3 Dehydrogenation of propane to propene 142
5.4 Conclusions 149

CHAPTER 6
A Pd/Alumina Functionalized Hollow Fibre Membrane Reactor for Water-Gas Shift Reaction 150
Abstract 150
6.1 Introduction 151
6.2 Experimental 153
6.2.1 Materials 153
6.2.2 Fabrication of Pd/functionalized HFMR 154
6.2.3 Characterization 154
6.2.4 WGS reaction using HFMR 155
6.3 Results and Discussion 157
6.3.1 Pt/CeO_2/SBA-15 catalyst for WGS reaction 157
6.3.2 Functionalized asymmetric alumina hollow fibres for WGS reaction 160
6.3.3 Pd/alumina functionalized hollow fibre membrane reactor for WGSR 163
6.4 Conclusions 171

CHAPTER 7
Conclusions and Recommendations 172
7.1 Asymmetric hollow fibre support 172
7.2 Palladium-based composite membrane 173
7.3 Palladium-based membrane reactor 174

7.4 Recommendations for future work 175
7.4.1 Membrane support and catalyst deposition 175
7.4.2 Catalyst activity 176
7.4.3 Membrane reactor design and long term stability studies 176
7.4.4 Reactor modelling 177

List of Publications 178

REFERENCES 179

Appendix A 194
GC Program 194
GC Calibrations 195
Appendix B 199

List of Tables

Table 2-1 Pd Membranes..... 58

Table 2-2 Pd-Ag Composite Membranes..... 59

Table 2-3 Classification of Membrane reactors..... 63

Table 2-4 Dehydrogenation in Palladium-based Membrane Reactors 77

Table 3-5 Hollow fibre precursor spinning conditions 85

Table 3-6 Bath compositions for Pd electroless plating 86

Table 4-7 Coating bath compositions of Pd/Ag electroless plating 106

Table 4-8 The weight gain of asymmetric alumina hollow fibre substrates after catalyst deposition..... 112

Table 4-9 Propane conversion and propene selectivity of iHFMRs 123

Table 4-10 Space-time yields (STY) of the 1st iHFMR and FBR 124

Table 5-11: Characteristics of functionalized and untreated alumina hollow fibre substrates..... 142

List of Figures

Figure 1-1 (a) conventional membrane reactor system and (b) integrated membrane reactor system. 16

Figure 1-2 Membrane Architecture 19

Figure 1-3 Structure of the thesis 22

Figure 2-4 Schematic representation of an asymmetric composite ceramic membrane 25

Figure 2-5 Pore size distribution of a four layered alumina membrane [25] 26

Figure 2-6 Diagrams of hollow fibre, tubular and flat membrane modules [34] 28

Figure 2-7 Hydrogen permeation through palladium membrane 30

Figure 2-8 pure gas permeation through porous support 34

Figure 2-9 Flow chart of the spinning process 39

Figure 2-10 Tube-in-orifice spinneret for fibre spinning 40

Figure 2-11 Possible mode for sensitization/activation of alumina surface [38, 64] 48

Figure 2-12 Principle of membrane reactors to promote reactions; (a) selective permeation of by-products of an equilibrium-limited reaction and (b) dosing a reactant through the membrane 62

Figure 2-13 Different membrane reactor concepts for a tubular configuration: (a) PBMR, FBMR (b) PBCMR, FBCMR and (c) CMR, CNMR 64

Figure 2-14 (a) bare silicon micro channels with 10 μm pillars and (b) coated with γ- Al_2O_3 69

Figure 3-15 Flow chart of Pd electroless plating process 87

Figure 3-16 Schematic diagrams of the apparatus for single gas permeation measurements 88

Figure 3-17 Dependence of nitrogen permeance at different temperatures on the dwelling time of Al_2O_3 hollow fibre substrates 90

Figure 3-18 Hydrogen and nitrogen flux through alumina hollow fibre support 91

Figure 3-19 SEM images of an Al_2O_3 hollow fibre spun with an air-gap of 15 cm and calcined at 1723 K for 4 h. (a) whole view (b) cross section (finger-like voids) (c) inner edge (x1000) (d) inner edge (x2000) (e) inner surface and (f) outer surface 93

Figure 3-20 Mercury intrusion data for asymmetric Al_2O_3 hollow fibre sintered at . 94

Figure 3-21 SEM images of (a) cross section and (b) surface of Pd/Al_2O_3 hollow fibre composite membrane..... 95

Figure 3-22 Relationship between pressure difference and hydrogen flux through palladium composite membrane 97

Figure 3-23 Arrhenius plot of hydrogen permeance for Pd/Al_2O_3 a hollow fibre composite membrane..... 98

Figure 4-24 Schematic diagram of the apparatus for the dehydrogenation of propane to propene..... 108

Figure 4-25 SEM images of the asymmetric alumina hollow fibre substrate sintered at 1723 K for 4 h: (a) whole view, (b) cross section, (c) inner surface and (d) outer surface 109

Figure 4-26 SEM images of catalyst deposition in the hollow fibre substrate: 112

Figure 4-27 Gas permeation of hydrogen and nitrogen through the hollow fibre substrates at room temperature 113

Figure 4-28 Weight gains of Pd and Ag during the electroless plating 115

Figure 4-29 SEM images of Pd/Ag composite membranes during “coating and diffusion” electroless plating: (a) surface of Pd layer, (b) cross section of Pd layer, (c) surface of Ag layer, (d) cross section of Pd and Ag layers before heat treatment, (e) cross section of Pd/Ag alloy after heat treatment and (f) surface of Pd/Ag alloy after heat treatment. 116

Figure 4-30 EDS analysis of Pd/Ag membranes: (a) before heat treatment and (b) after heat treatment..... 117

Figure 4-31 Relationship between square root of pressure difference and hydrogen permeation flux through Pd/Ag composite membrane at different temperatures. 119

Figure 4-32 Arrhenius plot of hydrogen permeance for Pd/Al_2O_3 hollow fibre composite membrane..... 121

Figure 4-33 Propane conversion (solid symbols), equilibrium conversion (--- dashed lines), propene selectivity (open symbols) of the inorganic hollow fibre membrane reactor (iHFMR) and fixed bed reactor (FBR) at 723 K 122

Figure 4-34 Propene yields of FBR and iHFMR..... 125

Figure 4-35 The performance comparison of a third iHFMR in the dehydrogenation of propane..... 126

Figure 5-36 SEM images of the asymmetric alumina hollow fibre substrate sintered at 1723 K for 4 h: (a) whole view, (b) cross section, (c) inner surface, (d) outer surface, ... 136

Figure 5-37 Mercury intrusion of asymmetric alumina hollow fibre substrates sintered at 1723 K for 4 h..... 137

Figure 5-38 Nitrogen adsorption/desorption isotherm plots and pore size distribution curve (inset) of SBA-15 sintered at 823 K for 6 h 138

Figure 5-39 SEM images of the functionalized alumina hollow fibre substrate: (a) whole view, (b) cross section, (c) inner surface and (d) top view from outer surface 139

Figure 5-40 Mercury intrusion of the functionalized alumina hollow fibre substrates 140

Figure 5-41 Pore size (< 100 nm) distribution and pore volume of functionalized and untreated alumina hollow fibre substrates..... 141

Figure 5-42 EDS analysis of the Pd/alumina composite hollow fibre membrane. 144

Figure 5-43 Propane conversion (solid symbols), equilibrium conversion (dashed lines) and propene selectivity (open symbols) of the Pt(1 wt.%)/SBA-15 catalysts. 144

Figure 5-44 Propane conversion (solid symbols), equilibrium conversion (dashed lines) and propene selectivity (open symbols) of the multifunctional HFMR-II..... 146

Figure 5-45 The space-time yields (STY) the FBR and the HFMR-II at 773 K 146

Figure 5-46 Propene yields of FBR and the HFMR-II at 773 K..... 147

Figure 6-47 Schematic diagram of the experimental set-up for the WGS reaction using HFMR 156

Figure 6-48 Pore size distribution (PSD) of SBA-15 and Pt/CeO_2/SBA-15 calculated from the adsorption branch of the isotherms using the BJH method .. 158

Figure 6-49 Effect of temperature on CO conversion and CH_4 selectivity over 50 mg of Pt/CeO_2/SBA-15 catalyst in a fixed bed reactor (atm pressure, S/C = 1, GHSV= 14,088 $cm^3/(g \cdot h)$, CO concentration = 4.2%) 159

Figure 6-50 Influence of GHSV on CO conversion and CH_4 selectivity over 50 mg of Pt/CeO_2/SBA-15 catalyst in a fixed bed reactor (atmospheric pressure, S/C= 1, feed flow rate 10-60 ml/min, CO concentration = 4.2%) 159

Figure 6-51 SEM images of asymmetric alumina hollow fibre with deposited SBA-15, (a) whole view, (b) cross section, (c) deposited SBA-15 and (d) inner surface 161

Figure 6-52 SEM-EDS analysis of functionalized an alumina hollow fibre..... 162

Figure 6-53 CO conversion and CH_4 selectivity as a function of temperature in a porous membrane reactor (PMR) with approximately 30 mg of deposited catalyst. (Ar sweep gas = 50 ml/min, S/C = 1, feed flow rate = 10 ml/min, CO concentration = 4.2 %)..... 163

Figure 6-54 SEM images of the Pd membrane coated on the functionalized alumina hollow fibre, (a) cross section and (b) Pd membrane surface 164

Figure 6-55 CO conversion, CH_4 selectivity and H_2 recovery rate as a function of temperature in HFMR with approximately 30 mg of deposited catalyst. (Ar sweep gas = 50 ml/min, S/C = 1, feed flow rate = 10 ml/min CO concentration = 4.2 %). 165

Figure 6-56 Effect of sweep gas to feed ratio on (a) CO conversion, CH_4 selectivity and H_2 recovery and (b) amount and concentration of H_2 produced, separated and retained of HFMR with approximately 30 mg of deposited catalyst (Ar sweep gas = 10-50 ml/min, S/C = 1, feed flow rate = 10 ml/min, 673 K) 166

Figure 6-57 Effect of reactant flow rate on (a) CO conversion, CH_4 selectivity and H_2 recovery and (b) amount and concentration of H_2 produced, separated and retained in an HFMR with approximately 30 mg of deposited catalyst (Ar sweep gas = 50 ml/min, S/C = 1, feed flow rate = 10-60 ml/min, 673 K) 169

Figure 6-58 Hydrogen yields of FBR, PMR and HFMR 169

CHAPTER 1

Introduction

1.1 Background

Polymeric membranes are at present used in a number of process applications, including filtration, desalination, gas separation and in membrane reactors. However, they have a major drawback in that they suffer in harsh chemical and thermal operating conditions. Inorganic membranes made from materials such as Al_2O_3, TiO_2, ZrO_2, SiO_2 etc have since been developed by various groups for similar applications, especially where high temperature operation precludes the use of existing polymeric membranes [1]. Futhermore, the application of inorganic membranes for hydrogen separation and purification processes and in membrane reactors is recognised as a promising component in a sustainable future hydrogen economy.

Inorganic membranes are currently produced usually in either finite sized tubes with diameters of at least several mm or as flat discs and consequently have low surface area/reactor volume ratios (typically 30-500 $m^2.m^3$). These low area/volume ratios compare unfavourably in, for example, polymeric hollow fibre permeation modules where area/volume ratios of several thousand are obtainable, which limits the application of conventional inorganic tubular and disc type membranes. This limitation is most evident in membrane reactors, where it is desirable to maximise the area of the membrane module to increase the permeation rate to remove product species from the reaction zone. Clearly this

limitation could be overcome by the use of a bundle of ceramic hollow fibres. Furthermore, unlike the disc membranes, there is much less difficulty in sealing a bundle of hollow fibres into a reactor module, because the seals can be outside of the hot zone of the reactor.

Recent advances in inorganic materials have extended the range of possibilites in which inorganic membranes can be potenitally applied, for example, in high temperature equilibrium-limited reactions. Within process industries, a number chemical reactions display equilibrium-limited conversion and hence cannot attain high productivity. Thus, there are significant economic and environmental incentives to devise strategies to overcome this difficulty, for example in the exploitation of geographically remote sources of natural gas and in increasing the conversion and selectivity of industrial dehydrogention reactions. A potentially valuable use is in hydrogen production.

In principle, increased conversion of a reactant can be achieved by continuously removing products from the reaction zone. Hence, by conducting chemical reactions in a membrane reactor which continuously removes the formed product from the reactor, equilibrium limitations can be “shifted” towards product side so that reactions may proceed to a much higher conversion. The membrane reactor method enables reactions to be carried out at an easily controlled temperature, minimising the occurrence of side reactions and resulting in a more favourable product distribution [2]. Conventional tubular membrane reactors have been demonstrated as an adequate means of controlling the supply of a reactant and as the key part of a reversible hydrogen storage / transport system [3, 4].

The underlying concept of membrane reactors involves combining chemical reaction and product removal via a permselective membrane in a single unit

(Figure 1-1). A membrane reactor, in which a permselective membrane is used to remove a product from the reaction zone as it forms, can increase the conversion of thermodynamically-limited reactions and / or decrease reaction temperature if it is endothermic.

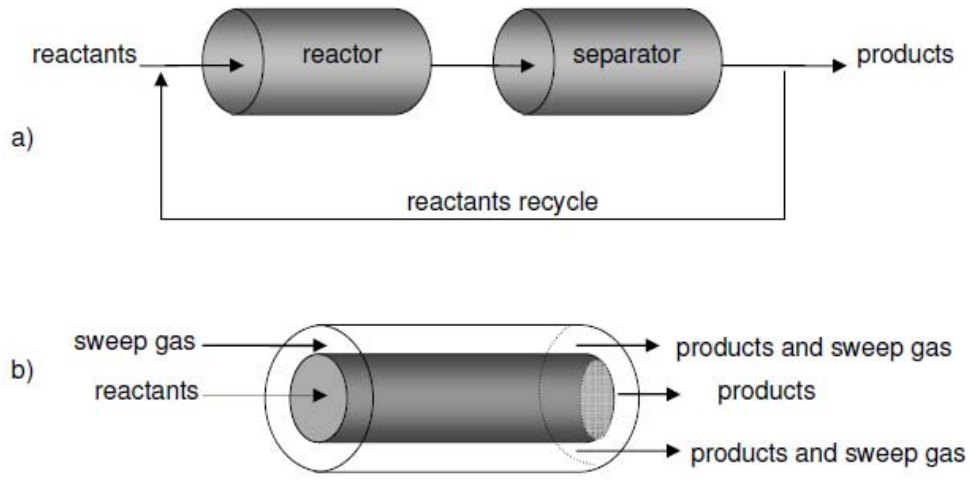


Figure 1-1 (a) conventional membrane reactor system and (b) integrated membrane reactor system.

Combining chemical reaction and separation into one unit simplifies downstream recovery and purification steps, and leads to potential savings in energy and reactant consumption. Furthermore, deploying membrane geometries with high packing densities can lead to a more compact process unit [2].

The idea of coupling chemical reaction and separation was first proposed in 1968 [5], and more recently, the concept has been proven experimentally using conventional inorganic membrane reactors for a range of reactions [6-11]. For the dehydrogenation of isobutane, Guo et al. [7] showed that a membrane reactor based on a Pd/Ag layer on an alumina tube (8 mm O.D.) resulted in a conversion of 51 %. This should be contrasted with the equilibrium value of 19 % at their

reaction temperature (723 K) and a value of just 16 % obtained in a conventional fixed bed reactor. Yildrim et al. [12] also reported conversion values exceeeding the thermodynamic limit for the catalytic dehydrogenation of light alkanes using membrane reactors. The catalytic dehydrogenation reaction could be carried out at lower temperatures and still attain comparable conversion. This would advantageously reduce the extent of side reactions, increasing the selectivity to the desired alkene and reducing catalyst deactivation from coke deposition. Furthermore, less energy would be required to attain the operating temperature, which is economically and environmentally favourable. Hence, there are many potential benefits of carrying out reactions such as catalytic dehydrogenation reactions of light alkanes in membrane reactors.

In this thesis, novel inorganic composite hollow fibre membranes are developed and are initally applied to catalytic dehydrogenation of propane and then extended further to the water-gas shift reaction. These membranes consist of a selective Pd or Pd-Ag layer coated onto a porous alumina hollow fibre support, which provides mechanical strength, increases the membranes permeability and reduces the amount of costly Pd required. The hollow fibre membranes will have advantages over the flat disc and tubular varieties hitherto examined for this purpose, in terms of packing density and reactive area. This is particularly advantageous in membrane reactor applications, where the membrane area must be maximised to remove the product from the reaction zone at a high rate.

Only a few groups worldwide have reported the preparation of useable ceramic hollow fibres [13-15]; a major problem in earlier attempts being the brittleness of the fibres. Recently, Kingsbury et al. [16], used a combined phase inversion and sintering method to successfully prepare asymmetric ceramic hollow fibres with two types of morphologies, a sponge-like region and finger-like region

(Fig.1-2(a)). This method confers additional benefits to previous fabrication attempts in that the asymmetric pore structure could simutaneously function as a porous support for coating of a gas separation layer and a porous matrix for catalyst deposition (Fig.1-2(b-c)). In other fabrication methods it is often necessary to coat the ceramic fibre, which usually has a symmetric pore structure, with additional ceramic layers to successively reduce the pore size.

For permselective permeation, asymmetric/composite hollow fibre membranes need to be prepared with a thin (typically 1-10 μm) dense separation layer. In this work, Pd and Pd-Ag separation layer is coated on the outer surface of the fibre using a well developed electroless plating method similarly reported by other groups for almunia tubes of larger diameters [17-19]. Because of the low specific surface area of the Pd-Ag separation layer on the outer surface of the fibre, this will not function as an effective catalyst and an additional catalyst is often necessary. This is provided by deposition/impregnation of a catalyst within the alumina support sturcture using a suitable depostion method. The avoidance of packing catalysts between fibres (tubes) confers a number of advantages since the problem of packing dozens of tubes uniformly with catalyst is eliminated; non-uniform packing leads to temperature excursions within a tube and gas flow variations between channels – both of which make it difficult to run the reactor optimally. An additional benefit of separating the catalytic and hydrogen permeation layers in this way is that one retains the option of using a reactive sweep gas on the permeate side of the membrane as has been shown by Gobina et al. [20] to further enhance conversions in dehydrogenation reactions.

This work focuses on three membrane architectures which are shown in Figure 1-2, and described below:

a) Asymmetric porous supports, where a membrane is formed using a phase inversion process to prepare a hollow fibre precursor, which is then sintered to create asymmetric porous structures.

b) Composite membranes, comprising a porous support formed by phase inversion and sintering and a second, distinct layer coated subsequently to provide the nonporous separation layer.

c) A variation on (b) is to deposit an active catalyst inside the asymmetric pore structure via impregnation or other suitable deposition methods.

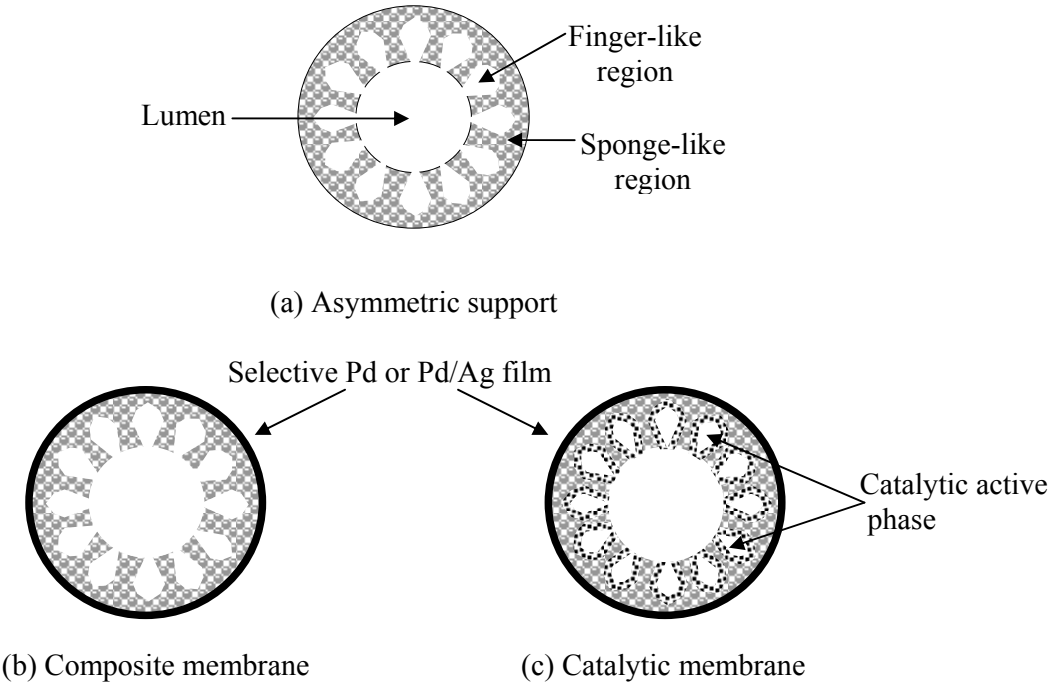


Figure 1-2 Membrane Architecture

1.2 Objectives

The broad aim of this thesis is to develop novel inorganic composite hollow fibre membranes for industrially relevant reactions and to also understand key engineering parameters that govern the membrane reactor performance.
The specific objectives are as follows:

1. Prepare an asymmetric alumina hollow fibre as a membrane support.
2. Develop a composite hollow fibre membrane reactor (HFMR):
    a) by functionalizing hollow fibre substrates through the deposition of catalysts within the fibre wall of hollow fibres and,
    b) by coating a thin and dense Pd or Pd-Ag hydrogen separation layer onto the outer surface of the hollow fibre support.
3. Determine the structural properties of the composite hollow fibre membrane reactor using gas permeation, SEM, XRD, BET and gas adsorption analytical techniques.
4. Test the effectiveness of the new membrane reactor design for catalytic dehydrogenation of propane and for water-gas shift reactions.

1.3 Thesis structure and presentation

This thesis is made up of seven separate chapters which describe preparation of Pd based composite membranes and their applications in chemical reactions. Figure 1-3 shows the overall scheme used in this work.

In Chapter 2, a literature review is given on the characteristics of inorganic membranes, various fabrication methods of Pd and Pd-Ag membranes, catalyst

deposition techniques in membranes and applications of palladium-based membrane reactors for dehydrogenation of light alkanes and water-gas shift reactions.

Chapter 3 describes the fabrication of a thin Pd membrane on porous asymmetric alumina hollow fibre supports prepared using the combined phase inversion and sintering method. A Pd layer is directly coated using an electroless plating method onto the outer surface of asymmetric supports to form a fully dense membrane.

A Pd-Ag inorganic hollow fibre membrane reactor (iHFMR) is developed for the catalytic dehydrogenation of propane to propene in Chapter 4. The Pd-Ag layer is coated on the outer surface of the asymmetric substrate and sub-micron sized Pt(0.5wt.%)/γ-alumina catalyst is deposited in the finger-like voids of the support to form a highly compact multifunctional reactor. A comparison of propane conversion and space-time yields is given between the iHFMR and a corresponding fixed bed reactor.

Following the successful development of the iHFMR, Chapter 5 describes the development of a highly compact multifunctional Pd/alumina membrane reactor for the same propane dehydrogenation reaction. In this design, the iHFMR consists of a thin and defect free Pd layer coated directly onto the outer surface of an alumina hollow fibre support with an asymmetric pore structure and a Pt(1wt.%)/SBA-15 catalyst deposited inside the substrate. The functionalized alumina hollow fibre substrates with a surface area/volume value of up to 1918.4 m^2/m^3 possess a catalyst surface area of 31.8 m^2/g. This is significantly higher than the surface area of 2.04 m^2/g, obtained for a Pt(0.5wt.%)/γ-alumina catalyst presented in Chapter 4.

In Chapter 6, the inner finger-like voids of hollow fibre substrates are functionalized with a Pt-ceria/SBA-15 catalyst and the outer surface is coated with a dense Pd layer. The resultant membrane reactor is tested for water-gas shift reactions.

And in Chapter 7, a summary of the results and conclusions of this thesis is presented with recommendations for future work.

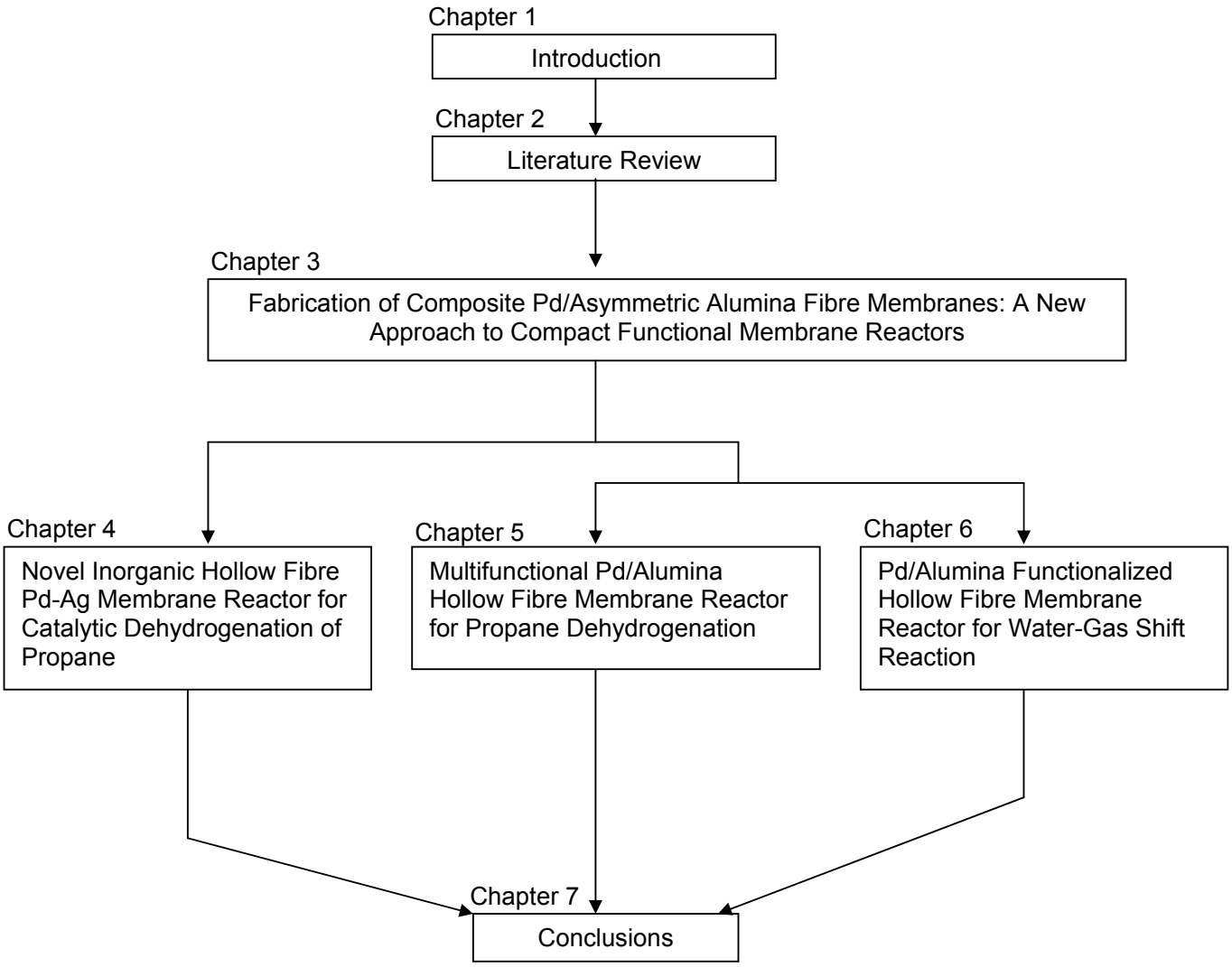


Figure 1-3 Structure of the thesis

CHAPTER 2

Literature Review

Abstract

In this chapter, an overview of the unique characteristics of ceramic membranes is presented with a particular focus on palladium-based composite membranes. Palladium and its alloys which are highly selective to hydrogen, can be fabricated and deposited on inorganic supports using a range of physical or chemical deposition methods. A novel phase inversion/sintering technique used in preparing asymmetric alumina hollow fibre supports is also described along with the various membrane and membrane/catalyst arrangements deployed in membrane reactors. The final section highlights experimental studies which demonstrate the use of palladium membrane reactors in catalytic membrane reaction processes and their economic potential.

2.1 CHARACTERISTICS OF CERAMIC MEMBRANES

A membrane is as a semi-permeable barrier between two phases [21]. The membrane is often in the form of a thin permselective film and controls the exchange of material between two adjacent fluid phases by either sieving or by controlling their relative rates of transport through the membrane. The transport processes across the membrane are typically driven by a gradient of concentration, pressure, temperature etc. and membranes are characterised by their permeability and selectivity. The permeability is defined as the flux through the membrane with respect to the thickness and driving force, while selectivity measures the ability of the membrane to separate a mixture containing two or more species.

Two main classes of membrane exist: dense (non-porous) and porous. Dense membranes are normally made from solid layers of metals (e.g. Pd alloys) for hydrogen separation [22], or of mixed electronic-ionic conducting oxides for oxygen separation [23]. Porous membranes often consist of a porous wall and/or porous top layer or layers (metal, oxide, glass) on a porous (metal-oxide) support. Membranes are also classified as having a symmetric (homogeneous) or an asymmetric structure. Homogeneous or symmetric membranes are self-supporting and mechanically stable. Asymmetric membranes on the other hand consist of a membrane deposited on a porous support, which provides mechanical strength. The porous support provides the mechanical stability for the membrane without causing too much resistance to mass transport. An asymmetric composite membrane is produced when a porous support is composed of a different material from the membrane layer.

Ceramic membranes are usually composites consisting of several layers of one or more different ceramic materials. They generally have a macroporous support, one or two mesoporous intermediate layers and a microporous or dense top layer (shown in Figure 2-4). The support layer provides mechanical strength while the intermediate layers bridge the pore size differences between the support layer and top layer where the actual separation takes place. Ceramic membranes are typically made from a range of materials including, Alumina, Zirconia, Titania, Silica, Carbon etc. or a combination of any of these materials.

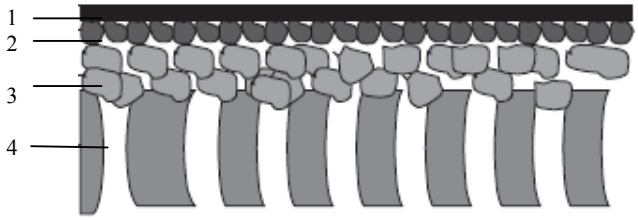


Figure 2-4 Schematic representation of an asymmetric composite ceramic membrane

1.) Modified separation layer (dense or < 2 nm);
2.) Separation layer (2-50 nm);
3.) Intermediate layer(s) (50-1000 nm);
4.) Porous support (1-15 μm)

The architecture of membrane and membrane-support combinations plays a crucial role in determining the mass transport properties of the membrane system. For example, in order to reduce the overall permeation resistance to the permeate flow, an asymmetric composite membrane requires a thin and defect-free separation layer with small pores deposited on a support with larger pores. However, producing a thin separation layer directly on top of a support with large pores is difficult because the precursor system from which the separation layer is made will significantly penetrate into the supporting pores (i.e., small particles from which small-pore membranes are made will penetrate much larger pores). This will result in a large increase in the resistance to flow. Furthermore, thin layers covering large pores are mechanically unstable and crack easily.

One possible solution is to fabricate a graded system by adding one or more intermediate layers with gradually decreasing layer thickness and pore size between the support layer and the separation layer. The larger the difference between the pore size of the support and the separation layer, the more intermediate layers that are required. An example of the pore characteristics of a four-layer alumina system is shown in Figure 2-5.

The multistep solution described above is used to enhance the layer quality by decreasing the number and size of defects by covering or filling the defects in an underlying layer with a layer on top of it. However, each step involves costly high temperature treatment and a more practical and economical solution was recently reported by Li et al. In their work they fabricated dense LSCF asymmetric membranes in a single step using the phase inversion process [24]. Scanning electron micrographs of the prepared membranes showed a dense and thin skin layer integrated with the porous support of the same ceramic material.

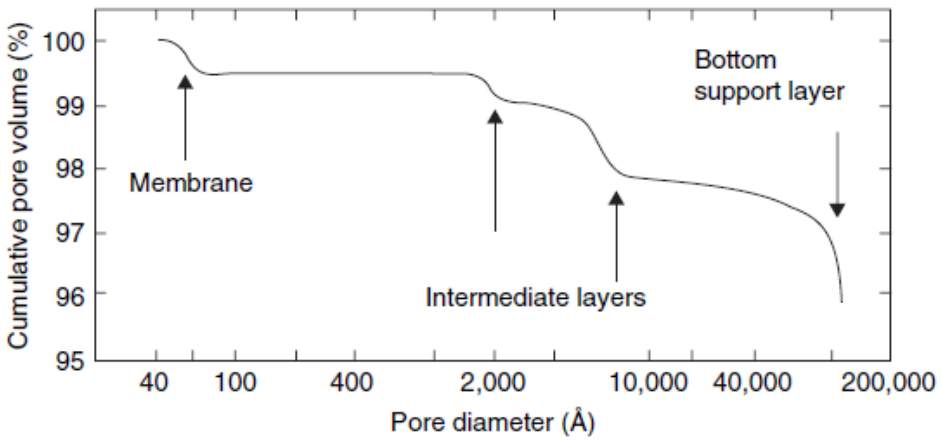


Figure 2-5 Pore size distribution of a four layered alumina membrane [25]

Ceramic membranes are commercially manufactured in a diverse range of geometries (flat discs, plate or tubular configurations) which are limited by low

surface area to volume (S/V) ratios. To improve this ratio, alumina multichannel monolithic elements were developed that can be combined into modules. Hsieh et al. showed that that S/V ratios are around 30-250 m^2 m^{-3} for tubes, 130-400 m^2 m^{-3} for multichannel monolithics and up to 800 m^2 m^{-3} for honeycomb multichannel monolithics [25].

To further increase mechanical robustness and packing density, disks, tubular and hollow fibre membranes are usually assembled into modules as shown in Figure 2-6. Hollow fibre modules offer the highest packing density, i.e. around 9000 m^2 m^{-3} in comparison to a packing density of around 30-500 m^2 m^{-3} offered by plate or tubular forms. However, despite the advantages of this configuration, widespread deployment of ceramic hollow fibres relies on overcoming the physical brittleness often associated with ceramic materials, especially for high temperature industrial applications. Furthermore, the small size of the internal bore in hollow fibres can present a problem when large quantities of gas are permeating (high pressure drop down the fibre bore). Notwithstanding the limitations of ceramic hollow fibres, they have still been produced both in porous and dense form for a range of applications that include, gas separations [26] [27], contactors [28], solid oxide fuel cells [29, 30], membrane reactors [31, 32], solvent recovery [33] etc.

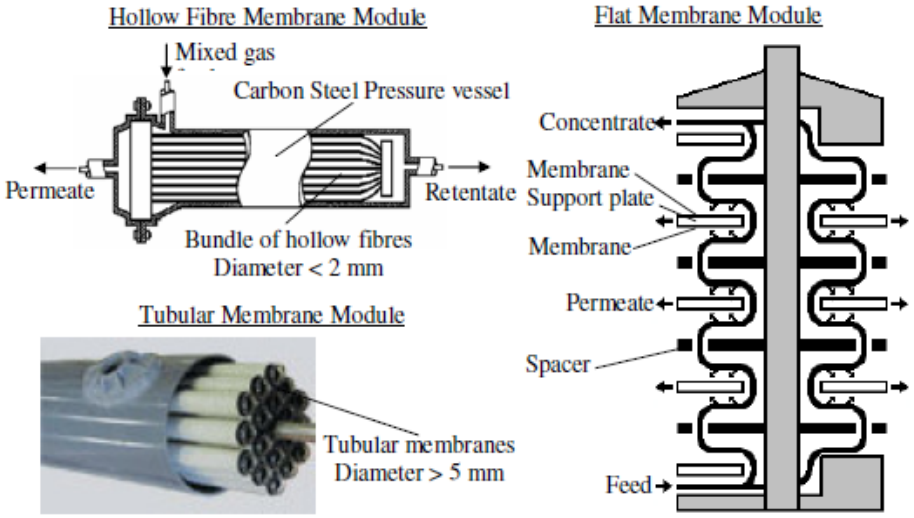


Figure 2-6 Diagrams of hollow fibre, tubular and flat membrane modules [34]

2.2 PALLADIUM COMPOSITE MEMBRANES

Inorganic membranes made up of palladium or palladium alloys were designed originally to purify hydrogen. The demand for hydrogen is driven by the ever growing energy consumption, estimated at 4.5 quadrillion Btu per yr, required for separation processes in plants [35]. Palladium membranes can reduce capital investment and energy consumption by extracting hydrogen from hydrocarbon streams and can be applied to sustainable energy systems such as fuel cells and distributed power [36]. Furthermore, as part of a process intensification strategy, palladium membrane reactors couple reaction and separation to increase efficiency.

In order for palladium membranes to compete or even replace other conventional hydrogen separation technologies such as pressure swing adsorption (PSA) or polymer membranes or to be used in membrane reactors, they must possess certain characteristics. These include: high flux and permselectivity for

hydrogen, high output per unit volume and a stable and predictable performance over a long period of time (>10000 h) at high temperature and pressure [37].

The following sections of this chapter describe gas permeation through supported palladium composite membranes. They focus on hydrogen permeation through Pd films, permselectivity and gas permeation through porous substrates.

2.2.1 Permeation of hydrogen through Pd membranes

Hydrogen permeates through palladium/palladium alloy membranes via a solution-diffusion mechanism that involves the following steps [38] shown in Figure 2-7:

1. Diffusion of H_2 molecules from the bulk gas to the metal surface through a boundary layer.
2. Adsorption of H_2 molecules on the membrane surface.
3. Dissociation into atomic hydrogen (dissociative chemisorption).

$$H_{2\ (gas)} \leftrightarrow 2H_{\ (chemisorbed)}$$

4. Diffusion of atomic hydrogen through the Pd lattice.
5. Transition of atomic hydrogen form the bulk Pd the Pd surface.
6. Recombination of H_2 atoms into hydrogen molecules on the permeate side (associative desorption).

$$H_{2\ (gas)} \leftrightarrow 2H_{\ (desorbed)}$$

7. Diffusion of H_2 molecules away from the membrane surface to the bulk gas through a boundary layer.

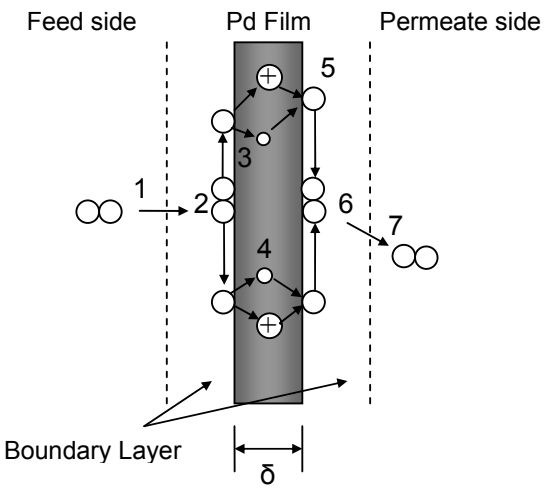


Figure 2-7 Hydrogen permeation through palladium membrane

Each step in the process can be described by a forward and reverse reaction, for example in step 2, dissociative chemisorption of hydrogen[39] :

$$H_{2(gas)} \underset{k_2 c^2{}_H}{\overset{k_1 p_H}{\rightleftharpoons}} 2H_{(surface)} \qquad (1)$$

Where k_1 and k_2 are the rate constants for adsorption and desorption respectively, p_H *(Pa)* is the partial pressure of hydrogen, and *c (mol/m^3)*, is the concentration of hydrogen in the metal. Assuming equilibrium between hydrogen molecules in the gas phase and hydrogen atoms at the gas/solid interface, the concentration of atomic hydrogen just within the metal, c_H *(mol/m^3)*, is proportional to the square root of hydrogen pressure (Sieverts' law) [40] Eq.2:

$$c_H = K_s p_H^n \qquad (2)$$

Where K_s (*mol/m^3. Pa$^{0.5}$*) is Sieverts' constant and p_H *(Pa)* is the partial pressure of hydrogen in the gas phase. The Sieverts' constant describes the solubility of atomic hydrogen in the lattice at low hydrogen concentration and when interactions between hydrogen atoms are minimal. The power dependency *n*, is 0.5 because hydrogen diffuses through the metal in atomic form [41].

In general, the atomic diffusion of hydrogen through a palladium film is driven by a partial pressure difference across the film and the surface processes (steps 2 and 5) can be neglected, while bulk diffusion (step 4) is rate limiting for hydrogen permeation through the membrane. Once inside the metal, the steady-state permeation rate is described by Fick's first law [42] (Eq. 3):

$$J_{H_2} = -D_H \frac{dc_H}{dx} \qquad (3)$$

Where, J_{H_2} is the hydrogen permeation flux *(mol/m^2. s)*, D_H is the diffusivity of hydrogen in the palladium membrane *(m^2/s)*. Substituting in the relationship for hydrogen concentration in the metal (Sieverts' law) Eq. 2 in to Eq. 3, and assuming a homogeneous solid and low hydrogen concentration (so that the diffusivity is independent of hydrogen concentration) and integrating, results in Eq.4:

$$J_{H_2} = \frac{Q}{l}\left(p_{H,1}^{0.5} - p_{H,2}^{0.5}\right) \qquad (4)$$

$$Q = D_H . S_H \qquad (5)$$

Where *Q* is the permeability *(mol/m^2 .s. Pa^n)*, *l* is the membrane thickness *(m)*, $p_{H,1}$ and $p_{H,2}$ *(Pa)* are partial pressures of hydrogen on the feed and permeate

side respectively and S_H represents hydrogen solubility in the palladium layer *(mol/m$_3$. Pa$^{0.5}$)*. The permeability can be further expressed as a function of temperature, composition and microstructure of the membrane layer, given by Eq. 6 and Eq. 7:

$$D_H = D_O \exp\left(\frac{E_A}{RT}\right) \qquad (6) \qquad\qquad S_H = S_O \exp\left(\frac{\Delta H_H}{RT}\right) \qquad (7)$$

In Eq. 6 and 7, E_A is the activation energy for hydrogen diffusion (*J/mol*), ΔH_H is the solubility enthalpy of hydrogen (*J/mol*), *R* is the universal gas constant and *T* is the absolute temperature (*K*). Combining equations 4 to 7 gives Sieverts' law:

$$J_{H_2} = \frac{Q}{l}\left(p_{H,1}^{0.5} - p_{H,2}^{0.5}\right) = \frac{Q_O}{l}\exp\left(\frac{-E_Q}{RT}\right)\left(p_{H,1}^{0.5} - p_{H,2}^{0.5}\right) \qquad (8)$$

Where, $$Q_O = D_O \,.\, S_O \qquad (9)$$

$$E_Q = E_A + \Delta H_H \qquad (10)$$

E_Q is the apparent activation energy of hydrogen diffusion through palladium (*J/mol*) and the *o* subscript represents the pre-exponential factor of the term.

In certain cases, for example, when the membrane is ultra thin or when the process stream has some contaminants, the surface (dissociation or recombination kinetics) processes become much slower than the diffusion of hydrogen and as such, Sievert's law is no longer valid [43]. The flux can alternatively be derived as

being proportional to the difference of the hydrogen partial pressure raised to an exponent with a value of *n*, shown below:

$$J_{H_2} = \frac{Q_o}{l} \exp\left(\frac{E_Q}{RT}\right).\left(p_{H,1}^{n} - p_{H,2}^{n}\right) \qquad (11)$$

The value of the pressure dependency, *n*, plays an important role in determining the rate-limiting step and consequently the determination of the values of the activation energy. Through nonlinear regression, the values of *n,* Q_o and the apparent activation energy, E_Q *(kJ/mol)*, can be obtained from the flux data taken at different temperatures and pressures [44]. By plotting permeance (Q_o/l) versus 1/T (where T is the temperature in *K*), the apparent activation energy for hydrogen diffusion through the metal can be determined through the Arrhenius relationship [45]. If the film contains defects (the permselectivity is not perfect), they should be accounted for by subtracting their contribution to flux when calculating the true hydrogen flux through the metal itself.

As palladium is very permeable to hydrogen and essentially impermeable to other gases, in theory, perfect permselectivity can be reached. However, in practice, purity is often limited due to small amounts of impurities that diffuse through the metal lattice and grain boundaries. The permselectivity of hydrogen through the palladium film can be expressed by measuring the flux of pure single gases rather than a mixture using Eq. 11.

$$S_{i/j} = \frac{J_i}{J_j} \qquad (11)$$

Where S_{ij} is a dimensionless number that describes the membrane permselectivity of component *i* and *j*, and $J_{i,}$ is the flux of component *i* through the membrane *(mol/m^2. s)*.

2.2.2 Permeation of gases through porous supports

Figure 2-8 and Eq. 12 show an illustration of the permeation flux of pure gas through a porous support without a selective Pd layer and a mathematical model of the process, respectively [46].

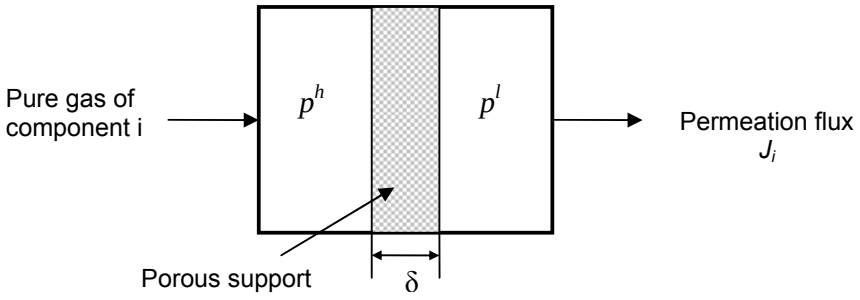


Figure 2-8 pure gas permeation through porous support

$$J_i = \frac{P_i}{\delta}\left(p^h - p^l\right) \qquad (12)$$

Where J_i is the flux *(mol/m^2. s) and* P_i is the permeability constant of component *i* through the support *(mol. m/.s. Pa^n)*

The separation of gas mixtures through porous supports with pore size distributions is achieved based on differences in molecular mass, size or shape, or on differences in the affinity of the gas molecules for the membrane surface.

Hence, a number of theoretical models can be used to analyze the transport of gases such as viscous flow, slip flow, Knudsen flow and molecular sieving effects. However, in porous supported Pd composite membrane systems, the supports offer minimal resistance to gas flow and are generally characterised by either viscous flow or Knudsen flow.

The gas flow behaviour is governed by interactions between gas molecules and between gas molecules and pore walls and is strongly influenced by the mean free path, i.e. the average distance a molecule travels between collisions. For viscous flow behaviour, the support pores are much larger than the mean free path of the gas molecules, this leads to more frequent collisions between gas molecules than with the pore walls and no separation takes place. For Knudsen flow behaviour, the support pores are much smaller than the mean free path, and hence gas molecules collide with the pore wall more frequently than with each other. For Knudsen flow, diffusion and separation take place as molecules with a lower molecular mass diffuse faster than molecules with a larger molecular mass. The Knudsen diffusion permselectivity for two molecules can be evaluated based on the molecular mass of each gas component using Eq. 13.

$$S_{i/j}^{Kn} = \frac{\sqrt{MW_j}}{\sqrt{MW_i}} \tag{13}$$

Where component *i* is lighter than component *j*

2.3 FABRICATION OF PALLADIUM COMPOSITE MEMBRANES

2.3.1 Membrane Supports

In palladium composite membrane systems, the porous support serves to improve the mechanical integrity of the membrane and as a suitable template to coat thin layers to give high permeance and selectivity. For hydrogen permeation, the separation layer has to be as thin as possible to ensure a high enough flux but not at the expense of being too weak to withstand moderate to high pressures and temperatures. Ceramic, Vycor glass, porous stainless steel (PSS), Quartz and Carbon are some of the most commonly used materials as supports in palladium composite membranes.

Each type of material has economic and performance trade-offs. For example, the merits of porous stainless steel (PSS) are sturdiness and weldability, however, PSS composite membranes have the disadvantage of relatively large pore size distributions, yielding thicker membranes and leading to intermetallic diffusion at high temperatures, causing a deterioration of hydrogen flux. Alumina supports are resistant to harsh chemicals and are stable at high temperatures but are prone to thermal expansion coefficient mismatches during thermal cycling [47]. Furthermore, the composition of the support, porosity and surface roughness determine largely the amount of palladium required to form a hydrogen permselective film without defects, and thus, the hydrogen flux and stability of the membrane.

Because of the influence of the support porosity and pore size distribution when coating thin and dense membranes, it has often been necessary to modify ceramics and porous stainless steel substrates. For example, a γ-alumina layer is

usually coated on top of a porous α-alumina support to narrow the pore size distribution without losing the porosity of the support [48]. Sol-gel derived γ-alumina (pore size 5-20 nm) layers produce a much smoother surface, ideal for coating Pd films with good adhesion, compared to a coarse α-alumina (pore size 50-500 nm) surface.

To improve the structural stability of Pd-Ag alloy stainless steel membranes, Shu et al. introduced an ultrathin intermediate layer of titanium nitride (0.1 μm thick) as a diffusion barrier between Pd-Ag and the SS substrate [49]. Auger electron depth profiling analysis indicated that the improved membranes were thermally stable at temperatures as high as 973 K. Coating an intermediate layer of silica using sol-gel processing, as a diffusion barrier between the porous stainless steel support and the Pd layer is also useful to improve stability and selectivity [50]. Jun and Lee modified the surface of a stainless steel support (pore size 0.5 μm) by dispersing submicron nickel granules on the surface and sintering the substrate at 1073 K for 5 h under vacuum [51]. This resulted in a smooth surface having pore sizes of about 0.05 μm.

2.3.1.1 Fabrication of ceramic hollow fibre membrane supports

Several techniques have been studied and used in developing ceramic membranes over the last few decades. Some of these include slip casting, tape casting, pressing, extrusion, sol-gel processing, dip coating and in the context of this thesis, the phase inversion/sintering method [1]. In general, they comprise three common successive steps: preparation of a starting dope, formation of a membrane precursor and finally a sintering/calcination step. The formation of the membrane precursor is the key differentiator among the various techniques. This intermediate step is determined by the desired application and type of

configuration, for example. pressing is commonly used to prepare disk membranes while the extrusion method is suitable for tubular supports that can weigh anything from a few grams to a ton.

The novel combined phase inversion/sintering method has been adopted for developing ceramic hollow fibre membranes because of its simplicity and versatility with a range of materials. For example, Tan et al. prepared and characterised alumina microporous membranes [14], Liu et al. produced mixed proton and electronic conducting hollow fibre SCYB fibres for chemical processing [52]. De Jong et al. fabricated a dual layer hollow fibre membrane using a triple orifice spinneret by the phase inversion and sintering method in a single step [53]. Zydorczak et al. prepared ultra thin LSCF hollow fibres for enhanced oxygen permeation [27]. Wang et al. also used the phase inversion technique to produce gas permeable mesoporous YSZ-SiO_2 hollow fibre membranes with a mean pore size of 3 nm [54].

The preparation of ceramic membranes via the combined phase inversion and sintering process involves three successive steps: preparation of the spinning suspension (dope), spinning of the membrane precursor via phase inversion into the desired shape and finally sintering of the precursor at high temperature to form the membrane. Figure 2-9 shows a schematic of the process, a brief description of which is given in the following sections.

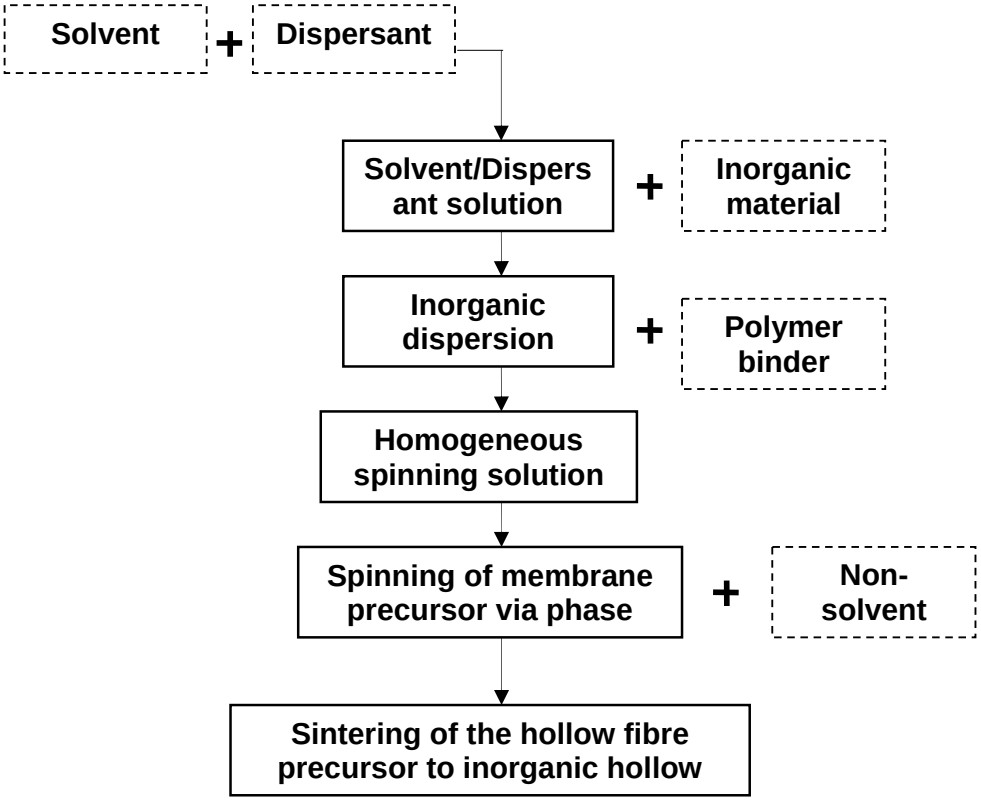


Figure 2-9 Flow chart of the spinning process

2.3.1.1.1 Preparation of the spinning suspension

The preparation of the spinning dope consists of mixing inorganic particles, additives and solvent to form a homogenous mixture. When preparing the dope, particular attention should be given to the particle size distribution as this effects the porosity and pore size distribution of the final membrane [25]. Additives such as dispersants, polymer binders, anti-forming agents, chelating agents etc. are used to improve the dispersion of the suspension. A key requirement of any polymer binder is that it must be invertible and burnt off easily during the sintering step. The solvent mainly acts a suitable medium to dissolve additives, binder and as an exchanging agent with non-solvent (coagulant) during the phase inversion process.

Detailed studies on the preparation of spinning dopes for alumina hollow fibres have highlighted how the composition of the various components affect the rheological behaviour of the dope and consequently the nature of the fibre precursors. For example, work done by Kingsbury et al. showed that by increasing the viscosity over a critical point, the fibre morphology can be varied greatly [16]. In general, the key to producing spinnable suspension (dope) lies in tuning the inorganic particles, solvent, additives and spinning conditions such as air-gap and dope viscosity.

2.3.1.1.2 Spinning

The second stage in the process involves spinning precursor fibres. Hollow fibre precursors are extruded through a tube-in-orifice spinneret, shown in Figure 2-10. First, the prepared spinning dope is transferred to a gas tight reservoir and degassed to remove bubbles and dissolved gas. The dope is then pressurised using nitrogen and is extruded through the orifice of the spinneret into a coagulation bath containing non-solvent (usually water), to form a membrane precursor. A non-solvent (usually water) is simultaneously pumped through the centre (tube) of the spinneret to form a hollow fibre. The fibre precursor is kept in the external coagulation bath for several hours to complete the phase inversion process. Following this, it is washed with tap water and dried.

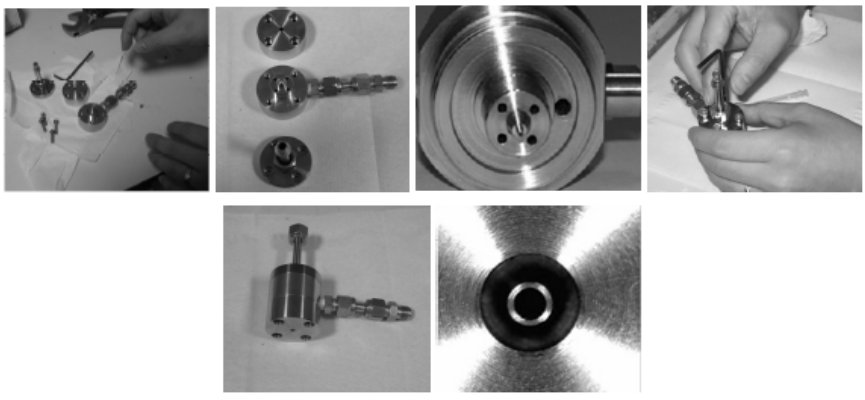


Figure 2-10 Tube-in-orifice spinneret for fibre spinning

The formation of membrane precursors using this phase inversion method results from early work carried out by Loeb and Sourirajan in the 1960s [55]. The process can be described in terms of a three-component system: non-solvent, solvent and polymer. After immersion of a polymeric solution into a non-solvent bath, the solvent diffuses out of the polymer solution, while the non-solvent diffuses into the solution. This exchange causes precipitation of the polymer to yield a polymer hollow fibre precursor [56]. By adding a small amount of polymer to a ceramic suspension, this technique has been adapted to prepare ceramic hollow fibres [14] [57].

2.3.1.1.3 Sintering

The final step involves subjecting membrane precursors to high temperature treatment (calcination) where the polymer binder is removed and ceramic particles are bonder together by sintering and is subdivided into three stages: presintering, thermolysis and final sintering. These are described in the following sections.

a.) Presintering

During pre-sintering, vaporisation of chemicals, water and water of crystallization from the surface of particles and removal of liquids and moisture adsorbed from the air takes place. It should be noted that adsorbed moisture may be held in the membrane precursors up to and exceeding 473 K.

b.) Thermolysis

Thermolysis occurs prior to sintering. Organic components such as dispersants, binders and additives decompose and are removed from the precursor fibre. Incomplete or uncontrolled thermolysis may cause defects in the membrane, which will be detrimental to the performance of the membrane. The thermochemistry of the binder, additives and the precursor configuration and heating profile also influence the thermolysis behaviour.

c.) Sintering

The final sintering step involves an initial, intermediate and final stage. All of which are associated with diffusion leading to a reduction in the surface free energy of the system. At the initial stage, there is rapid inter-particle neck growth (bonding) between particles which increases the strength of the fibre. Neck growth is initiated by mass transport mechanisms that can include any combination of surface diffusion, evaporation-condensation, grain boundary diffusion, lattice diffusion, viscous flow and plastic flow. However, only the latter four mechanisms are responsible for shrinkage and densification.

The intermediate stage, which covers most of the entire sintering process is characterised by shrinkage induced by grain growth and changes in the pore geometry. Grain and pore growth also known as coarsening, directly affects the microstructural features of the membrane. This grain growth is driven by the decrease in grain boundary energy that results from a decrease in the grain boundary area.

There are two types of grain growth in ceramic membranes: normal and abnormal growth. Normal grain growth is characterised by a relatively small change in the distribution of grain sizes while for abnormal growth, a few large grains develop and grow rapidly at the expense of smaller ones. Normal grain growth is favourable as abnormal growth may give rise to defects and non-uniformity [58].

During the final sintering stage, pores continue to shrink continuously and grains of a much larger size appear rapidly.

2.3.2 Palladium Membranes

Thin palladium and palladium alloy films are deposited by a variety of techniques. The type of method deployed depends largely on the type of substrate, its pore size and on the desired alloy composition. A review of some commonly used methods is given in the following sections.

2.3.2.1 Electroplating

In electroplating, metal electrodes are used to supply electrons to reduce metal ions from solution and deposit them onto a substrate. During the process, positive metallic metal ions formed at an anode migrate towards a cathodic membrane substrate in an applied electric field. For pulsed electrodeposition, the current is modulated in order to produce alternating metal deposition/removal cycling. In this manner, film parameters such as grain size, stress and composition can be well controlled.

Nam et al. used a vacuum electrodeposition technique to coat a pinhole free 1 μm Pd-Ni film onto a Cu/Ni/PSS support. The membrane containing 78 % Pd and 22 % Ni exhibited high hydrogen permeance and a hydrogen/nitrogen separation factor of 4700 at 823 K [50]. Amano et al. also tested a 1.2 mm thick V-Ni_{15} alloy foil with a 0.2 μm coating of palladium deposited by a pulse electroplating technique. Below 473 K, permeability was negatively affected by surface contamination and cracks developed at 300 kPa of pressure on the feed side [59].

2.3.2.2 Physical Vapour Deposition

Physical vapour deposition (PVD) involves depositing solid materials on a substrate from the vapour phase using a resistively heated piece of metal, such as a wire, as the metal source. PVD can be advantageous for deposition onto polymers

since the substrate can remain at room temperature. However, the drawbacks of PVD are the requirements of costly vacuum chambers and expensive metal alloy sources.

In its simplest form, the process involves vacuum evaporation of a heated metal or in a more complex manner by sputtering ions from the target surface with an electron beam. Although coating thickness is easily controlled using PVD, because the metal vapour flux impinges at a certain angle, the substrate must be rotated during deposition to avoid uneven coverage of the surface which may lead to voids and porosity.

Magnetron sputtering of ions takes place when a plasma (typically Ar) is introduced into a vacuum chamber and dislodges atoms and ions from the metal target which are then deposited on the substrate surface. A permanent magnetic field will increase ionization. Ample ionization, high current density and high sputtering rates are required to deposit a dense, continuous film. A variant of magnetron sputtering is referred to as ion plating. In this case, an ion gun is used instead of plasma to deposit chemical compounds or influence the properties of a deposited layer.

Jayaraman et al. sputtered a 1 μm Pd layer on sol-gel derived fine pore γ-alumina and course α-alumina supports. Although fairly gas tight films was formed on the former but not on the later, poor adhesion between the coated film and the γ-alumina support was noticed for films coated at room temperature to a thickness in excess of 300 nm. The results also indicated that at 353-873 K, the substrate type affects the grain size, nitrogen gas tightness and the adhesion of the deposited metallic film [48].

Franz et al. fabricated palladium micro-membranes with e-beam PVD onto a perforated silicon nitride/oxide bilayer composite on silicon wafers. A hydrogen/nitrogen permselectivity of 1800 was achieved. A thin layer of titanium was used to improve adhesion between the bilayer and wafer substrate. However, delamination occurred when the composite membrane was pressurised from the support side [60].

Tosti et al. used a dual ion beam to sputter Pd-Ag (0.5-5 μm) films on ceramic porous supports. In their study, complete selectivity was not obtained even with a 5 μm thick membrane due to shear stresses arising from differential elongation between the Pd coating and ceramic support under thermal cycling and hydrogen loading. The hydrogen/nitrogen separation factor was only slightly higher than in the ceramic support [47].

2.3.2.3 Chemical Vapour Deposition

Chemical vapour deposition (CVD) or metal-organic chemical vapour deposition (MOCVD) makes use of compounds with a sublimation temperature below their decomposition temperature. During composite metal membrane fabrication, a metallic material is usually sublimed in a separate chamber, transported using a carrier gas and thermally decomposed on the substrate surface or reacted with a gas such as hydrogen.

The major advantage of CVD is that the metal can be more easily deposited within the support pores as opposed to only on the surface as is the case with electroless plating and PVD. This enables much thinner palladium films to effectively block the pores of a porous support. The major drawbacks of CVD include contamination of the film with constituents of the metallic complex, such as carbon, as well as the build up of expensive precious metals on non-target surfaces.

Xomeritakis & Lin deposited thin (0.5-5 μm), palladium films onto asymmetric γ-alumina supports by counter-diffusion MOCVD. Although defects were found, as He permeated by Knudsen and viscous flow transport, the H_2/He permselectivity was still moderately high, >200 at 573 K [61].

Huang et al. deposited Pd and Pd-Ni films onto asymmetric γ-alumina (4 nm pore size) supports using counter diffusion MOCVD which promoted metal deposition within the pores of the membrane support. Pd-Ni alloy films (4 μm thick) were more permselective and crack-free compared to palladium. XPS showed that no oxygen or carbon impurities were deposited in the film [62].

Deshpande et al. deposited Pd-Ag films onto anodic γ-alumina followed by sintering of the porous deposit. By using flow-through aerosol-assisted CVD, they obtained a dense crystalline film approximately 1 μm thick, although some defects were present [63].

2.3.2.4 Electroless Plating

Electroless plating is commonly used to deposit Pd and Pd alloy films on various supports using chemicals as the source of both metals and electrons. The process relies on an autocatalytic reaction mechanism that is initiated by an activated surface. Initially, to remove contaminants and ensure a uniform and dense film, the support is cleaned in a dilute acidic solution, rinsed in alcohol or acetone and deionised water. The surface is then 'activated' to initiate the autocatalytic plating process using a *sensitization* and *activation* bath. Following this, the support is immersed in an electroless plating bath containing the required chemicals at about 333 K for a set period of time to coat a metal film with a certain thickness. The metal deposition rate and film morphology can be controlled by adjustments of both the plating bath concentration and plating temperature.

Compared to other deposition techniques, electroless plating has excellent throwing power (coverage of surface), can coat on non-conductors with proper surface activation, and requires very simple equipment with low costs. However, the major drawback of electroless plating is that it uses highly toxic chemicals and generates hazardous liquid wastes. If the plating surface is non-conducting or non-catalytic, it must be well activated, relatively smooth and free of macro defects. Hence, it is important to have a fundamental understanding of the variables that affect the electroless plating process in order to consistently produce uniform Pd and Pd alloy films. The focus of the following section is on surface activation, plating bath chemistry and the interplay among the many parameters required in the plating process to make thin, stable and selective membranes.

2.3.2.4.1 Surface activation

The activation process is carried out using tin and palladium chloride, either in a sequential or mixed method. In the sequential method, substrates are immersed in separate tin chloride and palladium solutions with rinsing with water in between. Mixed activators consist of a combination of tin and palladium salts in one bath. The sequential sensitizing/activation procedure begins with immersion in an acidic $SnCl_2/SnCl_4$ colloidal sensitizing solution followed by an acidic palladium containing activating solution. The colloidal tin solution is required to anchor the palladium to the surface. Upon immersion in the palladium activating solution, tin binds palladium to the surface via the reaction below, to create a Pd-Sn alloy on the substrate.

$$Sn^{2+} + Pd^{2+} \rightarrow Sn^{4+} + Pd^{0} \qquad (14)$$

The tin re-solubilises in the acidic palladium activation solution, but in practice, much remains on the surface. Tin-rich surface layers usually cover the active palladium

cores and although activity has been found to depend on the Sn/Pd ratio, excess tin accumulating on top of the palladium crystallites blocks their activity in catalyzing hydrazine oxidation. Rinsing after activation is required to prevent ‘‘drag-in’’ of the sensitizing and activation bath components into the plating bath. Otherwise, spontaneous decomposition of the bath may occur as the catalyst creates many nucleation sites throughout the plating solution.

Charbonnier et al. provided a good overview of tin and palladium activation processes and mechanisms. They concluded that tin chemisorbs preferentially onto substrate oxygen followed by palladium attachment via chlorine ions adsorbed on the tin. Although their work involved polymers, the mechanism can probably be extended to alumina with its surface hydroxyl groups [64]. When the colloidal tin particles contact the substrate, Sn^{2+} adheres to the surface, probably by a mechanism shown in Figure 2-11.

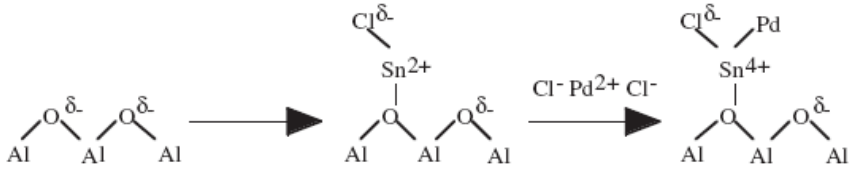


Figure 2-11 Possible mode for sensitization/activation of alumina surface [38, 64]

The structure of the Pd clusters on an activated substrate, surface morphology as well as the number and size of metal grains affect the quality of the palladium composite membranes. The presence of tin compounds with low melting points between the layers of metal film may cause the formation of pinholes and cracks due to melting and decomposition of the impurities at higher temperatures, thus affecting the long-term stability of the membrane. Paglieri et al. compared the long term stability of membranes prepared by using the conventional activation process and membranes activated with a new tin free activation process [65]. The

new technique consisted of dip coating of substrates with Pd acetate, calcination and reduction to metallic Pd in an H_2 atmosphere. The N_2 flux through membranes activated with the new method was more stable at 973 K for a period of a 1 week compared to the conventional procedure. However, the hydrogen permeability decreased at 873 K and above because of annealing problems.

Nanoscale metal clusters on the substrate created by impregnation, incipient wetness or ion exchange could serve as sites for initiation of electroless plating or actually create the permselective layer. This notion was studied by Li et al. who used a sol-gel technique in which Pd-modified boehmite sol was deposited on the surface of porous α-alumina. This was followed by calcinations at 823 K and treatment with H_2 to reduce Pd on the surface [66]. The sol-gel activated surface had a uniform distribution of palladium seeds compared to the Sn-Pd activated substrate.

In theory, any technique may be used to deposit a metal seed layer to promote electroless plating deposition, as long as the metal catalyzes decomposition of the reducing agent. Wu et al. activated a porous Titania membrane by using a photocatalytic reaction and $PdCl_2$. A thin Pd film (0.3-0.4 μm) was produced with a high H_2/N_2 permselectivity (1140 at 773 K) [67]. Schwartz et al. developed an activation technique for ceramic supports that involved the deposition of palladium acetate from solution, followed by heat treatment to burn off the organic fraction and leave behind palladium particles. An advantage of this procedure is the elimination of wastewater generated from sensitizing and activation procedures [68].

2.3.2.4.2 Electroless plating bath

After the activation procedure, the porous support is placed in an electroless plating bath for metal deposition. The electroless plating bath generally consists of a metallic salt, complexing agent, reducing agent and a stabilizing agent. Electroless

plating processes occur at the solid liquid interface between the support and the plating solution, where electrons are released by the anodic partial reaction and consumed by the cathodic partial reaction:

$$R^0 \rightarrow R^{Z+} + ze^-$$
$$M^{Z+} + ze^- \rightarrow M^0 \qquad (15)$$

Here, *R* is the reducing agent, *M* is the metal and *z* is the number of electrons transferred. For deposition to occur the sum of the standard redox potentials (E^o) of the oxidation and reduction reactions must be positive and ΔG^o (Gibb's free energy) be negative so that the reaction is thermodynamically favourable. In electroless palladium plating baths, shown in the equation below, a palladium-amine complex is usually stabilised by a chelating agent such as Na_2EDTA and a suitable reducing agent N_2H_4. The bath pH is usually kept around 11 depending on the ammonium hydroxide (NH_4OH) content.

$$2Pd(NH_3)_4^{++} + N_2H_4 + 4OH^- \rightarrow 2Pd^0 + 8NH_3 + N_2 + 4H_2O \qquad (16)$$

Several Pd metal sources such as $(Pd(NH_3)_4(NO_3)_2$, $Pd(NH_3)_4Cl_2$, $Pd(NH_3)_4(NO_3)_2$ and $PdCl_2$, were found to be the best salts to achieve high conversions. Also, a few reducing agents have been utilized in the electroless plating process including hydrazine, hypophosphite and formaldehyde

Shu et al. established that hydrazine oxidation is the rate-limiting step in electroless palladium deposition onto stainless steel, i.e. hydrazine adsorption and dehydrogenation controls the rate of palladium deposition [11]. Zhao et al. found that higher hydrazine concentrations in the plating bath produced more compact and permselective palladium films. The Pd particle size decreased as the concentration of hydrazine increased. The palladium membranes composed of

finer palladium particles produced at higher palladium deposition rates were more compact [69].

The structural evolution of the palladium film during electroless plating, i.e. grain size, cluster size, compactness and morphology, which have significant influences on the performance of membranes, are very dependent on the bath chemistry and plating rate. Hitherto, hydrazine is the most common and suitable reducing agents for electroless plating of palladium.

Cheng and Young compared the morphologies of Pd membranes prepared from hydrazine-based and hypophosphite-based solutions. The hypophosphite bath had a slower but constant plating rate, providing better efficiency than the hydrazine based plating bath. However, the oxidation of hypophosphite produced hydrogen gas, leading to a β-hydride phase at low temperatures and caused delamination of the Pd membrane. Therefore, chemical reducing agents that generated hydrogen were not suitable for Pd plating [70].

2.3.2.4.3 Electroless plating process

During the plating process, it is important to know that both the metal and reducing agents deplete over time and so have to be replaced depending on the plating kinetics of the bath and support. The support is plated until the activity of the support diminishes and pores are fully covered with Pd and the membranes become dense. As discussed earlier, plating rate and film morphology depend on the concentration of the plating bath constituents and the plating temperature, so understanding the fundamentals of electroless plating is key to optimizing the conditions for producing usable Pd and Pd alloy films on supports. The palladium film structure in composite membranes has been linked to limitations in high

temperature stability, resistance to thermal cycling and minimization of the defect-free film thickness.

Kikuchi et al., Uemiya et al. and Konno et al. were the first groups to develop composite membranes using electroless plating, depositing thin 5-20 μm films onto porous alumina or glass supports [71-73]. In some cases, their membranes had infinite permselectivites and were used for various reactions. Collins and Way also deposited palladium films between 11-20 μm on asymmetric alumina supports. They reported hydrogen/nitrogen selectivity of 1170 at 823 K and transmembrane pressure of 124 kPa and 380 at a transmembrane pressure of 1500 kPa [74].

Zhao et al. used vacuum infiltration to plate palladium to a thickness of 1 μm onto a palladium-modified Boehmite sol-gel layer [69]. The membrane peeled during annealing in inert gas so membranes prepared using electroless plating without vacuum were tested for permeability instead. The hydrogen/nitrogen ideal separation factor was 23 at ΔP of 1 atm and 723 K.

Quicker et al. were most able to consistently produce permselective palladium films using electroless plating compared to other methods of deposition [10]. A 3 μm thick film on porous (0.1 μm) ceramic had a hydrogen/nitrogen separation factor of 250 at room temperature.

Huang et al. studied the permeability of 7 and 15 μm thick palladium films deposited by electroless plating onto α-alumina and supported γ-alumina supports [44]. By modelling the diffusion through the palladium film and the porous supports, it was determined that the resistance of the support to permeation was substantial.

The selectivity coefficient of hydrogen/nitrogen through the composite membrane reached infinity.

Zheng and Wu made a comparison of pore size shrinkage between palladium deposited on α-alumina supports in a closed (hydrothermal) system, so that the pressure increased during plating, and in a conventional (open) system. The results showed a decrease in pore size from 0.8 to 0.36 μm when Pd was deposited hydrothermally and a pore size of 0.55 μm after conventional electroless plating. A systematic increase of pressure forced the plating solution to penetrate more deeply inside the pores, yielding better pore size shrinkage [75].

Pan et al. prepared thin 2-3 μm dense Pd membranes on macroporous γ-alumina/α-alumina hollow fibres using electroless plating techniques [18]. The membrane exhibited a high hydrogen permeance of 10 m^3/m^2 h bar at 723 K, which remained stable for 800 h. They reported a hydrogen/nitrogen separation factor of 1000. Sun et al. also prepared thin 1.5-5 μm Pd composite membranes on alumina hollow fibre substrates. They reported a hydrogen flux of 19.1 m^3/m^2.h at 723 K and selectivity of 3115 at a transmembrane pressure of 1 bar. They reported a highest flux of ~ 35 m^3/m^2 h at 773 K, at a transmembrane pressure of 1 bar and activation energy of 13.3 kJ/mol [78].

In order to optimise the microstructure and thickness of deposited films, the electroless plating can be combined with osmosis to prepare composite membranes. Pd films plated under osmotic conditions have been shown to exhibit much smaller metal grain sizes and narrower distributions that lead to much finer, uniform and thinner Pd films than otherwise would have been the case. The decrease in the Pd film thickness and finer microstructure enhances hydrogen permeation flux.

Souleimanova et al. prepared thin Pd/Vycor composite membranes using an electroless plating and osmosis technique [76]. The average Pd grain size gradually decreased from 350 nm (without osmosis) to 150 nm (with osmosis) with 9 M sucrose solution. As a result, Pd penetrated deeper inside the porous support compared with a conventional process, enhancing the interaction between the film and substrate. This improved the thermal stability and mechanical properties of the composite membrane. The same group carried out further experimentation and showed a reduction in the membrane thickness from 8 to 3 μm for regular plating and osmotic plating, respectively [77]. Furthermore, films of finer Pd clusters and more uniform microstructures were synthesised by the use of osmotic plating. The hydrogen permeation flux through the membrane increased by approximately 2-fold as the concentration of osmotic solution employed during plating increased from 0 to 9 M.

2.3.3 Palladium/silver Composite Membranes

A common problem encountered with the use of pure palladium is that it suffers from hydrogen embrittlement under certain critical conditions (Temp, 573 K and pressure, 2 MPa). In this environment, Pd undergoes a phase (α→β) transition, which alters its microstructure causing it to become brittle and subsequently fracture. This problem can be reduced by alloying other metals with palladium. Essentially, alloying lowers the critical temperature for the α → β phase transition by narrowing the α/β-Pd hybrid miscibility gap that is present in pure palladium at temperatures below 566 K.

Many metal alloys hitherto studied such as $PdAg_{25}$, $PdCu_{40}$, $PdRu_6$, PdY_{10} have been shown to increase the permeability of palladium while substantially enhancing its mechanical properties. Pugachev et al. showed that $PdAg_{25}$ adsorbs hydrogen more quickly and is up to 1.5 times as permeable as pure palladium. In addition, palladium alloys have higher tensile strength and hardness. This helps to eliminate membrane rupture, warping or cracking associated with thermal cycling [79]. Similarly, Shu et al. reported that at 673 K and 2.2 MPa, a $Pd_{77}Ag_{23}$ membrane exhibited a maximum permeability 1.7 times greater than that of pure palladium [80].

Table 2-1 and Table 2-2 show a summary of the characteristics and performance of Pd and Pd-Ag membranes prepared using various techniques discussed in this work. The main emphasis in recent years has been focused on producing much thinner membranes that exhibit higher permeance and selectivity for separation of hydrogen from a hydrogen/nitrogen mixture. In preparing Pd-Ag composite membranes a common problem was encountered in controlling the film composition and as a result a possible alternative could be to deposit the metals separately and then anneal. However, to obtain an alloy film from two distinct metal layers in a practical amount of time, a high temperature must be utilized to promote complete metallic interdiffusion. Therefore, the necessary control and temperature criteria have favoured the use of electroless plating techniques by researchers for the fabrication process.

The two possible ways to form alloys by electroless plating; coating and diffusion and co-deposition methods, are discussed below.

2.3.3.1 Coating and Diffusion method

In coating and diffusion, two films are deposited sequentially followed by inter-diffusion at high temperature. Although bulk compositions can be precisely

controlled with this method, a common problem in depositing a uniform film throughout the support is often encountered.

Uemiya et al. studied the separation selectivity and permeation rate of Pd-Ag alloy membranes on porous ceramic supports. The results showed that the rate of hydrogen permeation increased with silver content and reached a maximum at 23 wt% Ag. The $PdAg_{23}$ membrane exhibited 100 % selectivity for hydrogen permeation at 746 K. They concluded that the performance of the membrane at such low temperature is attributed to inhibition of the coexistence of α- and β-phase palladium hybrids. This is due mainly to a lowering of the spinodal decomposition temperature which resulted in enhanced hydrogen permeability and high hydrogen solubility [22].

Shu et al. prepared Pd-Ag/PSS composite membranes using the sequential deposition technique. After annealing for 5 h at 773 K under a hydrogen atmosphere a non-homogeneous alloy layer with a rich silver content on the top surface was formed. To further enhance the structural stability of the membrane, a titanium nitride diffusion barrier (0.1 μm thick) between the PSS and the Pd-Ag layer was introduced for higher annealing temperatures. The barrier slightly modified the pore structure of the substrate according to permeation measurements but effectively separated the Pd-Ag layer from the substrate [11].

Keuler et al. investigated the effect of the palladium and silver deposition sequence on coating adhesion and metal distribution in the alloy matrix after heating. Pd-Ag layers were obtained by first depositing palladium and then silver or vice versa. Heat treatment was carried out under a hydrogen atmosphere at 923 K. When silver was deposited first, the palladium to silver ratio across the thickness of the film remained constant after heat treatment and resulted in only a small amount of alloy penetrating into the membrane pores. However, when palladium was

deposited first, the alloy penetrated to at least 3 μm inside the pores and the alloy composition was not homogeneous across the film thickness [81].

Guo et al. used the coating and diffusion method to prepare an 8.6 μm thick Pd-Ag/PSS membrane. The membrane was treated with Argon at 1173 K for 12 h, and the Ag content was estimated using ICP measurements at 23.1 %. They reported a H_2 permeation flux of 0.759 mol s^{-1} at 773 K (ΔP = 1.936 atm). The separation factor of hydrogen/nitrogen or argon was close to infinity [7].

To produce homogeneous Pd-Ag alloy membranes, high temperatures have to be used. However, the temperature must be limited to avoid inter-metallic diffusion of elements from for example, in PSS support to the membrane layer and to avoid deterioration of the pore microstructure in glass supports.

An alternative alloy formation method involves the co-deposition of two metals from the same plating bath simultaneously. An obvious advantage of using this technique is that lower temperatures can be used to anneal submicron Pd-Ag particles to form a homogeneous layer.

Table 2-1 Pd Membranes

Reference	Plating method	Support	Film thickness (μm)	H_2 flux ($mol.m^{-2}\ s^{-1}$)	H_2/N_2 selectivity	n value	E_A (kJ/mol)	Operating conditions
Uemiya et al. [82]	ELP	porous glass tube with 0.3 um pores	13	0.378	-	-	10	773 K ΔP = 1.7 bar
Uemiya et al. [22]	ELP	Al_2O_3 tube with a thin layer containing mean pore size of 0.2 um	4.5	0.326	infinite	0.5	-	673 K ΔP = 0.7 bar
Li et al. [83]	ELP & osmosis	α-Al_2O_3 tube with sol gel layer containing 0.16 um pores	10	0.477	infinite	0.65	12.3	793 K ΔP = 1.7 bar
Pan et al. [84]	ELP	α-Al_2O_3 hollow fibre with sol gel layer containing 5.7nm pores	~2-3	0.204	~1000	1	14.6	693 K ΔP = 2 bar
Sun et al. [78]	ELP	α-Al_2O_3 hollow fibre containing 0.2 um pores	1.5	0.237	3115	1	13.3	723 K ΔP = 1 bar
Nair et al. [85]	ELP	3-5 um gamma-Al_2O_3 (5-20 nm pores) coated from boehmite sol on α-Al_2O_3 hollow fibre with 0.15 um pores	5	0.190	700	0.5	-	730 K ΔP = 1.8 bar
Tong et al. [86]	ELP & polymer	α-Al_2O_3 hollow fibre with 0.15 um pores coated with Pd acetate, PPO and Chlorofoam	5	0.333	infinite [b]	-	-	773 K ΔP = 1 bar

ELP electroless plating

subscript b H_2/He

Table 2-2 Pd-Ag Composite Membranes

Reference	Alloy content (wt. %)	Plating method	Support	Film thickness (μm)	Annealing conditions	H_2 flux ($mol.m^{-2} s^{-1}$)	H_2/N_2 selectivity	n value	E_A (kJ/mol)	Operating conditions
Kikuchi et al. [87]	Pd_{77}-Ag_{23}	ELP (coat & diff)	α-Al_2O_3 tube with sol gel layer containing 200 nm pores	~5.8	1173 K, 12 h	0.473	infinite	0.5	7	673 K ΔP = 1.94 atm
Guo et al. [7]	$Pd_{76.9}$-$Ag_{23.1}$	ELP (coat & diff)	α-Al_2O_3 tube with sol gel layer containing 150 nm pores	8.6	1173 K, 12 h	0.759	infinite	0.5	8.216	773 K ΔP = 1.936 atm
Hou et al. [88]	Pd-Ag	ELP (coat & diff)	α-Al_2O_3 tube with sol gel layer containing 90 nm pores	~5.5	873 K, 12 h	0.180	>2000	0.614	9.8	623 K ΔP = 2 bar
Tanaka et al. [89]	Pd_{85}-Ag_{15}	ELP (co-deposition)	α-Al_2O_3 tube containing 150 nm pores	~4-5	773, 4 h	0.45	528	0.7	16	573 K ΔP = 2 bar
Tong et al. [90]	Pd_{80}-Ag_{20}	ELP (co-deposition)	asymmetric PSS tube	2	773, 4 h	~0.15	infinite	1	25.5	573 K ΔP = 1 bar
Pizzi et al. [91]	Pd_{80}-Ag_{20}	ELP (coat & diff)	α-Al_2O_3 tube containing 100 nm pores	2.5	-	0.20	infinite	0.5	17	573 K ΔP = 0.4 bar

ELP electroless plating
PSS porous stainless steel
coat&diff coating and diffusion method

2.3.3.2 Co-deposition method

In electroless co-deposition, both palladium and silver metal constituents are contained in the starting plating solution used to deposit the metal alloy on the support. Consequently, the deposition rate is influenced by a range of factors that include the total amount of metals, silver content, hydrazine concentration, temperature of the plating bath and the substrate roughness and quality. Differences in the plating dynamics of the two metals and the stability of the plating bath can hinder the formation of uniform defect-free dense alloy membranes.

Shu et al. annealed a co-deposited Pd-Ag film for 150 min at 673 K and compared it to a sequentially deposited Pd-Ag film annealed for 5 h at 823 K. Their results showed Pd deposition is inhibited to an extent by Ag in the plating bath. The Pd deposits was slightly improved by pre-deposition on the substrate followed by drying for 3 h at 393 K prior to introducing the silver precursor into the plating bath [11].

Cheng and Yeung studied the kinetics of Pd-Ag co-deposition on Vycor tubes from a mixed electroless plating bath. They showed that plating baths with higher hydrazine to metal ratios and at higher temperatures yielded membranes with higher Pd concentrations. The highest plating rate was achieved when the initial plating rate of Pd was 2-3 times higher than Ag. When a Pd (87.5%)/Ag (12.5%) membrane was compared to a pure palladium membrane, it produced a H_2 flux about 1.4-1.7 times higher and formed a single phase alloy after annealing at 773 K for 8 h [70].

Tanaka et al. prepared thin and homogeneous Pd-Ag membranes on porous alumina tubes using an optimised activation method that involved seeding Pd nano-

particles followed by co-deposition by an electroless plating method. By removing Sn completely from the activation step, problems such as loss of catalytic activity and inhibition of hydrogen sorption activity caused by Sn colloidal particles shielding activated palladium nuclei on the substrate are eliminated. After simultaneous deposition, alloying of palladium and silver was achieved after heat treatment at 773 K for 4 h under an H_2 atmosphere, due to interdiffusion of the two metals. The highest hydrogen permeance achieved was 2.13 x 10^{-3} mol m^{-2} s^{-1} $Pa^{-0.5}$ with a hydrogen/nitrogen separation factor of 528 at 573 K at a transmembrane pressure of 100 kPa [89].

2.4 MEMBRANE APPLICATIONS

2.4.1 Palladium Membrane Reactors

Membrane reactors combine two distinctly different functions, i.e. reaction and separation, into a single unit. By integrating catalytic and separation functions, chemical processes are simplified and the number of units is reduced, which leads to savings in both capital and operating costs. Other advantages of membrane reactors relate to the synergy between reaction and separation that can be achieved. This synergy is obvious in thermodynamic equilibrium limited reactions, for example, the membrane can promote the reaction by selectively removing one product from the reaction zone through the membrane and thus shift equilibrium towards the product side. Furthermore, membrane reactors can control the supply of reactant to the reaction zone to optimise the concentration ratio of the reactant stream. As a result, product yields and selectivity can be improved by suppressing undesired reactions and the formation of by-product(s). The two main functions of a membrane reactor are illustrated in Figure 2-12.

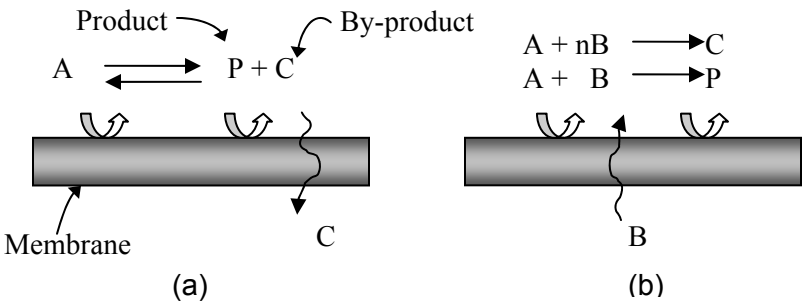


Figure 2-12 Principle of membrane reactors to promote reactions; (a) selective permeation of by-products of an equilibrium-limited reaction and (b) dosing a reactant through the membrane

Palladium-based membrane reactors have been mainly used for equilibrium-limited dehydrogenation reactions. The role of the membrane is to selectively remove the hydrogen product efficiently from the reaction zone and shift the reaction equilibrium to the product side. By removing hydrogen, higher yields can be realised at much lower temperatures whilst reducing or eliminating side reactions and catalyst deactivation [21].

2.4.1.1 Membrane reactor configurations

Several membrane reactor configurations have been proposed over the last few decades, but they are all generally classified according to the function of the membrane and catalyst as shown in Table 2-3 and Figure 2-13 [34]. The most commonly referred to reactor is the packed bed membrane reactor (PBMR), in which the reaction function is provided by a packed bed of catalyst in contact with the membrane and the membrane itself is inert and only provides a separation function. A fluidized bed membrane reactor (FBMR) configuration is similar to PBMR but the packed bed is replaced by a fluidised bed. FBMRs are useful to better control the reaction temperatures, however, they have yet to gain widespread acceptance. In a catalytic membrane reactor (CMR) configuration, the membrane is catalytic and provides both the separation and the

reaction function although this concept has found wider acceptance in the bioreactor field than in the chemical industry. A catalytic non-permselective membrane reactor (CNMR) is similar to a CMR but the membrane is not permselective and only provides a reactive interface. Finally, a packed bed catalytic membrane reactor (PBCMR) and fluidized bed catalytic membrane reactor (FBCMR) both use a catalytic bed and a permselective membrane. This configuration is ideal for situations where a bi-functional catalytic function is desirable. Other reactor configurations and concepts also exist, such as hybrid concepts, where the membrane reactor is used as an add-on stage to an already existing conventional reactor. This particular configuration has a number of attractive features, especially for applications involving conventional type porous membranes, which are characterized by moderate (Knudsen-type) permselective properties [34].

Table 2-3 Classification of Membrane reactors

Acronym	Description
CMR	Catalytic membrane reactors
CNMR	Catalytic non-permselective membrane reactors
PBMR	Packed bed membrane reactors
PBCMR	Packed bed catalytic membrane reactors
FBMR	Fluidized bed membrane reactors
FBCMR	Fluidized bed catalytic membrane reactors

In catalytic membrane reactors the coupling of the membrane with the catalysts can be achieved in several ways, as illustrated in Figure 2-13 [1]; a.) The membrane can be coupled with catalyst pellets packed on the surface of the membrane, b.) The membrane itself is inherently catalytic and coupled with catalyst pellets, and c.) The catalyst is impregnated (superficially catalytic) into the pores of a microporous material either as individual particles or as a layer. This design benefits from mass and/or heat

transfer improvements and the catalyst can be ten times more active than when in pellet form [92]. The following section focuses on superficially catalytic membrane reactors.

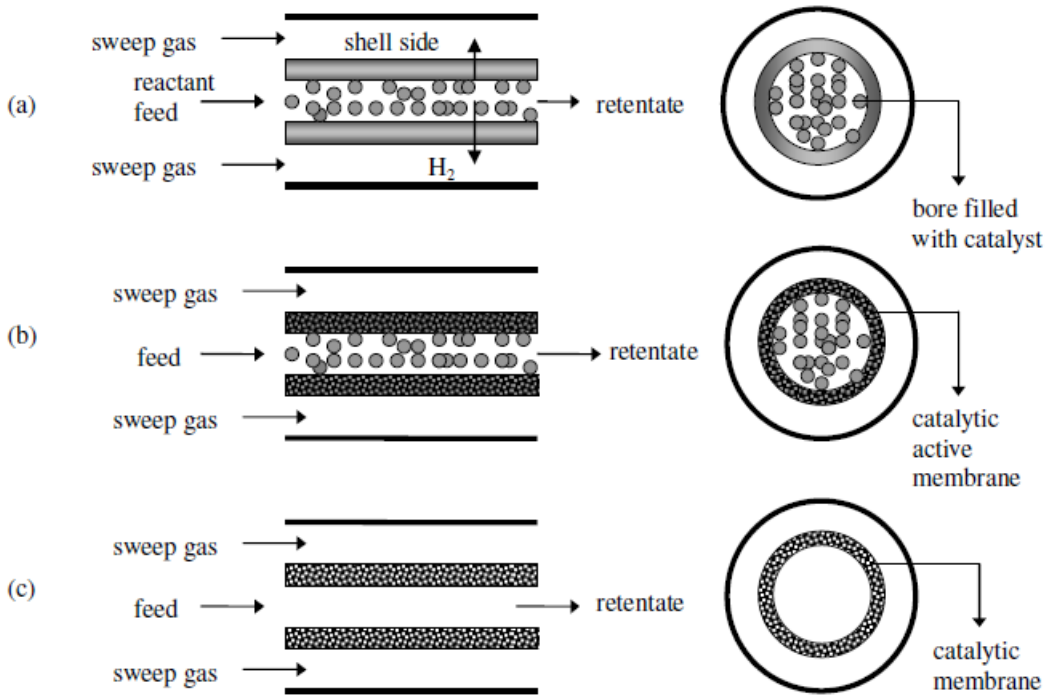


Figure 2-13 Different membrane reactor concepts for a tubular configuration: (a) PBMR, FBMR (b) PBCMR, FBCMR and (c) CMR, CNMR

2.4.1.2 Catalyst deposition techniques

Gonzalez et al. [93] and Meille [94] have attempted to review the myriad of techniques used to deposit catalysts onto structured surfaces or within the pores of porous membranes in order to achieve high catalyst specific surface areas. It is obvious from the literature that the deposition method used depends very much on the surface properties of the substrate and on the type of catalyst deposited. Some of the most commonly used methods to disperse catalysts onto mesoporous supports are as follows:

2.4.1.2.1 Deposition-precipitation method

The deposition-precipitation method involves impregnating the porous support with a solution containing the catalyst metal precursor and a suitable precipitating agent. After the reaction, metal oxide precursors precipitate out of solution and undergo decomposition by drying and subsequent thermal treatment to form the active catalyst metal.

Zhao et al. deposited nickel onto α-Al_2O_3 filter supports using a deposition-precipitation method with nickel nitrate as a precursor and urea as the precipitating agent. Alumina disks were evacuated in a sealed vessel to remove any air that could lead to poor wetting of the support and then the impregnation solution was sucked into the vessel. The disks were then dried to complete hydrolysis of urea in the pores of the disks and were calcined at 723 K for 4 h to decompose precipitated nickel oxide precursors. SEM and X-ray mapping of the modified nickel supports indicated that careful control of the reaction time and the urea/nickel molar ratio is needed to attain high fixation of the nickel oxide precursors during the slow decomposition of urea. After calcination, the urea method gave a fairly uniform distribution of nickel precursor throughout the support [95].

Belochapkine et al. also used a coating method based on deposition-precipitation of aluminium hydroxide from aluminate solutions to deposit a γ-alumina catalyst support layer in a glass microreactor [96]. The catalytic coating prepared demonstrated good adhesion, suitable for liquid/gas applications, and good compatibility with the complex microreactor geometry. Furthermore, the phase composition and specific surface area of the coating were very similar to a conventional powdered γ-alumina catalyst support.

2.4.1.2.2 Impregnation method

The impregnation method is the simplest and most commonly used method to deposit catalyst supports/layers inside the pores of membranes. Usually, the support is immersed in a solution containing the metal precursor, dried and then heated to obtain a dispersed layer on the support material.

There are two types of impregnation techniques: wet impregnation and incipient wetness impregnation. Yeong et al. utilised both types to deposit palladium catalysts in the microstructure of a falling film reactor (FFR) for application in the hydrogenation of nitrobenzene to aniline. For wet impregnation, a γ-Al_2O_3 layer was deposited on a stainless steel support using an aqueous solution containing γ-Al_2O_3 particles with binder and acid. Excess suspension was removed from the surface and the support was calcined at 973 K for 2 h. Platinum was then deposited onto a γ-Al_2O_3 layer using a solution of palladium (II) acetate for 2 h, after which excess solution was removed from the surface and the support was left to dry in air for 2 h. The support was heated to remove moisture, calcined at 673 K for 3 h and finally rinsed with distilled water and ethanol. For the incipient wetness impregnation case, a γ-Al_2O_3 layer was deposited as above but the catalyst precursor solution was left to dry in a fume cupboard before being calcined at 673 K for 3 h and rinsed with distilled water and ethanol [97].

Vralstad et al. employed the incipient wetness impregnation technique for cobalt functionalization of mesoporous silica supports [98]. MCM-48 and MCM-41 were impregnated with an aqueous solution of $Co(NO_3)_2.6H_2O$ followed by drying at 373 K for 3 h and calcination in flowing air at 573 K for 16 h. The ICP method provided a high

dispersion of cobalt oxide particles whilst maintaining the mesoporous structure and high surface areas.

Pina et al. used an impregnation technique to deposit platinum on a γ-Al_2O_3 support layer to fabricate a Pt/γ-Al_2O_3 catalytic membrane for application in the combustion of volatile organic compounds [99]. A γ-Al_2O_3 phase was deposited on top of an α-Al_2O_3 support by means of successive cycles, each involving vacuum filtration of 1 M boehmite sol, followed by drying and calcination at 773 K. Platinum catalyst was introduced to the γ-Al_2O_3 phase by wet impregnation with chloroplatinic acid, followed by drying and calcination steps.

Perez et al. deposited platinum on a ceramic porous multilayered membrane by immersing the membrane in a solution of chloroplatinic acid for 4 h [100]. The membrane was then washed with nitric acid, dried under nitrogen at 373 K for 1 h and sintered to decompose the impregnated platinum precursor. SEM and TEM characterisation confirmed platinum crystallites were successfully loaded inside the mesoporous layer.

2.4.1.2.3 Sol-gel method

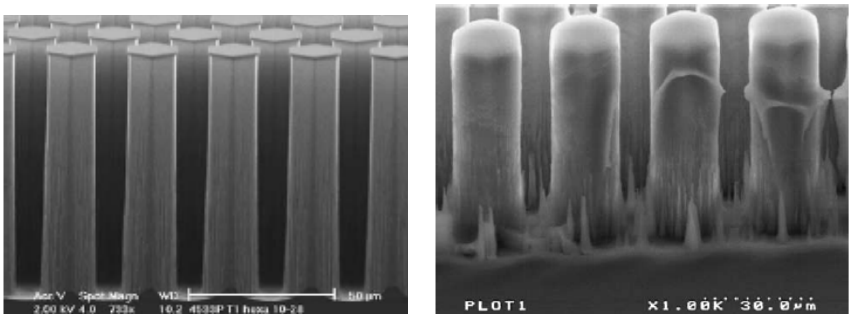
Sol-gel deposition has been used by a large number of groups to coat γ-Al_2O_3 membranes on α-Al_2O_3 substrates. It involves mixing metal-organic precursors with metal precursors to form a homogeneous solution. The metal-organic precursor is hydrolyzed by the addition of water while carefully controlling the pH and the reaction temperature. As hydrolysis and polymerization occur, colloidal particles or micelles with an approximate diameter of 10 nm are formed. These particles continue to grow and until a metal oxide gel is formed. The solvent is eventually removed by heat treatment in air [93] [101].

Saracco et al. carried out studies on sol-gel derived porous catalytic filters for applications in catalytic abatement of gaseous pollutants, such as NOx, VOCs etc. [102]. Catalytic filters were prepared by depositing γ-Al_2O_3 layers on the pore walls of highly resistant α-Al_2O_3 porous candles using vacuum assisted impregnation of the starting sol. The catalytic activity of the modified filters was characterized directly using isopropanol dehydration as a model reaction (catalyzed by the acidity of γ-Al_2O_3 itself without the need for further activation with metal precursors) to simulate the suitability of the filter to abate pollutants. A 95 % conversion was easily achieved at industrially relevant superficial velocities of 10^{-2} Nm^3 m^{-2} s^{-1}, and with acceptable pressure drop increases compared with virgin filters.

Alfonso et al. used the sol-gel process to deposit a homogeneous γ-Al_2O_3 layer containing dispersed vanadium to produce a V/γ-Al_2O_3 catalytic membrane reactor for oxidative dehydrogenation of propane. In making the sol, 2.5 g of hydrated aluminium hydroxide as pseudo-boehmite was dissolved in deionised water at 353 K. The sol was then cooled to room temperature and mixed with HNO_3 and NH_4VO_3. Polyvinyl alcohol was included in the sol to improve the rheological properties and to avoid crack formation during drying and calcination. Following this, the sol was slip cast on top of the α-Al_2O_3 support and subsequently dried and calcined to 923 K for 2 h [103].

Various microreactor technologies also involve the use of coated supports, for example. Meille et al. reported using a sol-gel method to coat γ-Al_2O_3 onto silicon micro channels, Figure 2-14 [104]. After impregnation of the oxide phase from a platinum precursor, the microreactor was used to catalyze the oxidation of carbon monoxide. The

Pt/Al_2O_3 catalyst showed a better ignition temperature (298 K) compared to a Pt-sputtered (373 K) microstructured reactor [105].



(a) (b)

Figure 2-14 (a) bare silicon micro channels with 10 μm pillars and (b) coated with γ- Al_2O_3

2.4.1.2.4 Ion exchange method

The ion exchange method involves exchanging either hydroxyl groups or protons from the support with anionic or cationic species in solution [93]. This method requires careful adjustment of the pH in order to maximise the electronic interaction between the support and the metal precursor and knowledge of the isoelectric point is essential to attain adequate dispersions.

Uzio et al. deposited platinum using an aqueous solution of hexachloroplatinic acid on a multi-layered γ-Al_2O_3/α-Al_2O_3 tubular support via the ion-exchange method [106]. The membrane was initially dipped in water and then in acidic solution (0.1 g Pt/l) with a contact time between 1 and 4 h. The support was washed twice in nitric acid solutions (pH 4), dried for 4 h and calcined at 723 K for 2 h under nitrogen gas. Finally, the platinum was then reduced to the metallic state under flowing hydrogen at 673 K for 2 h. EDX-SEM analysis showed that the platinum loadings and the concentration profiles across the membrane are related to the time of exchange due to slow diffusion of

platinum precursors from the exchange solution into the pores of the membrane. Interestingly, the catalytic performance of the membrane was very similar to a conventional catalyst prepared using a similar support in a toluene hydrogenation test. This indicated that the physico-chemical properties of the membrane did not seem to affect the catalytic properties of the supported platinum.

Capannelli et al. loaded 1.55 weight percent of vanadium on γ-Al_2O_3 to fabricate a thin V_2O_5/γ-Al_2O_3 layer on a cylindrical ceramic support via an ion exchange technique. The catalytic performance of the functionalized support was compared with γ-Al_2O_3 supported vanadium catalysts in the form of granules for oxidehydrogenation of propane to propene. A considerable enhancement in the catalytic performance was seen with the functionalized support because side reactions responsible for the decrease in selectivity seen at high temperatures in packed bed reactors were minimized [3].

2.4.1.2.5 Other methods

Other techniques used to functionalise porous supports include: chemical vapour deposition (CVD), physical vapour deposition (PVD), flame assisted vapour deposition (FAVD) [94].

CVD, which is described in section 2.3.2.3, is similar to the sol-gel method but without the need for a solvent and only the volatile precursor and substrate are present in the deposition chamber. This method has been used to deposit catalyst on powdered surfaces [107] and Al_2O_3 coatings on stainless steel micro-channels prior to impregnation with a catalyst metal precursor [108]. The PVD method which is also described in section 2.3.2.2, includes mechanical methods (cathodic sputtering) and thermal methods (evaporation and electron-beam evaporation) that are used for catalyst

deposition on structured surfaces [97]. FAVD deposition takes place in an open atmosphere without the complex deposition chamber and/or vacuum system used in PVD or CVD. In this method, the atomised chemical precursor of the catalyst is burned in a flame and the substrate is placed in the combustion zone at a controlled distance and temperature [109].

2.4.2 Catalytic Membrane Reaction Processes

The following sections outline some of the applications of inorganic membrane reactors in chemical reactions. In particular, the focus is on dehydrogenation and water-gas shift reactions.

2.4.2.1 Dehydrogenation Reaction

Dehydrogenation of hydrocarbons to produce hydrogen is a key process in the modern petrochemical industry. As most dehydrogenation reactions are endothermic and as such are limited at low temperatures, the employment of a membrane reactor to selectively separate hydrogen from the reaction mixture can greatly increase the conversion and enable the reactor to operate at lower temperatures. Some of these reactions are reviewed in Table 2-4.

From the literature, the most commonly used membrane reactor configuration is the shell-and-tube arrangement. In this scheme, platinum-based catalysts are usually packed either in the annulus between the membrane and module casing (shell side) or inside the lumen of tubular membranes (tube side) in order to maximize the surface contact between the reactants and the catalyst. Furthermore, this catalyst/membrane

arrangement corresponds to the packed bed membrane reactor (PBMR) type, where the membrane is itself not active and the reaction function is carried out by catalysts placed in the reactor. The main advantage of this system is its simplicity in design and in case of catalyst poisoning, a new catalyst can easily be introduced.

2.4.2.2 Water-Gas Shift (WGS) Reaction

The water-gas shift reaction is one of the important routes for the industrial production of CO-free hydrogen from light hydrocarbons. In the reaction, carbon monoxide is reacted with excess steam to form carbon dioxide and hydrogen (17). Because the reaction is mildly exothermic and reversible, a higher temperature leads to a higher rate of reaction but at the expense of a lower final equilibrium conversion.

$$CO + H_2O \leftrightarrow CO_2 + H_2 \qquad \Delta H_{298} = -41.1 \text{ kJ/mol.} \qquad (17)$$

To overcome the thermodynamic limitations at high temperatures, the reaction is carried out in two stages: a high temperature (HT) stage operated between 593-723 K using ferrochrome catalysts and a low temperature (LT) stage operated between 473-523 K using copper-zinc based catalysts with cooling in between stages. By operating an HT catalyst at higher temperatures, favourable kinetics can be exploited, and the volume of catalyst can be minimised. At the same time, by cooling the syngas between HT and LT stages, an active catalyst can take advantage of the thermodynamic equilibrium at low temperatures [110].

The application of palladium or palladium alloy membranes combines the WGS reaction with removal of hydrogen through a permselective membrane. Therefore, the

equilibrium can be shifted towards product formation. In comparison to the two-stage conventional reactors, palladium-based membrane reactors offer several advantages: 1.) The continuous removal of hydrogen allows CO conversion to exceed the thermodynamic equilibrium limit. 2.) The reaction can be carried out in a single step and feed pressure has a positive effect on CO conversion when H_2 is removed and 3.) the reaction can be carried out at high temperature and high pressure, which benefits both the reaction and membrane permeation kinetics.

Over the last decade, several successful studies have been reported on the use of Pd based membranes for WGS reactions, including; Uemiya et al. [111], Basile et al. [112], Xue et al. [113], Cruscuoli et al. [114, 115] and Tosti et al. [116]. Most of the studies typically used a tube-in-shell configuration with WGS catalysts packed inside the membrane or within the annular spacing between the membrane and module casing, where sweep gas is injected. Sweep gas has often been used to promote hydrogen permeation in previous experiments, although recently, Barbieri et al. and Brunetti at al. [117, 118] reported CO conversion exceeding 90 % at 573 K and 600 kPa using a Pd-alloy membrane packed with $CuO/CeO_2/Al_2O_3$ catalysts with no sweep gas.

In parallel to membrane development, significant effort has been invested into finding highly active and stable catalysts to carry out WGS reactions. Commercial low temperature $Cu/ZnO/Al_2O_3$ catalysts are sensitive to temperature excursions above 573 K and are not suitable for application at the higher temperatures needed in membrane reactors. In addition, robust high temperature ferrochrome catalysts are not active enough to fully realise the potential of WGS membrane reactors. A recent trend has been the shift to using noble metal catalysts supported on CeO_2 and Ce-Zr mixed oxides

that exhibit high-temperature kinetics compared to conventional ferrochrome catalysts and are not inhibited by CO_2 [119, 120].

In this work, palladium membrane reactors based on hollow fibre alumina asymmetric support coated with a thin and dense palladium layer is fabricated for the WGS reaction. The support will be functionalised by depositing both ceria and a silica (SBA-15) based catalyst support to maximise the catalytically active area, which is beneficial in catalytic membrane reactors. The support is then impregnated with a catalyst and coated with a thin permselective Pd layer using electroless plating. This compact multifunctional reactor will possess high surface area to volume ratios which are beneficial for WGS reactions and will demonstrate a novel way to integrate catalytic and separation technologies for membrane based reaction separation processes.

2.4.2.3 Economic Feasibility of Pd-based Membrane Reactors

The deployment of palladium-based membrane reactors on an industrial scale depends largely on the price of the palladium material [121]. If membrane systems are to compete with traditional systems, a number of other issues also have to be addressed; the membrane itself would have to be thin (< 20 μm) and dense, the membrane and catalyst must be stable under high temperatures and pressures, and in harsh chemical environments for a number of years.

In addition to the development of membranes, the process economics is dependent on the design of the whole membrane system (i.e. module and integration) [121]. The module design determines the mass transfer efficiency and pressure drop inside the membrane reactor. For example, the fluid dynamics in the reaction zone must

permit both the required permeation rate through the membrane and the required residence time of the reactants inside the module. Furthermore, low partial pressures at the permeate side must be ensured to control pressure drop, which affects energy usage. With regard to energy consumption, the membrane area can be reduced or increased depending on whether a high conversion, a high hydrogen recovery or both are desired. A large membrane area is necessary to attain high conversions and high recovery rates, however, for lower yields, lower membrane areas are suitable albeit at the expense of further downstream processing of the retentate.

Only a few studies focusing on commercialization of membrane reactors are available in the literature. Recently, Moparthi et al. carried out a feasibility study of silica and palladium membrane reactors for two dehydrogenation reactions: ethyl benzene to styrene and propane to propene [122]. They used a conceptual design based methodology that accounted for non-linear and combinatorial trade-offs between reaction zone volume, membrane area and other operating parameters (thickness, pressures, sweep gas flow rates etc). In their study, the propene production scheme was evaluated to provide between 60-70 % excess profits using a membrane reactor compared to a conventional reactor, although there was no difference in gross profit profiles for the styrene production case. They concluded that the use of membrane reactors for the reactions in their study is only feasible when the cost contribution of the membrane together with other auxiliary equipment does not exceed more than 20 % of the total costs. However, their model did not account for catalyst deactivation, which also influences the process and profitability.

Criscuoli et al., also carried out a comparison of a conventional two-stage reactor plus separator with a palladium-based membrane reactor for the water-gas shift reaction

[115]. The results showed that membrane systems bring about a reduction in the amount and volume of catalyst used in the reaction although the high cost of palladium means it is not cost effective compared to conventional reactors. They concluded that the manufacture of a defect free palladium membrane with a thickness of 20 μm or less is required to make the membrane systems competitive.

In terms of membrane system kinetics, better control of the interactions between the catalyst and membrane, and the influence of the membrane on the reaction kinetics is needed to enhance the viability of catalytic membrane reactors. This is important because the catalyst behaviour has been shown to vary under different reaction conditions, for example when adding or removing species through the membrane [123], and kinetic expressions also differ between conventional and membrane reactor systems [114].

Table 2-4 Dehydrogenation in Palladium-based Membrane Reactors

Reaction	Membrane / configuration	Reaction Conditions		Conclusions	References
		Temp (K)	Catalyst		
Dehydrogenation of ethane	Pd-Ag/Vycor tubes PBMR	660	3 mm pellets 0.5 % Pt/Al_2O_3 catalysts placed in membrane lumen	Under optimal conditions, an 8-fold increase in conversion was achieved with the membrane reactor compared to equilibrium. There was a good agreement between experimental data and simulation when pure N_2 was used as sweep gas but not with air, possibly due to oxidation of the Pd surface.	Gobina & Hughes [20]
Dehydrogenation of n-butane	Pd/Al_2O_3, tubular membrane PBMR	670	2.55 g 0.5% Pd/Al_2O_3 cylindrical catalyst pellets packed in the membrane lumen	Conversion increased 4 and 6 fold when CO and O_2 were used as sweep gas respectively in comparison to the equilibrium value.	Gobina & Hughes [6]
Dehydrogenation of propane	Pd-Ag/Vycor tubes PBMR	673-848	2.55 g 0.5% Pt/Al_2O_3 cylindrical catalyst pellets packed in the membrane lumen	Four-fold improvement on C_3H_8 conversion at 673 K. Use of reactive sweep gas significantly increased conversion.	Yildrim [12]
	Pd/silica/γ-Al_2O_3 CMR		0.5% Pt/Al_2O_3 cylindrical catalyst dispersed within pores of the membrane tube	No conversions at low temperatures. At higher temp of 843 K, C_3H_8 conversion was 47 % compared to the equilibrium value of 40 %.	

	Pd/silica/γ-Al_2O_3 PBCMR		similar to arrangement above plus 0.5 % Pt/Al_2O_3 cylindrical catalyst pellets packed tube side	At low temperatures of 708 - 738 K, conversion increased by two-fold compared to CMR case.	
Dehydrogenation of propane	Pd/Al_2O_3, tubular membrane PBMR	833	7.0 g of commercial catalyst packed on shell side	Membrane reactor achieved higher propane conversion of 35.4 % and propene yield of 26.1% compared to 29.0 % and 22.2 % in a packed bed reactor, respectively.	Quicker [10]
	Pd/PSS tubular membrane PBMR			Higher conversion of 39.0 % achieved compared to Pd/alumina due to higher hydrogen removal rate.	
Dehydrogenation of propane	Pd/γ-Al_2O_3 tubular membrane PBMR	773	1 g Pt/K/Sn/Al_2O_3 cylindrical catalyst pellets packed tube side	C_3H_8 conversion was 52 % compared to 28 % at equilibrium level. High hydrogen permselectivity was confirmed as a key factor in terms of conversion and selectivity.	Jong-San Chang et al. [124]

Dehydrogenation of isobutane	Pd-Ag/α-Al_2O_3 tubular membrane PBMR	623-773	4 mm of Cr_2O_3-Al_2O_3 catalyst packed shell side	Conversion of isobutane (50.5% at 723 K) in the membrane reactor compared to equilibrium of 18 % and a fixed bed reactor of 15.5 %. Partial pressure of H_2 in reaction zone critical to delaying catalyst deactivation and carbon formation	Guo et al. [7]
Dehydrogenation of isobutane	Pd-Ag/PSS tubular membrane PBMR	723-793	3 mm pellets 0.5 % Pt/Al_2O_3 catalysts placed inside membrane lumen	Isobutane/H_2 feed ratio of 4:1 was needed to surpress catalyst deactivation. Higher yields and selectivity to isobutene attained in the membrane reactor. 10-fold increase in sweep gas flow, increased conversion to 45-55 %	Liang and Hughes [125]
Dehydrogenation of cyclohexane	Pd/α-Al_2O_3 tubular Micro reactor	573	-	Integration of stainless steel rods inside the membrane increased the surface area per vol. of Pd membrane. This increased catalytic reaction and doubled the benzene yield.	Yamamato [126]
Dehydrogenation of cis-3-hexen-1-ol	Pd-Ag/SS PBMR	443-503	1 g of CuO-ZnO packed on the shell side	Selectivity of cis-3-hexenal was significantly enhanced with membrane reactor and increased with temperature.	Sato [127]
Dehydrogenation of propane	Pd/Al_2O_3 hollow fibre in a two-zone fluidized bed reactor TZFBR	773-823	15 g of Pt-Sn/Al_2O_3 packed on shell side	MR effectively removed H_2 produced in the reaction and achieved stable state. However, yields were low due to catalyst deactivation and coke formation.	Gimeno [128]

CHAPTER 3

Fabrication of Composite Pd/Alumina Asymmetric Hollow Fibre Membranes: A New Approach to Compact Multifunctional Membrane Reactors

Abstract

This chapter describes the fabrication of thin Pd membranes on porous asymmetric alumina hollow fibre supports prepared via a combined phase inversion and sintering technique. A spinning suspension (dope) containing well dispersed Al_2O_3 particles (1μm, 0.05 μm and 0.01 μm), Arlacel P135, Polyethersulfone (PESf) and N-methyl-2-pyrrolidone (NMP) as ceramic membrane material, dispersant, polymer binder and solvent respectively is prepared to fabricate a hollow fibre precursor, which is then sintered at elevated temperatures. The prepared support shows an asymmetric morphology characterised by a porous inner surface from which finger-like voids extend across approximately 80 % of the fibre cross section with the remaining 20 % consisting of a denser sponge-like outer region where the gas permeation behaviour is mainly determined by Knudsen diffusion. A thin palladium membrane is directly coated onto the outer surface of the asymmetric support without the need for any pre- or post-treatment, to form a fully dense composite membrane. Finger-like macro voids formed in asymmetric membrane supports of this type could be used as a matrix for catalyst deposition, forming a functional support for the development of compact multifunctional catalytic membrane reactors, which will be discussed in the following chapters.

3.1 Introduction

Due to the increasing world-wide demand for high purity hydrogen [129, 130], Pd-based membranes have attracted considerable attention as an effective way for separating H_2 from mixtures with the advantages of high permeability and selectivity [18, 38, 131]. In the last several decades, a lot of research work on Pd and Pd alloy membrane technology has been focused on coating thin membranes (usually 2-10 μm) onto flat discs or tubular porous substrates. In this way sufficient mechanical strength can be achieved with less material costs without compromising on permselectivity [38, 131]. However, the surface area/volume ratio of the membrane configurations mentioned above is very limited (around 30 and 250 m^2/m^3 for flat sheet and tube type substrates, respectively [25]. Owing to the fast development of membrane technology, porous ceramic hollow fibres with stable thermal and chemical properties have been successfully achieved [1, 14]. These fibres are suitable as substrates for Pd-based membranes due to their smaller diameters and thinner wall thickness. When made into a bundle, the advantage of a high area/volume ratio (as high as 3000 m^2/m^3 [1, 19, 84]) makes these fibres extremely attractive for industrial processes.

More recent work on coating thin Pd and Pd alloy membranes onto ceramic hollow fibre substrates with symmetric pore structures for hydrogen separation has been carried out by various researchers. Due to the importance of the substrate's surface properties in determining the microstructure and performance of Pd separation layer, coating of γ-Al_2O_3 intermediate layers (several microns in thickness, pore size of about 5-10 nm) as a multi-step surface modification was always considered to be necessary [18, 19, 85, 132]. Although Tong et al. [86] developed a novel combined organic and

inorganic process for coating a uniform Pd membrane onto porous Al_2O_3 hollow fibres (o.d. 2.9 mm, id 2.2mm, pore size 150 nm) without any intermediate layers, multi-step post-treatment was still needed to obtain a defect-free Pd separation layer. Another way to improve the surface properties as well as mechanical strength of hollow fibre substrates was to use fine α-Al_2O_3 particles (about 0.2 μm) in the preparation of symmetric hollow fibre membranes [78]. While direct Pd plating can be achieved in this way, resistance for gas transport in the substrate was obviously increased at the same time.

Li and Tan et al. [1, 14] were one of the first groups to develop a combined phase inversion/sintering process for producing ceramic hollow fibres with an asymmetric pore structure. Due to different polymer precipitation rates, ceramic hollow fibres fabricated in this way possess finger-like voids near the inner and outer walls with a sponge-like layer in the middle. Rapid precipitation occurring at the outer layer leads to the formation of a thin and denser skin layer, as has been explained by the authors. This skin layer can be considered as a kind of surface modified layer for electroless plating processes and Pd-based membranes can be directly coated onto such hollow fibres without any further pre- or post-treatment. This eliminates the need for a γ-Al_2O_3 intermediate layer, which reduces costs because no extra coating and calcination steps are required.

Further experimental work on the formation of these asymmetric structures was recently carried out by Kingsbury and Li [16]. They showed that by varying operating parameters such as air-gap and the viscosity of the spinning suspension (dope) using water as a non-solvent additive, the formation of finger-like voids can be systematically tuned to extend from the inner surface alone and extend across the hollow fibre with an

outer sponge-like region. The finger-like void region could be extended from 0 % of the fibre thickness (i.e. symmetric sponge-like membrane structure) to approximately 80 % or above of the fibre cross section. In contrast to the outer layer, finger-like voids in the inner substrate can act as a matrix for catalyst deposition and by depositing a separation layer onto such fibres a compact multi-functional membrane reactor can be realised. In addition, by integrating catalysts in the membrane substrate instead of using of a packed bed type configuration, a great reduction in reactor volume can also be realized.

In this chapter, Al_2O_3 hollow fibres with such asymmetric pore structures are prepared and directly utilized as substrates for coating Pd membranes without any pre- or post-treatments. The performance of the resultant Pd/Al_2O_3 hollow fibre composite membrane is correlated with the membrane microstructure and operating conditions. Palladium-based composite membranes described here are assessed for their suitability for use in multifunctional membrane reactors (MR). MR studies utilizing these membrane supports are presented in the chapters 4-6.

3.2 Experimental

3.2.1 Materials

Al_2O_3 1 μm (alpha, 99.9 % metals basis, S.A. 6-8 m^2/g), 0.05 μm (gamma-alpha, 99.5 % metals basis, S.A. 32-40 m^2/g) and 0.01 μm (gamma-alpha, 99.98 % metals basis, S.A. 100 m^2/g) from Alfa Aesar (Johnson Matthey company) were used as supplied. Polyethersulfone (Radal A300, Ameco Performance, USA), N-methyl-2-pyrrolidone (HPLC grade, Rathbone) and Arlacel P135 (Polyethyleneglycol 30-dipolyhydroxystearate, Uniqema) were used as binder, solvent and additive,

respectively. Tap water and de-ionized water were used as the external and internal coagulants, respectively.

3.2.2 Fabrication of asymmetric inorganic hollow fibre membranes

In the preparing the spinning dope, the required mass of NMP was measured in a glass bottle using a Precisa 1000C-3000D mass balance. Following this, Arlacel P135 heated in an oven, added into the NMP solution. The required mass of each powder was measured and gradually added to the well mixed NMP-Arlacel P135 solution. The mixture was then milled with 20 mm agate milling balls with an approximate Al_2O_3/agate weight ratio of 2 for 48 h. After this period, PESf (6.1 wt %) was introduced into the mixture in a single measure and stirred for a further 48 h using the same ball mixer. The composition of the resulting spinning dope is outlined in Table 3-5.

The prepared spinning dope was transferred to a gas tight stainless steel reservoir and degassed under vacuum using a Welch model 2025 vacuum pump. The vacuum degree was initially set at 200 mbar for 20 min and increased to 400 mbar for a further 40 min. Degassing of the spinning dope was carried out to remove any bubbles which would cause defects in the fabricated hollow fibre precursors. Immediately after degassing, the spinning dope was pressurised to 7 psig using nitrogen gas and extruded through a tube-in-orifice spinneret (O.D./I.D. 3.0mm/1.2mm) (Figure 2-10 in page 40) to obtain hollow fibre precursors.

Table 3-5 Hollow fibre precursor spinning conditions

Spinning parameters	
Dope composition (wt %)	
Al_2O_3 (1.0 μm)	41.09
(0.05 μm)	11.74
(0.01 μm)	5.87
PESf	6.1
NMP	33.9
Arlacel	1.3
Dope temperature (K)	293
Coagulation bath temperature (K)	293
Internal coagulant temperature (K)	293
Internal coagulant flow rate (ml s^{-1})	0.17
Nitrogen pressure (psi)	7
Air gap (cm)	15

The resulting hollow fibre precursor was extruded into an external coagulation bath containing tap water. The air-gap between the spinneret and external bath was kept at 15 cm. Deionised water was employed as the internal coagulant at a flow rate of 0.17 ml/s. The resulting hollow fibre precursors were left in the coagulation bath overnight to allow the full exchange of solvent and non-solvent phases, ensuring the solidification process was complete.

Subsequently, the hollow fibre precursors were cut to lengths of approximately 40 cm and were then heated in a CARBOLITE furnace at about 873 K for 2 h to remove the organic polymer binder and were then sintered at different temperatures (1673-1823 K) with varied dwelling times (0.5-12 h) with heating and cooling rates of 5K/min to allow particle fusion and bonding to occur.

3.2.3 Fabrication of Pd/Al_2O_3 hollow fibre composite membranes

The sintered substrates (about 25 cm in length) were covered with a gas-tight glaze on the outer surface with the exception of the central part (about 5 cm in length and 2.28 cm^2 in surface area) which was left for purpose of Pd coating. Also, one end of the fibre substrate was sealed with glaze whilst keeping the other end open. The electroless plating of Pd membranes requires seeding the substrate with Pd nuclei to initiate uniform deposition [133]. This was accomplished by a conventional two-step process comprising sensitization ($SnCl_2$) and activation ($Pd(NH_4)_2Cl_4$) steps. Before Pd plating, the central unglazed part of the substrates were washed with DI water and dried at 393 K overnight. Details of the plating process and bath composition are provided in Figure 3-15 and Table 3-6.

Table 3-6 Bath compositions for Pd electroless plating

Activation bath		Plating bath	Composition
Sn activation bath		$Pd(NH_4)_2Cl_4$	4 g l^{-1}
$SnCl_2 \cdot 2H_2O$	1 g l^{-1}	$EDTA \cdot 2H_2O$	67.2 g l^{-1}
HCl (37%)	1 ml l^{-1}	$NH_3 \cdot H_2O$ (28%)	350 ml l^{-1}
Pd activation bath		N_2H_4 (0.5M solution)	10 m l^{-1}
$Pd(NH_4)_2Cl_4$	1 g l^{-1}	pH	11.2
HCl (37%)	1 ml l^{-1}	Temperature (K)	333

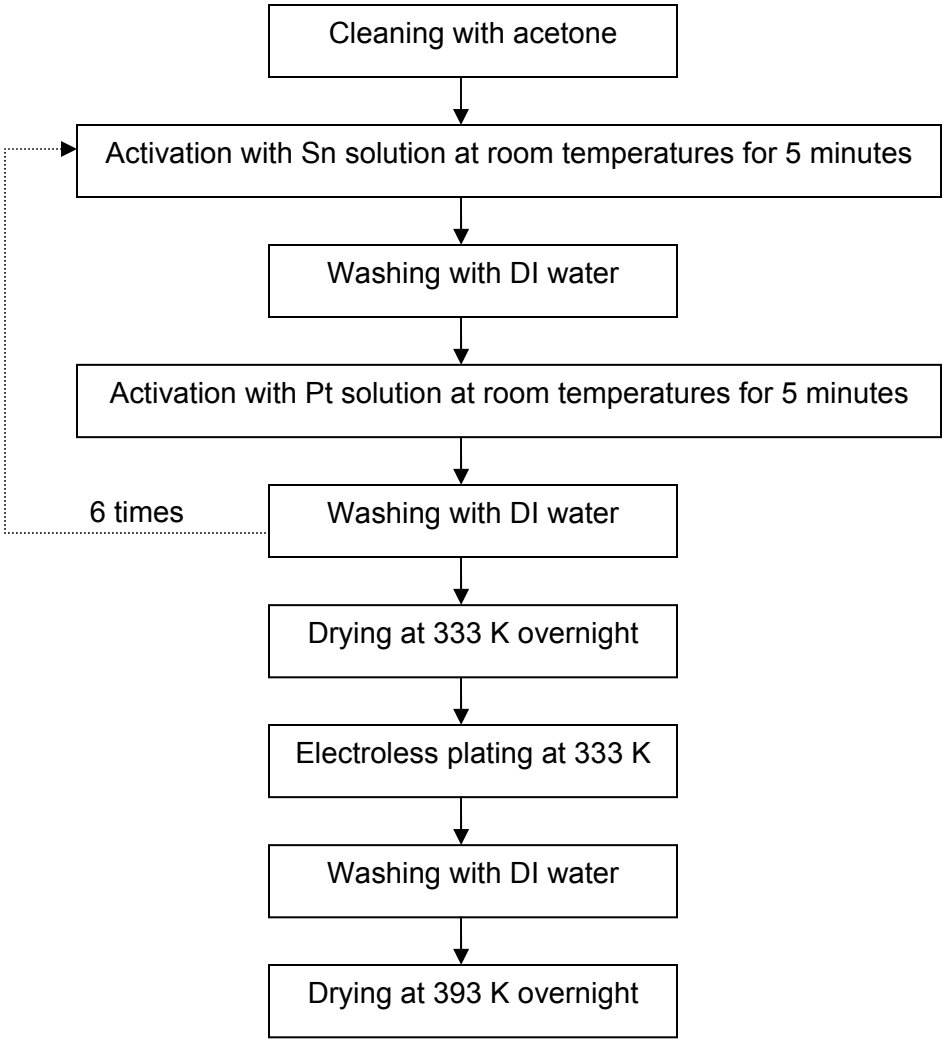


Figure 3-15 Flow chart of Pd electroless plating process

3.2.4 Membrane characterization

The morphology of the prepared hollow fibre substrates and Pd composite membranes was visually observed using a scanning electron microscope (JEOL JSM-5610LV, Tokyo, Japan). A clear cross-sectional fracture of the hollow fibre substrates was obtained by directly snapping the fibre. All the samples were positioned on a metal holder and gold coated using sputter-coating operated under vacuum. The SEM micrographs of both surface and cross section of the samples were taken at various magnifications.

Single gas (H_2 or N_2) permeation measurements of both the Al_2O_3 hollow fibre substrates as well as the Pd composite membranes were carried out using the apparatus shown schematically in Figure 3-16. The open end of the fibre was sealed into the module with quick-set epoxy resin. Feed gases of pure hydrogen or nitrogen (99.99 %) were introduced into the shell side of the module. Operating pressure was controlled by a back pressure valve and read from a KN2200 electronic pressure gauge. Pressure in the lumen was kept at atmospheric pressure and the gas permeating through the Al_2O_3 hollow fibre substrate and the Pd composite membrane was measured with bubble flow meters. The module was placed into a CARBOLITE tube furnace (total length of 15 cm), where the effective length of the constant-temperature heating zone was about 5 cm. The temperature within the furnace was controlled by a microprocessor temperature controller.

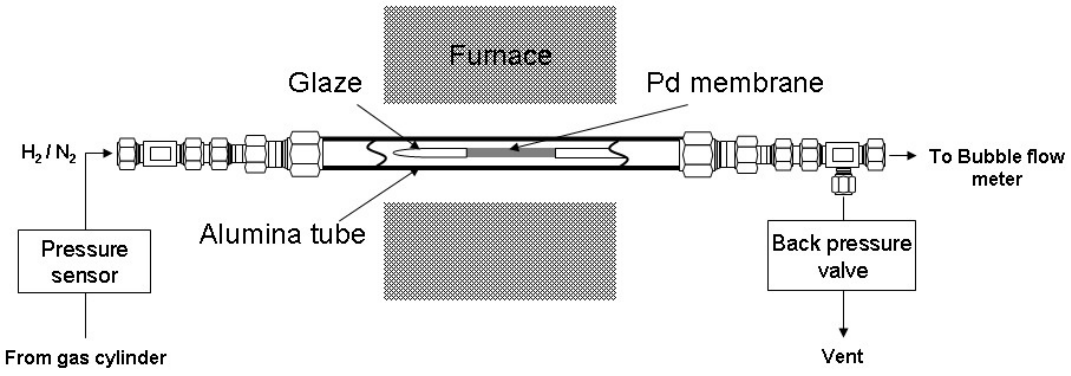


Figure 3-16 Schematic diagrams of the apparatus for single gas permeation measurements

3.3 Results and Discussion

3.3.1 Microstructure of Al_2O_3 hollow fibre substrates

As the fabrication, microstructure and performance of Pd-based composite membranes are closely dependent on the surface properties of the substrates [38], Al_2O_3 hollow fibres substrates with controlled microstructures must be obtained first. This was achieved by sintering Al_2O_3 hollow fibres at different temperatures with varied dwelling times. Based on the fact that gas permeance is governed by membrane microstructures (pore size, pore size distribution etc.) and can provide comprehensive information on porous substrates, gas permeation of nitrogen (room temperature) was chosen to characterize these hollow fibre substrates. Figure 3-17 shows nitrogen gas permeance of Al_2O_3 hollow fibre substrates after different dwelling times. Gas permeance (5-20 psi) of nitrogen decreased with the increasing of temperature and dwelling time, which resulted from the temperature induced reduction of the pore size. The obvious decrease of the gas permeance from 1723 K is due to fast fusion between Al_2O_3 particles and an apparent shrinking of the pore size. The higher the sintering temperature the shorter the dwelling time needed to achieve a “stable” gas permeance. This indicated that temperature was more effective in reducing mean pore size of Al_2O_3 hollow fibre substrates than dwelling time. As membrane reactors are preferentially operated at atmosphere pressure [1], having a small pore size/pore size distribution greatly increases resistance to gas transport. However, in order to coat thin and dense Pd membranes, as small a pore size as possible is required [38]. Based on the trade-off relationship between the requirements for reactor operation and of the substrates for the Pd membrane, Al_2O_3 hollow fibre substrates were sintered at 1723 K for about 4 h before coating with the Pd membrane.

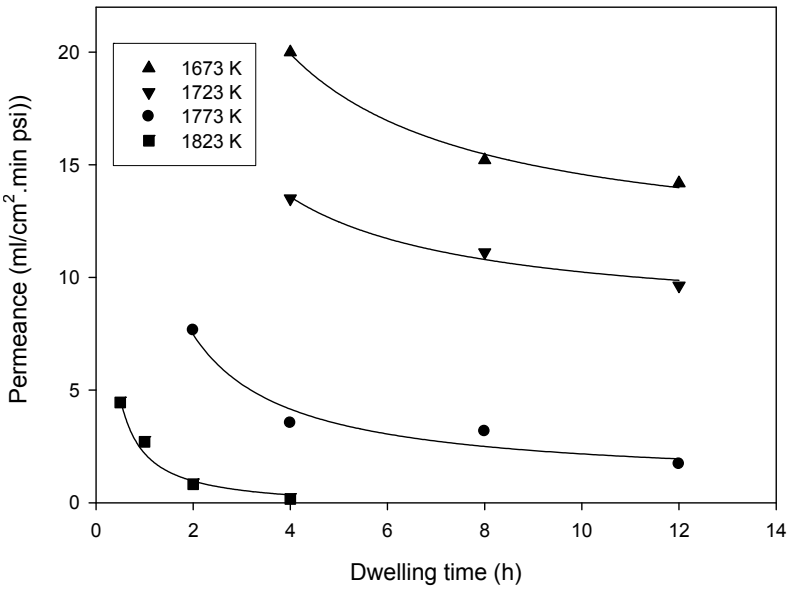


Figure 3-17 Dependence of nitrogen permeance at different temperatures on the dwelling time of Al_2O_3 hollow fibre substrates

In order to coat a thin and fully gas-tight Pd membrane, it is necessary to minimize the amount of pinholes or defects in the substrate. The integrity of Al_2O_3 hollow fibre substrates (sintered at 1723 K for about 4 h) was further characterized by H_2/N_2 gas permeation at different temperatures and transmembrane pressures, as shown in Figure 3-18. The support had an H_2 flux of 328-1168 $ml.cm^{-2}min^{-1}$ and an N_2 flux of 95-327 $ml.cm^{-2}min^{-1}$ at 723 K and at transmembrane pressures of 0.3-1.4 bar. Both H_2 and N_2 permeation fluxes through Al_2O_3 hollow fibre substrates varied linearly with increasing pressure and decreased at elevated temperatures. The separation factor (α) of H_2/N_2 at room temperature was about 3.5, which indicated that the gas transport through such substrates is very close to Knudsen diffusion. Compared with the previous reports [18, 78], the separation factor (α) here is close to the ideal value for Knudsen diffusion ($\alpha^*=3.7$), which indicated only small defects in the substrates and due to the existence of a thin and smooth outer surface of the fibres [1], it was assumed that these substrates

could be directly used for coating a thin and dense Pd film, which is presented in the next section.

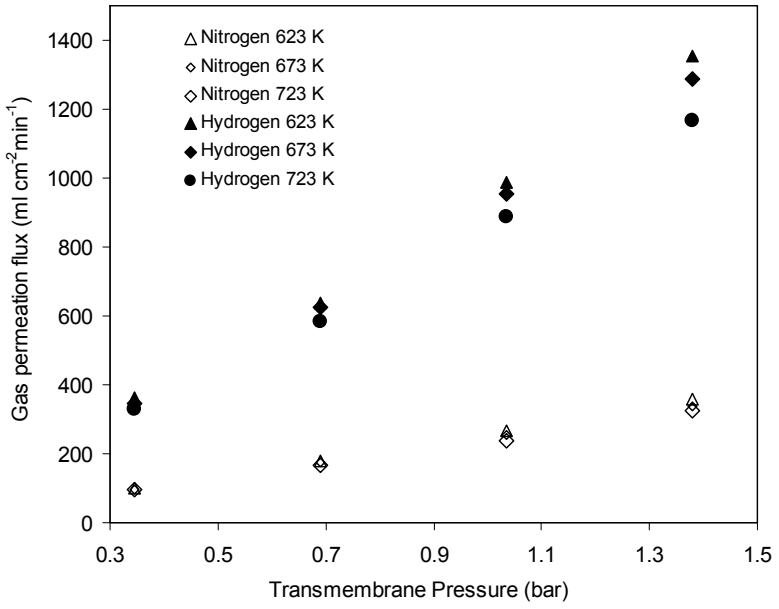


Figure 3-18 Hydrogen and nitrogen flux through alumina hollow fibre support

Figure 3-19 shows SEM images obtained from alumina hollow fibres supports spun with a 15 cm air-gap and sintered at 1723 K for 4 h. It is clear that a uniform asymmetrically structured support with an O.D. of 1893 μm and I.D. of 964 μm is formed as a result of the phase inversion method. In Figure 3-19(a)-(d), long finger-like macrovoids extend ~ 80 % from the inner surface to the outer surface, with the remaining 20 % consisting of a sponge-like layer. Figure 3-19(e)-(f) shows a more porous inner surface and a denser outer surface, respectively, resulting from the phase inversion process. This is confirmed from the mercury intrusion data of the sintered alumina hollow fibres shown in Figure 3-20. The data shows a bimodal pore size distribution with a narrow peak at 6 μm and a weaker broad peak at 0.15 um, which represent the pores of the entrance to the inner porous region and denser sponge-like outer layer respectively.

Hydrodynamically unstable viscous fingering has been suggested as a phenomenon associated with the formation of finger-like and sponge-like structures and occurs when a less viscous fluid (non-solvent) is in contact with a higher viscosity fluid (spinning suspension) [16]. During the phase inversion process, solvent/non-solvent exchange takes place which causes an influx of the non-solvent into the suspension film and an increase in the suspension viscosity and finger-like voids may result from non-solvent influx under certain circumstances. Due to the high concentration of non-solvent at the interface between the non-solvent and the suspension, polymer precipitation is instantaneous and viscosity rapidly increases. Previous studies have shown that when the suspension viscosity exceeds a critical value no further morphological change may take place and the size of the entrances to the finger-like voids is determined at this point [16, 134]

The exposure of the outer nascent fibre surface to the atmosphere also causes an increase in viscosity in the outer region due to simultaneous solvent evaporation and non-solvent (moisture) condensation from the surrounding atmosphere. The hollow fibre membranes prepared in this study has exceeded the critical suspension viscosity is in the outer region of the fibre before immersion in the non-solvent bath takes place. Consequently, finger-like void growth is not observed at the outer fibre surface and a sponge-like structure results.

Further examination of fibre microstructure in Figure 3-19 (f), reveal a sufficiently smooth outer surface for the direct deposition of thin membrane layer. Also, in comparison with symmetric structured fibres, the sponge-like layer near the outer wall is much thinner. The void morphology (i.e. large pore size of the inner surface compared to the outer surface) offers the possibility to accommodate the deposition of catalysts within

the fibre wall and to essentially functionalize the support using several methods: an incipient wetness impregnation method using an aqueous solution of catalyst supported on submicron particles, or a deposition-precipitation method using a homogeneous solution containing both the catalyst and catalyst substrate precursor compounds [135, 136].

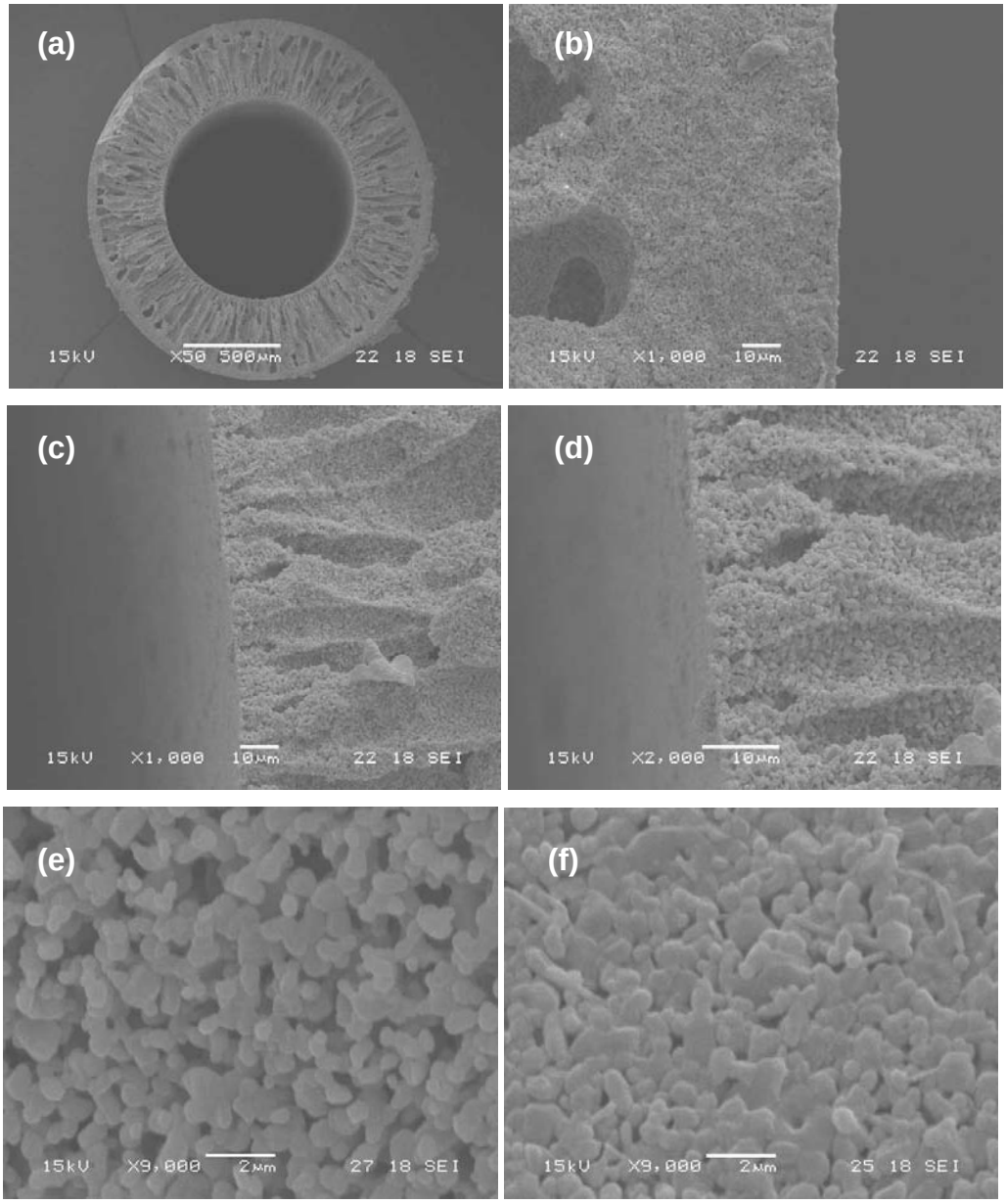


Figure 3-19 SEM images of an Al_2O_3 hollow fibre spun with an air-gap of 15 cm and calcined at 1723 K for 4 h. (a) whole view (b) cross section (finger-like voids) (c) inner edge (x1000) (d) inner edge (x2000) (e) inner surface and (f) outer surface

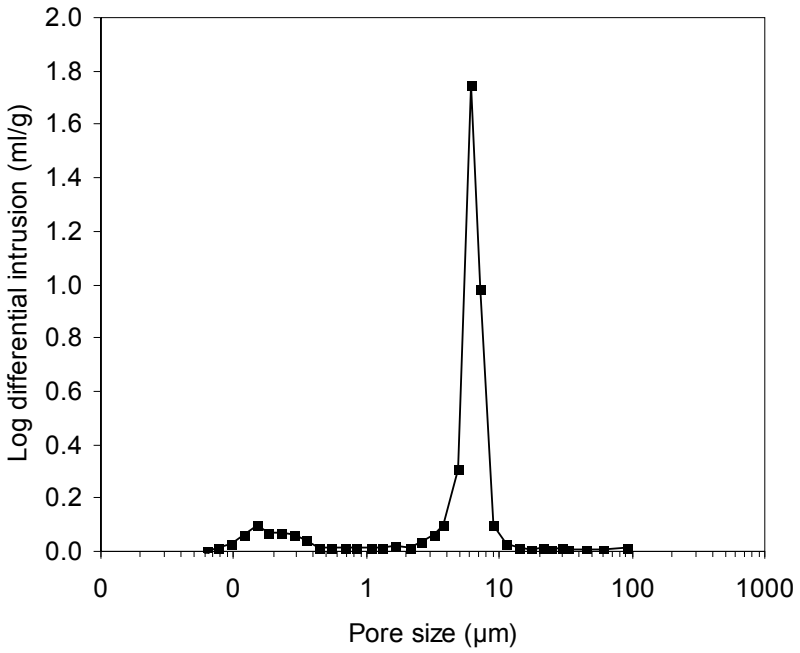


Figure 3-20 Mercury intrusion data for asymmetric Al_2O_3 hollow fibre sintered at 1723 K for 4 h

3.3.2 Morphology of Pd/Al_2O_3 hollow fibre composite membranes

A Pd membrane was directly coated onto the outer surface of Al_2O_3 hollow fibre substrates using the electroless plating method previously outlined. After plating, a thin and dense layer (3-4 μm) was formed on the outer skin layer of substrates with an asymmetric pore structure Figure 3-21(a). The appearance of the Pd surface, consisting of hills and valleys of tightly clustered Pd grains, shown in Figure 3-21(b), is consistent with similar studies where electroless plating was used [137, 138]. It is believed that as the process proceeds, deposition takes place initially on seeded Pd nuclei and when the metal grains begin to overlap, Pd is still mostly deposited on the higher areas of the formed film, resulting in hills and valleys.

The Pd layer prepared in this study appears to be very dense because no apparent gaps between Pd clusters were found. This was also identified by gas-tight characterization (room temp, N_2, 3 bar transmembrane pressure), in which no detectable pressure drop was observed over a period of about 24 h.

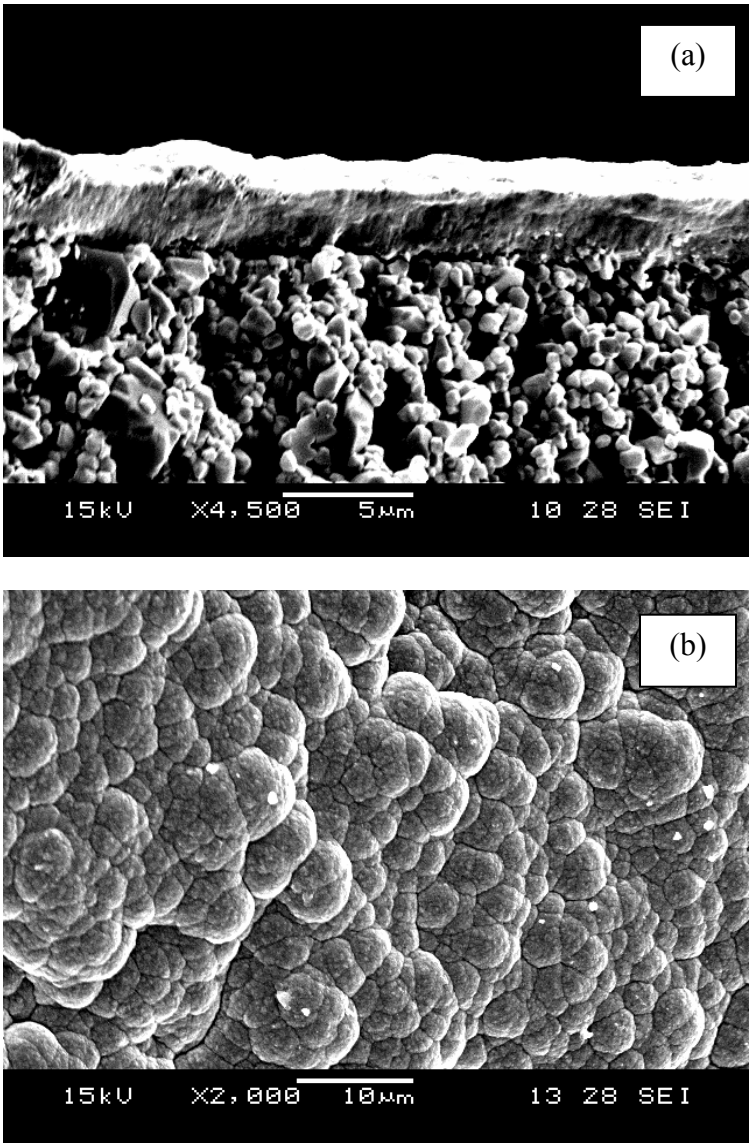


Figure 3-21 SEM images of (a) cross section and (b) surface of Pd/Al_2O_3 hollow fibre composite membrane

3.3.3 Performance of Pd/Al_2O_3 hollow fibre composite membranes

High temperature gas permeation measurements of Pd/Al_2O_3 hollow fibre composite membranes was carried out using gas permeation apparatus (Figure 3-16). Before hydrogen was introduced, both the sealing and the gas-tightness of the composite membranes at high temperatures were tested at 573-823 K with a transmembrane pressure (N_2) up to about 4 bar. The fact that no detectable nitrogen was found ensured the reliability of the measurements and demonstrated a perfectly sealed and a fully dense Pd membrane with super high selectivity. Figure 3-22 shows the effect of pressure difference on hydrogen permeation of Pd/Al_2O_3 hollow fibre composite membranes. Hydrogen permeation flux increased with an increase in operating temperature and transmembrane pressure, with the flux increasing from 32.8 $ml.cm^{-2}min^{-1}$ at 723 K to 60.9 $ml.cm^{-2}min^{-1}$ at 723 K.

The linear relationship between hydrogen flux and pressure difference indicated that the pressure exponent (n) was close to 1 over the temperature range (Appendix B, Table B-1). The n value was determined by taking the sum of the greatest least squares regression value for all the temperatures. This is in agreement with previous studies that showed exponent values can reach 0.9 for Pd/alumina composite hollow fibre membranes [86] [38]. This indicates that surface processes (adsorption, desorption steps) dominate the permeation process.

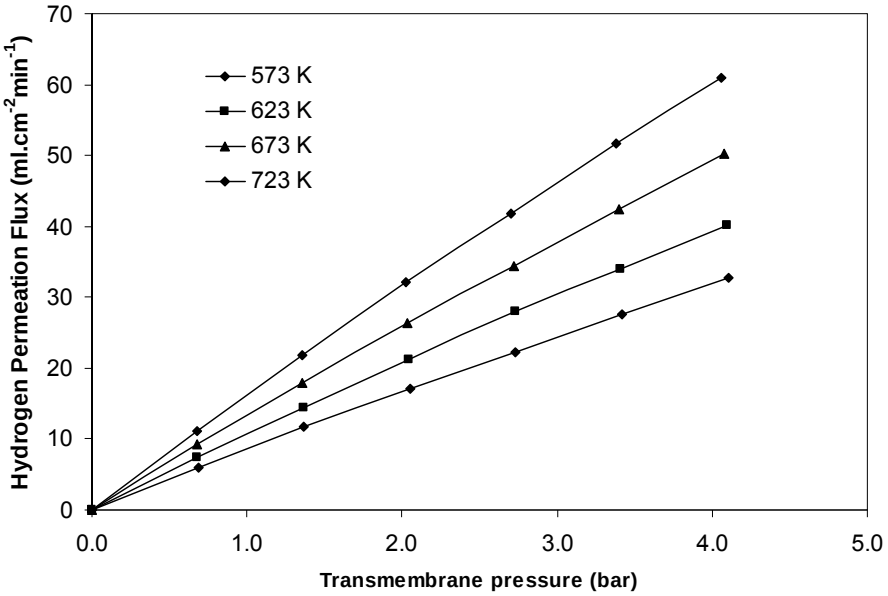


Figure 3-22 Relationship between pressure difference and hydrogen flux through palladium composite membrane

It has been widely known that, in the electroless plating process, the morphology (pore size and roughness) of the substrate's surface is critically important for the growth of a Pd layer and ultimately determines its microstructures [38]. In addition to operating parameters (temperature and transmembrane pressure etc.), the microstructure of the Pd separation layer governs hydrogen transport through the composite membrane. Deriving from non-surface modification of the support, inferior surface properties led to a lower surface coverage of Pd seeds in the activation process. This resulted in the formation of hills and valleys of Pd clusters when forming a dense Pd layer because Pd particles or clusters grow in a 3-dimensional way during the electroless plating process [11]. Also, the observed slight substrate penetration also decreased the effective porosity of the support and contributed to the further decrease of hydrogen permeance [86].

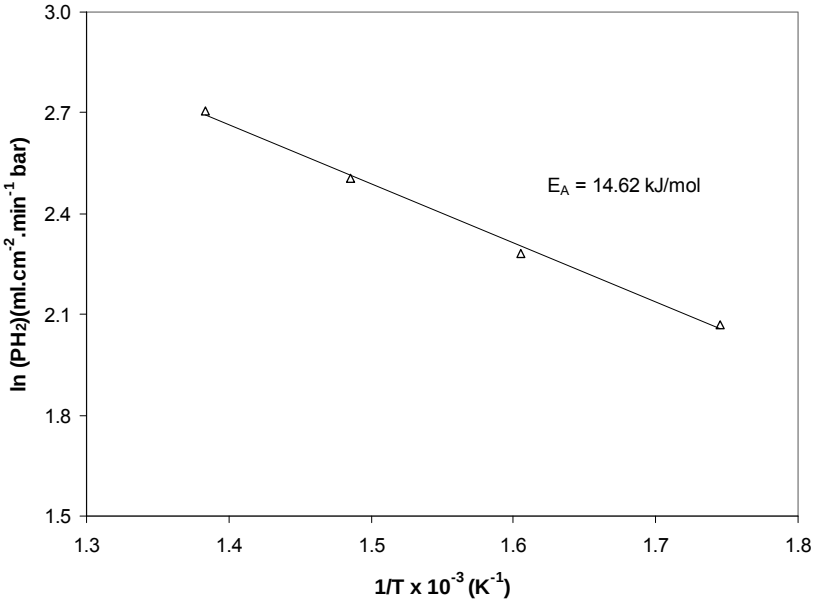


Figure 3-23 Arrhenius plot of hydrogen permeance for Pd/Al_2O_3 a hollow fibre composite membrane

Figure 3-23 shows the Arrhenius relationship of hydrogen permeance as a function of the temperature in the range 573-723 K from which the activation energy was calculated to be 14.62 kJ/mol. This value is in agreement with similar studies on Pd based membranes [18, 19, 78, 132].

3.4 Conclusions

Al_2O_3 hollow fibres with an asymmetric pore structure were prepared by a combined phase inversion and sintering technique. The fibres show an asymmetric structure which is characterised by a very porous inner surface from which finger-like voids extend across approximately 80 % of the fibre cross section with the remaining 20 % consisting of a denser sponge-like outer layer. It is believed that finger-like void formation in asymmetric ceramic membranes is initiated by hydrodynamically unstable viscous fingering developed when a less viscous fluid (non-solvent) is in contact with a higher viscosity fluid (ceramic suspension containing invertible polymer binder).

SEM characterisation showed that the outer sponge-like layer of the substrate provides a sufficiently smooth surface to coat dense membrane films for hydrogen separation by a suitable plating method. Thin and fully dense Pd membranes were directly deposited onto the outer surface of such fibres without any modification process. However, this can lead to substrate surface properties in which Pd particles or clusters are non-uniformly formed during the electroless plating process. The Pd membrane achieved a hydrogen permeation flux of 60 $ml/cm^2.min^1$ at 723 K and 4 bar transmembrane pressure with an activation energy of 14.62 kJ/mol. The composite membrane together with its unique structure offers the possibility of depositing sub-micron sized catalyst particles into the finger-like voids to develop a highly compact multifunctional membrane reactor.

CHAPTER 4

A Novel Inorganic Hollow Fibre Membrane Reactor for Catalytic Dehydrogenation of Propane

Abstract

A novel inorganic hollow fibre membrane reactor has been developed and applied to the catalytic dehydrogenation of propane to propene. Alumina hollow fibre substrates, prepared by a phase inversion/sintering method, possess a unique asymmetric structure which can be characterised by a very porous inner surface from which finger-like voids extend across approximately 80 % of the fibre cross section with the remaining 20 % consisting of a denser sponge-like outer layer. In contrast to other existing Pd/Ag composite membranes where an intermediate γ-Al_2O_3 layer is often used to bridge the Pd/Ag layer and the substrate, the Pd/Ag composite membrane prepared in this study was achieved by coating the Pd/Ag layer directly onto the outer surface of the asymmetric substrate. After depositing sub-micron sized Pt(0.5wt.%)/γ-alumina catalyst in the finger-like voids of the substrates, a highly compact multifunctional iHFMR was developed. Propane conversion as high as 42 % was achieved at the initial stage of the reaction at 723 K. In addition, the space-time yields (STY) of the iHFMR were approximately 60 times higher than that of a fixed bed reactor (FBR), demonstrating the advantages of using iHFMR for dehydrogenation reactions.

4.1 Introduction

Due to the production of polypropylene from propene, the direct dehydrogenation of propane ($C_3H_8 \leftrightarrow C_3H_6 + H_2, \Delta H° = 124\,kJ/mol$) to propene has been extensively studied both theoretically and experimentally in the past several decades [139, 140]. High temperatures (773-873 K) and low pressures (0.3-1 atm) are industrially employed to obtain commercially acceptable conversions due to the endothermic nature of the reaction [139]. For instance, the conversion of propane in the Catofin™ process is between 48-65% per pass at 823 K when the operating pressures are at 0.3-0.5 bar[139]. Besides the considerable amount of extra energy needed, high operating temperatures promote undesirable side-reactions that quickly deactivate the catalysts. Severe coking is often observed and frequent catalyst regeneration after short time intervals of only 15-30 min is necessary [139]. In the case of the UOP Oleflex™ process, a longer cycle duration of about 7 h can be achieved at 823 K by adding hydrogen to the feed to reduce the coke formation, although propane conversion is limited to around 40% for thermodynamic reasons [140].

Use of membrane reactors allows the continuous removal of hydrogen from the reaction zone during the dehydrogenation of propane to propene, thus offering the possibility of substantially increasing the conversion and/or lowering the reaction temperature in endothermic, equilibrium-limited reactions of this type [13, 38, 141]. Compared to porous membrane reactors, dense membrane reactors, such as Pd-based membranes, possess much better performance due to their extremely high hydrogen selectivity [12, 13, 142]. Thin and defect-free Pd-based membranes are usually

deposited onto porous ceramic or metal substrates to achieve high permeation flux, reduced membrane cost and sufficient mechanical strength etc. without compromising the hydrogen permselectivity [38, 143]. In most cases, Pd-based membranes cannot be directly deposited onto the porous substrates with symmetric structures due to their large surface pore size. As a result, a γ-Al_2O_3 intermediate layer, which is usually prepared by a sol-gel based technique, is widely employed before the subsequent membrane deposition [38, 143].

Following the recent success by Tan et al. in fabricating porous alumina hollow fibres with extremely high surface area/volume ratios [144], various studies have been carried out to deposit Pd-based membranes onto substrates of this type for hydrogen separation [19, 85, 132, 145], in which a γ-Al_2O_3 intermediate layer was often employed as discussed previously. Although Tong et al. [86, 146] developed a novel combined organic and inorganic process to avoid the need for the mechanically weak, intermediate γ-Al_2O_3 layer, a multi-step post-treatment was still necessary. Alumina hollow fibre substrates with symmetric structures featured in a study by Sun et al.[78], involving the elimination of finger-like voids in fibres to give greater mechanical strength. No intermediate layer was required when a Pd membrane as thin as around 1.5 μm was deposited onto hollow fibre substrates consisting entirely of a sponge-like structure.

In contrast to the substrates used above, the alumina hollow fibre substrate prepared in this study possesses a unique asymmetric pore structure that is characterised by a very porous inner surface from which finger-like voids extend across approximately 80 % of the fibre cross section with the remaining 20 % consisting of a denser sponge-like outer layer. This unique structure confers several advantages, as the

sponge-like outer layer with its narrow pore size distribution provides a sufficiently smooth surface for the direct deposition of a thin and defect-free hydrogen separation layer without any pre- or post-treatment, whilst long finger-like voids in the substrate wall provide an extensive surface for deposition of catalysts as shown in the insert of Figure 4-24.

In this chapter, Pd/Ag alloy membranes with a composition close to 77wt.% Pd and 23 wt.% Ag, which have been widely studied due to their great H_2 permeation flux and stability, have been selected as the H_2 separation layer. They have been coated onto the denser sponge-like outer layer of the substrate, while sub-micron sized Pt (0.5 wt.%)-γ-alumina catalyst particles have been deposited into the finger-like voids through the very porous inner surface, forming a highly compact multi-functional membrane reactor for simultaneous dehydrogenation of propane to propene and hydrogen separation. Due to the limitation on the stability of the catalyst, the operating temperature was inevitably fixed at 723 K at which the equilibrium conversion of propane is low. However, in comparison with the traditional fixed bed reactor (FBR), the highly compact multi-functional inorganic hollow fibre membrane reactor (iHFMR) proposed in this study clearly demonstrates its advantages.

4.2 Experimental

4.2.1 Materials

Aluminium oxide powders of 1 μm (alpha, 99.9% metals basis, S.A. 6-8 m^2/g), 0.05 μm (gamma-alpha, 99.5% metals basis, S.A. 32-40 m^2/g) and 0.01 μm (gamma-alpha, 99.98% metals basis, S.A. 100 m^2/g) particle sizes were purchased from Alfa

Aesar and were used as supplied. Polyethersulfone, (PESf, Radel A-300, Ameco Performance, USA), N-methyl-2-pyrrolidone (NMP, HPLC grade, Rathbone) and Arlacel P135 (Uniqema, UK) were used as binder, solvent and additive, respectively. DI water and tap water were used as the internal and external coagulants, respectively, when fabricating Al_2O_3 hollow fibre precursors. $Pd(NH_4)_2Cl_4$ (Ammonium tetrachloropalladate, 99.99%, Aldrich), $SnCl_2{\cdot}2H_2O$, $Na_2EDTA{\cdot}2H_2O$, HCl (37%), N_2H_4, $AgNO_3$ and $NH_3{\cdot}H_2O$ (28%) (Fisher Sci. Ltd) were used for preparing the Pd/Ag hydrogen separation layer using an electroless plating method. H_2PtCl_6 (99.995%, Aldrich) and 60 nm gamma-aluminium oxide powders (99% metal basis, S.A. 180 m^2/g, Alfa Aesar) were used for preparing the Pt (0.5 wt%)/γ-Al_2O_3 catalyst using a traditional impregnation method.

4.2.2 Preparation of multifunctional membranes

4.2.2.1 Asymmetric Al_2O_3 hollow fibre support:

Asymmetric Al_2O_3 hollow fibre substrates were fabricated via a phase inversion/sintering technique [144]. Arlacel P135 (0.1 wt%/alumina surface area) was dissolved in NMP prior to the addition of aluminium oxide powders (1 μm: 0.05 μm: 0.01 μm = 7:2:1). The dispersion was rolled with 20 mm agate milling balls with an Al_2O_3/agate weight ratio of 1.9 for 48 h and milling was continued for a further 48 h after the addition of PESf. The spinning suspension was then transferred to a gas tight reservoir and degassed under vacuum for 2 h. After degassing, the suspension was pressurized at 7-20 psig using nitrogen gas and was extruded through a tube-in-orifice spinneret (ID 1.2 mm, OD 3.0 mm) into a coagulation bath containing 120 litres of water with an air-gap of 15 cm. DI water was used as the internal coagulant and the flow rate ranged from 10 to 30 ml/min. The formed precursor fibres were first heated in a

CARBOLITE tube furnace at about 873 K for 2 h to remove the organic polymer binder and were then sintered at 1723 K for 4 h with heating and cooling rates of 5 K/min. The outer surface of the prepared substrates (about 30 cm in length after sintering) was coated with a thin and gas-tight layer of glaze with the exception of the central part of the fibre (of around 5 cm in length), left for electroless plating of the Pd/Ag membrane.

4.2.2.2 Catalyst preparation and deposition:

Sub-micron sized Pt (0.5wt.%)/γ-Al_2O_3 catalyst was prepared by impregnation of 60 nm γ-Al_2O_3 powders of with an aqueous solution of H_2PtCl_6 at room temperature. After impregnation, the catalyst was dried at 383 K overnight and calcined at 773 K for 4 h with heating and cooling rates of 2 K/min. Prior to catalyst deposition, the catalyst was reduced under flowing H_2 at 773 K for 2 h. The deposition of the catalyst particles into the finger-like voids of the substrates was performed by uniformly dispersing the prepared catalyst in an aqueous medium using Arlacel P135 as a dispersant. The hollow fibre substrates were vacuumed for 1 h to remove the air trapped inside. A volume of the suspension containing catalyst particles was then sucked into a closed vessel containing the substrates. After 1 h, the vessel was opened to the atmosphere which applied an additional driving force for the suspension to penetrate into the finger-like voids within the substrates. Prior to drying the substrates in an oven over night at 383 K, the remaining suspension in the substrate lumen was expelled using compressed air. This catalyst deposition process was repeated three times for sufficient loading of catalyst in the finger-like voids before the dehydrogenation reaction.

4.2.2.3 Pd/Ag coating:

The Pd/Ag membranes were coated onto the outer surface of asymmetric alumina hollow fibre substrates by an electroless plating technique[38]. Prior to the coating, the substrates were cleaned and activated by the conventional Pd-Sn activation procedure. The activation process consisted of successive immersion of the substrates in the tin (II) chloride ($SnCl_2$) solution and the palladium chloride ($PdCl_2$) solution at room temperature. Deionised water and 0.1 M HCl were used to rinse the samples between the immersions. The activation process was repeated 6 times, after which the substrate surface turned brown. The Pd/Ag membrane was then coated by a "coating-diffusion" process[38] using the plating baths having the compositions shown in Table 4-7.

Prior to the Ag coating, a Pd layer was coated onto the activated substrate surface. The thicknesses of the Pd and the Ag layer were determined by controlling the plating process, in which the plating solution was refreshed every hour. The homogeneous Pd/Ag alloy membrane was obtained by heat treatment of the samples at 923 K for 12 h.

Table 4-7 Coating bath compositions of Pd/Ag electroless plating

Compounds	Pd Bath	Ag Bath
$Pd(NH_3)_4Cl_2 \cdot H_2O$ (g/l)	4	-
$AgNO_3$(g/l)	-	0.519
$Na_2EDTA\ 2H_2O$ (g/l)	40.1	40.1
NH_4OH (28%) (ml/l)	198	198
N_2H_4(1 M) (ml/l)	5.6	5.6
pH	10-11	10-11
Temperature (K)	333	333

4.2.3 Characterization of multifunctional hollow fibre membranes

The morphology of the alumina hollow fibre substrates, the Pd/Ag composite membranes and the catalyst deposited in the finger-like voids were visually observed using a scanning electron microscope (JEOL JSM-5610LV, Tokyo, Japan). A clear cross-sectional fracture of hollow fibre substrates was obtained by directly snapping the samples. All the samples were positioned on a metal holder and gold coated using sputter-coating operated under vacuum. The SEM micrographs of both the sample surface and cross section were taken at various magnifications. EDS analysis (INCA Energy by Oxford Instruments) was employed to investigate the elemental distribution across the Pd/Ag membranes.

Single gas (H_2 or N_2) permeation measurements of both the asymmetric Al_2O_3 hollow fibre substrates with and without catalyst loading and the Pd/Ag composite membranes were carried out. The gas permeation module was placed into a CARBOLITE tube furnace equipped with a microprocessor temperature controller. The effective heating zone of constant temperature was approximately 5 cm of length. Pressurized hydrogen or nitrogen (99.99%) was introduced into the shell of the module. The operating pressures were adjusted by a pressure regulator (PRG-101-60, Omega) and monitored using a KN2200 electronic pressure gauge. The pressure in the lumen was kept at atmospheric pressure. The flow rates of gas permeating through the substrates or the Pd/Ag composite membranes were measured using bubble flow meters.

4.2.4 Dehydrogenation of propane to propene

The apparatus for the dehydrogenation of propane to propene is schematically shown in Figure 4-24. A gaseous stream containing propane (5%) and hydrogen (4.5%) with balanced nitrogen was introduced at 30 ml/min into the lumen of the reactor. Argon with a flow rate of 50 ml/min was used as a sweep gas to carry the permeated hydrogen to a TCD gas chromatograph (Varian-3900) for analysis. The membrane reactor was operated at atmospheric pressure and the effluent gases from the reactor were analyzed on-line using a FID gas chromatograph (Varian-3900). It should be noted that the above operation is only used for lab-scaled apparatus. For a commercial unit, it would be logical to use vacuum instead of using Ar as a sweep gas. Also, the iHFMRs would be constructed with a bundle of the fibres instead of a single fibre to obtain a surface area/volume ratio suitable for commercial applications.

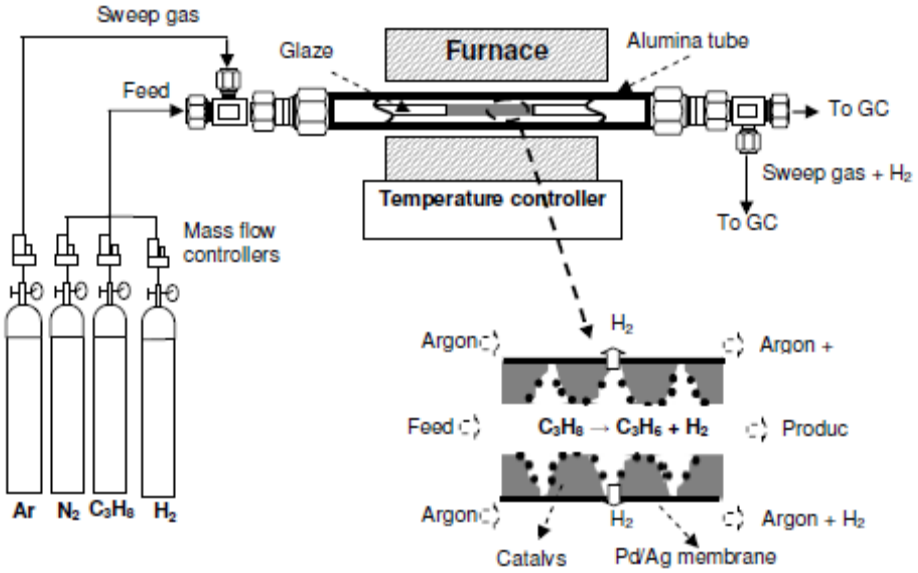
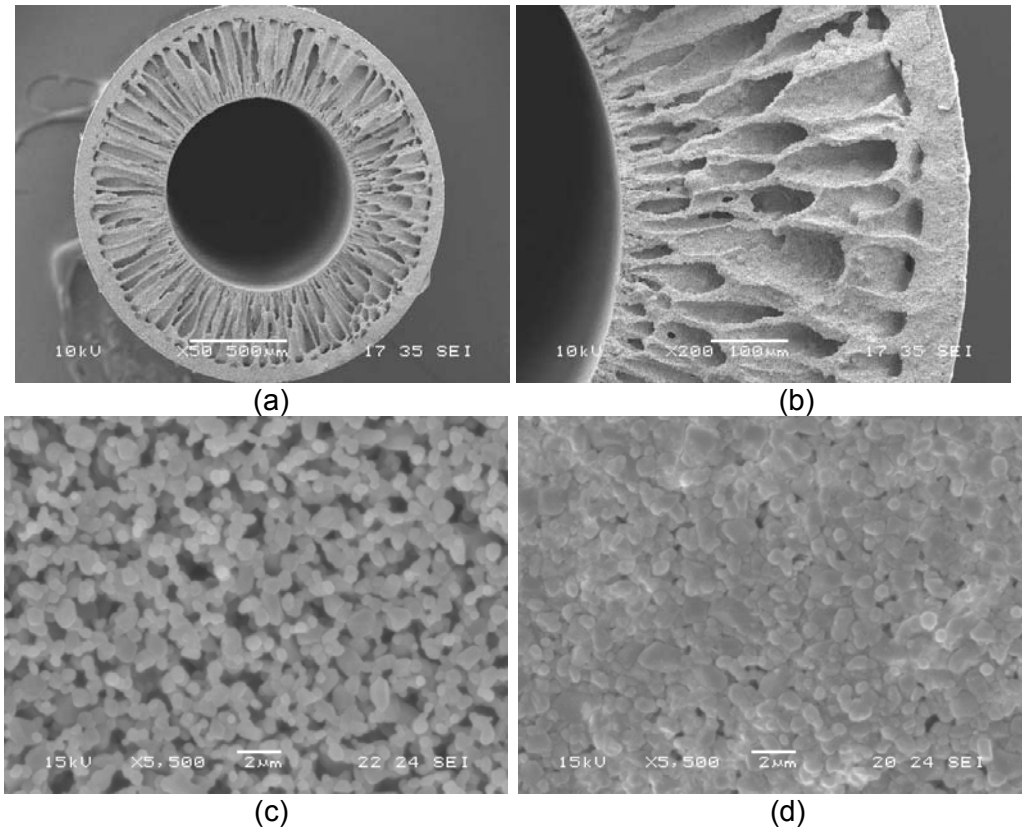


Figure 4-24 Schematic diagram of the apparatus for the dehydrogenation of propane to propene

4.3 Results and Discussion

4.3.1 Microstructure of asymmetric Al_2O_3 hollow fibre substrates

Figure 4-25 shows morphologies of the asymmetric Al_2O_3 hollow fibre substrates sintered at 1723 K for 4 h, which are similar to the ones fabricated in Chapter 3. The OD and ID of the fibres with uniform wall thickness were measured at approximately 1893 μm and 964 μm respectively. As can been seen, the hollow fibre substrates prepared possess a unique asymmetric structure composed of long finger-like voids and a thin and uniform sponge-like layer, Figure 4-25(a) and (b), with a very porous inner surface (Figure 4-25 (c)) and a relatively denser outer surface (Figure 4-25d).



(a) (b)

(c) (d)

Figure 4-25 SEM images of the asymmetric alumina hollow fibre substrate sintered at 1723 K for 4 h: (a) whole view, (b) cross section, (c) inner surface and (d) outer surface

The formation of finger-like voids at the inner fibre surface is believed to be initiated by instabilities at the interface between the non-solvent and the suspension. Finger-like void growth then proceeds as a result of non-solvent influx into the suspension as a result of the viscous fingering phenomenon. Due to the high concentration of non-solvent at the interface, polymer precipitation is instantaneous resulting in a rapid, large increase in the viscosity of the suspension in this region. Consequently, the suspension viscosity exceeds the critical value at which further morphological change may take place and the size of the entrances to the finger-like voids is determined at this point. Non-solvent influx through these entrances into the suspension results in finger-like void growth. However, the polymer precipitation rate within the suspension is lower than that at the interface with non-solvent due to the lesser availability of non-solvent in this region. As a result the suspension viscosity remains below the critical value for longer and finger-like void growth may proceed, giving rise to the characteristic finger-like shape. Finger-like void growth cannot proceed above a critical suspension viscosity and consequently growth is halted when this value is exceeded. Exposure of the outer fibre surface to the atmosphere causes an increase in viscosity in this region due to simultaneous solvent evaporation and non-solvent condensation from the surrounding atmosphere. For fibres prepared as substrates in this work the critical suspension viscosity is exceeded in the outer region of the fibre before immersion in non-solvent takes place. Consequently, finger-like void growth is not observed at the outer fibre surface and a sponge-like structure results.

Accompanied by the growth of the finger-like voids, a highly porous inner surface and a relatively denser outer surface are formed as shown in Figure 4-25(c) and (d). In contrast to other existing alumina substrates with symmetric structures, the sponge-like

layer near the outer wall prepared in this study is much thinner. In addition, the employment of fine particles contributes to both the narrow pore size distribution and the sufficiently smooth outer surface for the direct deposition of Pd/Ag membranes. Moreover, catalyst could be deposited into the finger-like voids of the substrates. Thus, highly compact multi-functional membranes can be further fabricated.

4.3.2 Catalyst preparation and deposition

Sub-micron sized Pt(0.5wt.%)/γ-alumina catalyst was prepared using a traditional impregnation method and deposited into the substrate of hollow fibre membrane reactor (iHFMR). Prior to catalyst deposition, the catalyst particles were dispersed in an aqueous medium using Arlacel P135 as a dispersant. Only the catalyst particles suspended evenly in the aqueous medium were used for subsequent catalyst deposition. As a result, a very small amount of the catalyst was deposited uniformly in the finger-like voids of the asymmetric alumina substrates. As can be seen from Figure 4-26a, the surfaces of the finger-like voids were covered by a thin layer of sub-micron sized catalyst particles, while the sponge-like regions of the substrate remained unaffected. Figure 4-26b shows the finger-like void surface at high magnification and indicates that the catalysts are sparsely deposited on the surface of the finger-like voids. This agrees with the result that, after the catalyst deposition, the average weight gain of the asymmetric alumina hollow fibre substrates (30 cm in length) is only approximately 0.74 %, as listed in Table 4-8.

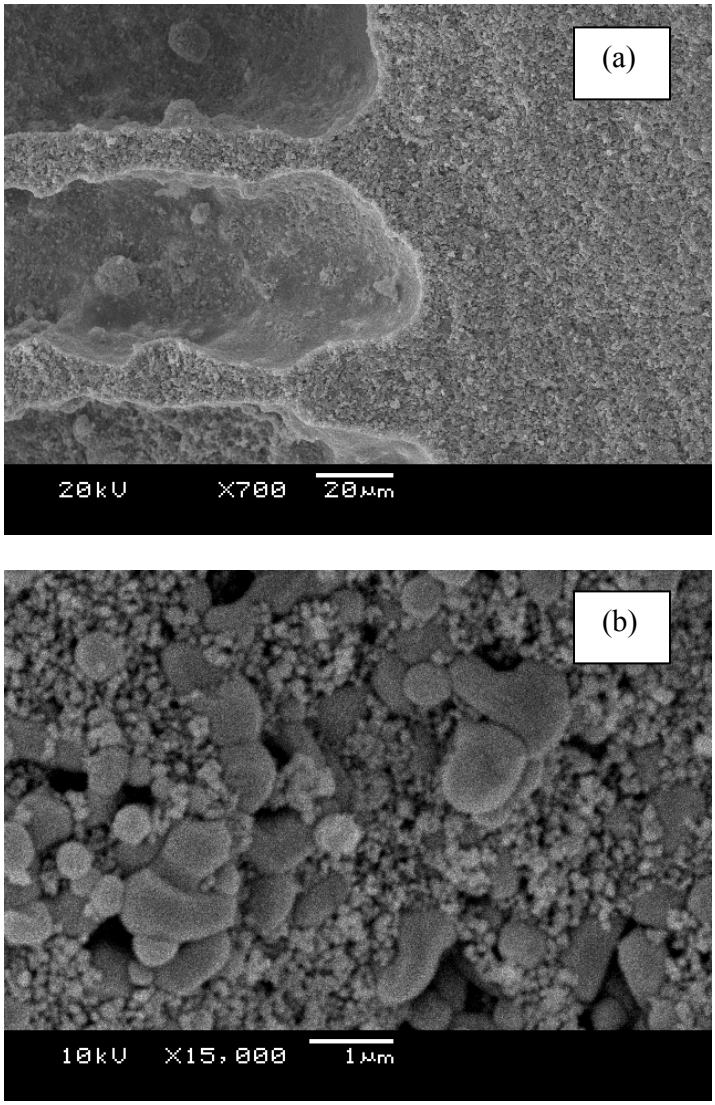


Figure 4-26 SEM images of catalyst deposition in the hollow fibre substrate: (a) catalyst particles deposited into the finger-like voids, (b) finger-like voids with high magnification.

Table 4-8 The weight gain of asymmetric alumina hollow fibre substrates after catalyst deposition

Catalyst deposition	Whole weight of samples (mg)	Weight gain (%)
Before deposition	935.6	-
After 1st one hour deposition	936.5	0.10
After 2nd one hour deposition	940.4	0.51
After 3rd one hour deposition	942.5	0.74

4.3.3 Gas permeation of Al_2O_3 hollow fibre substrates

The permeation characteristics of Al_2O_3 hollow fibre substrates were investigated using H_2 and N_2 gas permeation measurements. The permeation results are shown in Figure 4-27. As can be seen, the permeance of H_2 and N_2 slightly increase as the mean pressure across the substrates is increased, indicating that the total flow through the alumina hollow fibre substrates (sintered at 1723 K for 4 h) is described by the combined contribution of Knudsen diffusion and Poiseuille flow [78, 147]. The separation factor (α) of H_2/N_2 was measured to be 3.2, which is slightly lower than those of 3.3-3.5 achieved by modifying the substrates with a γ-Al_2O_3 intermediate layer [38, 78]. Figure 4-27 further illustrates that the H_2 and N_2 permeation fluxes of the substrates with and without the catalyst are very close; indicating that the mass transfer resistance created due to the catalyst deposition is negligible.

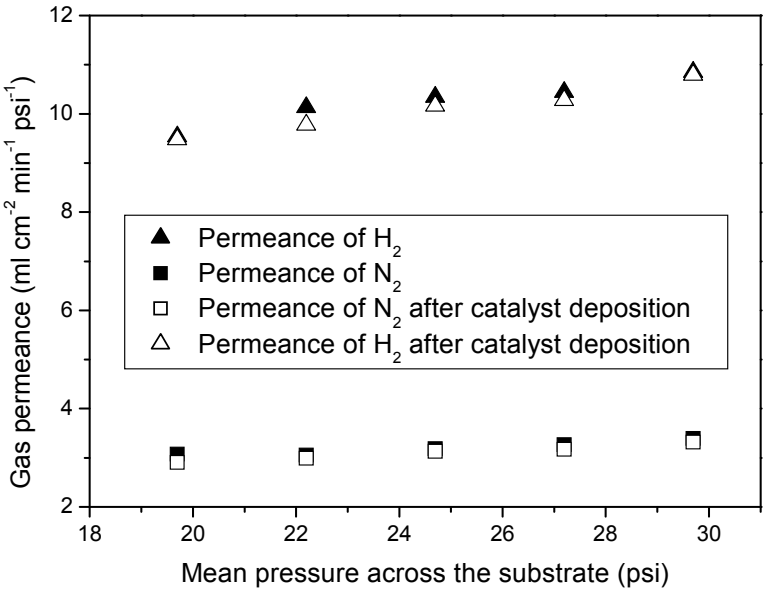


Figure 4-27 Gas permeation of hydrogen and nitrogen through the hollow fibre substrates at room temperature

4.3.4 Sequential electroless plating of Pd/Ag membranes

The Pd/Ag composite membranes were coated onto the outer surface of the substrates prepared above by a “coating-diffusion” electroless plating method[38] where the plating bath was refreshed every one hour. Prior to deposition of Ag, the surface of the Pd membrane was reactivated so as to produce uniform Ag plating. The composition of the Pd/Ag membranes was controlled by the plating rates of Pd and Ag as shown in Figure 4-28. The weight gain of Pd and Ag increases linearly with time during the electroless plating. The mechanism of the electroless plating (ELP) technique is based on the controlled autocatalytic reduction of the metastable metallic salt complexes on the target surfaces [67]. Nonlinear behavior can be observed when the ELP is carried out continuously without changing the ELP solution, in which the number of the Pd nucleation sites and the concentration of the metallic salt complexes change with time. In contrast, the ELP solution in this study was refreshed every hour, as a result of which the Pd and Ag plating behaviors were linear with respect to time. The plating rate of Pd is approximately 6.5 times higher than that of Ag. This plating profile was further confirmed by preparing Pd/Ag membranes with different thicknesses, which were calculated based on the theoretical densities of Pd and Ag. The calculated membrane thicknesses agree well with that of the SEM characterizations.

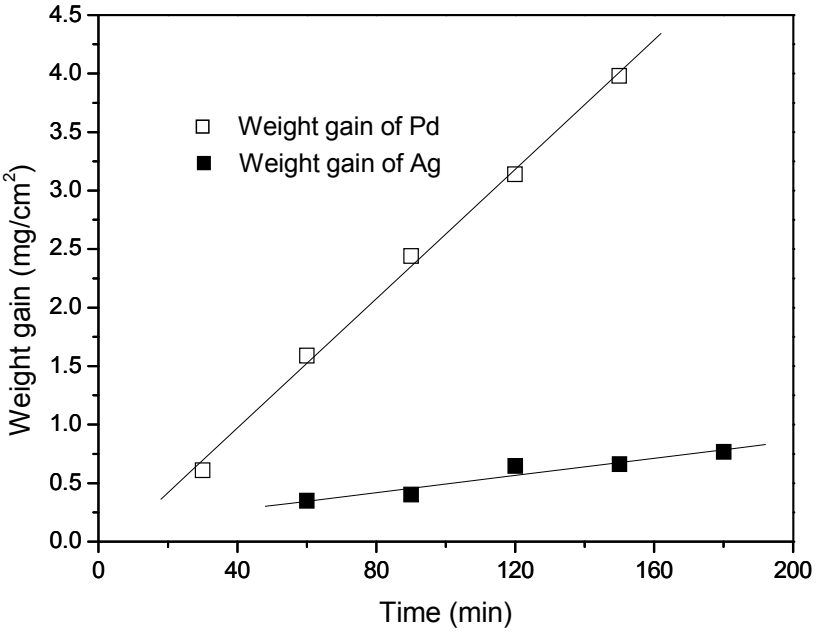


Figure 4-28 Weight gains of Pd and Ag during the electroless plating

Figure 4-29 shows the morphology of a Pd/Ag membrane with a thickness of around 8 μm. The reason for choosing a relatively thick membrane for SEM as well as the subsequent EDS analysis is to highlight the micro-structural change of the membranes during the electroless plating process. As can be seen from Figure 4-29(a) and (b), a uniform Pd layer was first deposited on the activated substrate with the Pd grains tightly bound on the surface without observable defects. A less defined grain boundary on the surface of the Ag layer is shown in Figure 4-29(c). A clear double-layer structure was obtained after the deposition of Ag as shown in Figure 4-29(d). Figure 4-29(e) illustrates that the boundary between the Pd and Ag layers disappeared after heat treatment at 923 K for 12 h in Ar due to intermetallic diffusion between the layers. Although some small pores were found on the surface of the composite membrane after the heat treatment Figure 4-29(f), these pores are dead volumes, as the membrane as a whole is gas-tight with excellent H_2/N_2 selectivity.

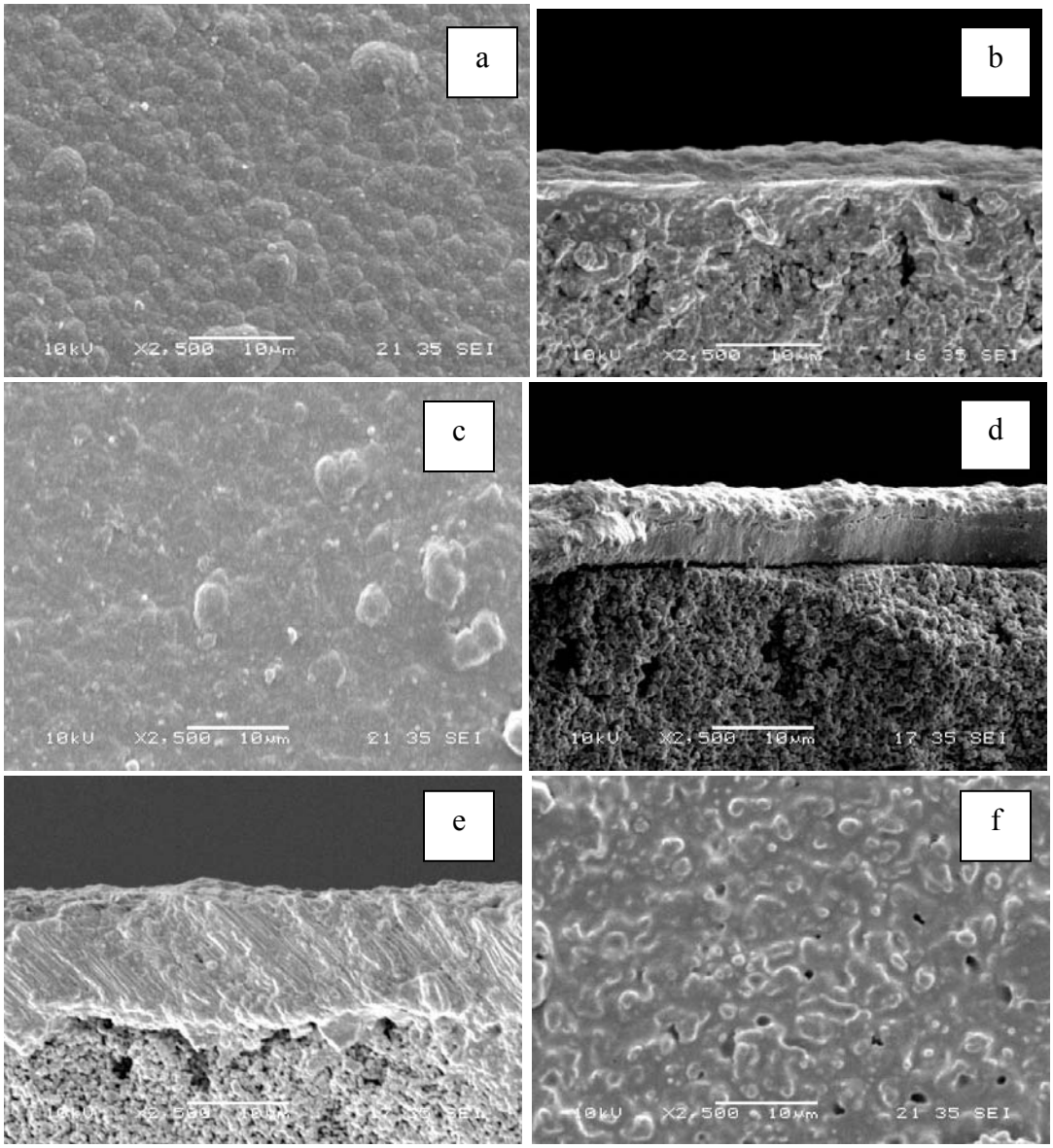
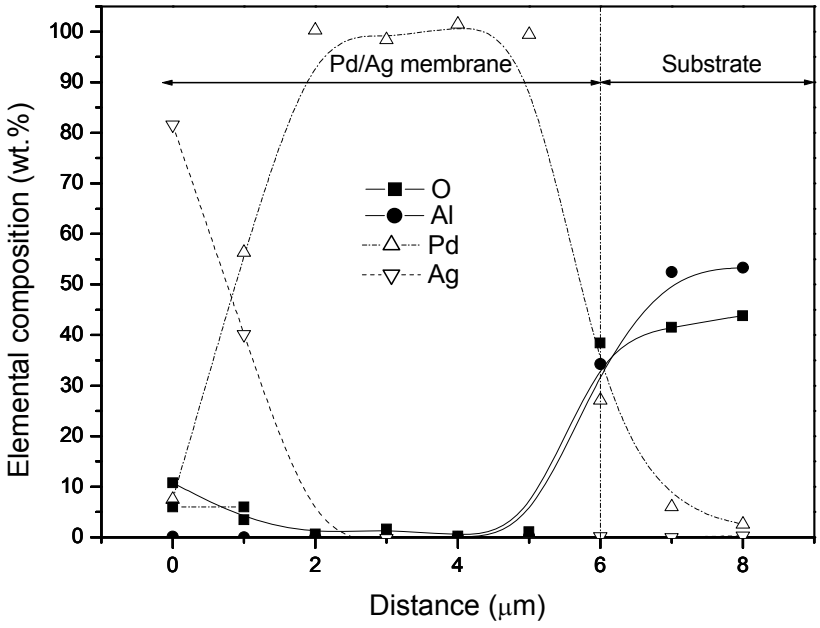


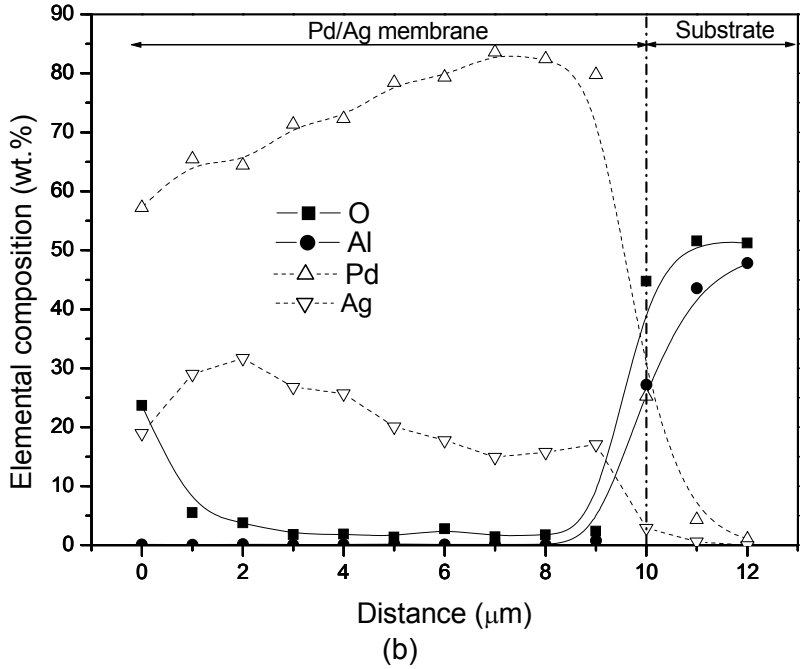
Figure 4-29 SEM images of Pd/Ag composite membranes during “coating and diffusion” electroless plating: (a) surface of Pd layer, (b) cross section of Pd layer, (c) surface of Ag layer, (d) cross section of Pd and Ag layers before heat treatment, (e) cross section of Pd/Ag alloy after heat treatment and (f) surface of Pd/Ag alloy after heat treatment.

EDS analysis was also carried out to investigate the elemental distribution across the Pd/Ag membrane cross section before and after heat treatment. As shown in Figure 4-30(a), a small amount of Pd was observed at approximately 2 μm beneath the

substrate surface before heat treatment, which indicated that the Pd plating solution penetrated slightly into the substrate during the electroless plating process.



(a)



(b)

Figure 4-30 EDS analysis of Pd/Ag membranes: (a) before heat treatment and (b) after heat treatment

In contrast to Figure 4-30(a), significant change in the elemental distribution across the membrane occurred after heat treatment as shown in Figure 4-30(b). The Tamman temperature (TM) is defined as the temperature at which considerable thermal vibration occurs in a lattice and is estimated at half the melting point (K) of a material [49]. As the TM of Ag, which is about 617 K, is much lower than that of Pd (914 K), it is reasonable to assume that silver atoms migrate significantly into the palladium layer during heat treatment. As can be seen in Figure 4-30(b), the concentration of Ag decreased slightly towards the substrate, while the concentration of Pd was increased. This indicates that a higher temperature and/or longer time would be required for a more uniform elemental distribution in such a thick membrane. Although a number of studies on metallic inter-diffusion have been carried out to determine the diffusion coefficient of Ag in Pd, it is still difficult to accurately predict the alloying process. For example, the diffusion coefficients from several groups are quite different from each other [49]. One of the possible reasons is that, apart from the material nature of Pd and Ag, the alloying process can be determined by the membrane microstructure, which is closely related to the preparation processes and the surface properties of the substrates. Hou et al. [88] obtained homogeneous Pd/Ag membranes by annealing the membrane at 873 K for 10 hours, which is quite similar to our work. While Uemiya et al. [22] concluded that high temperatures of above 1073 K were necessary to obtain a homogeneous Pd/Ag alloy membrane. However, area scans performed randomly on the cross section of other thinner samples revealed an average Pd/Ag ratio of 78:22, which was considered to be an indication that the Pd/Ag membranes used in subsequent experiments have a homogeneous distribution of Pd and Ag.

4.3.5 Gas permeation of Pd/Ag-Al_2O_3 composite hollow fibre membranes

Figure 4-31 shows the effect of the pressure difference on hydrogen permeation through a 5 μm Pd/Ag composite membrane between 723 K and 873 K. Before the introduction of hydrogen, the sealing of the module and the gas-tightness of the composite membrane were tested using nitrogen with the transmembrane pressure up to 3 bar. A 1 ml bubble flow meter with a minimum detectable scale of 0.01 ml was used to measure the flow rate of nitrogen. No soap bubble movement was observed at every operating temperature and pressure, indicating that the hydrogen/nitrogen selectivity in this study is close to infinity. In addition, a technique for testing the fibre gas tightness developed by Tan et al. [148] was also employed, further confirming that the membrane employed is gastight.

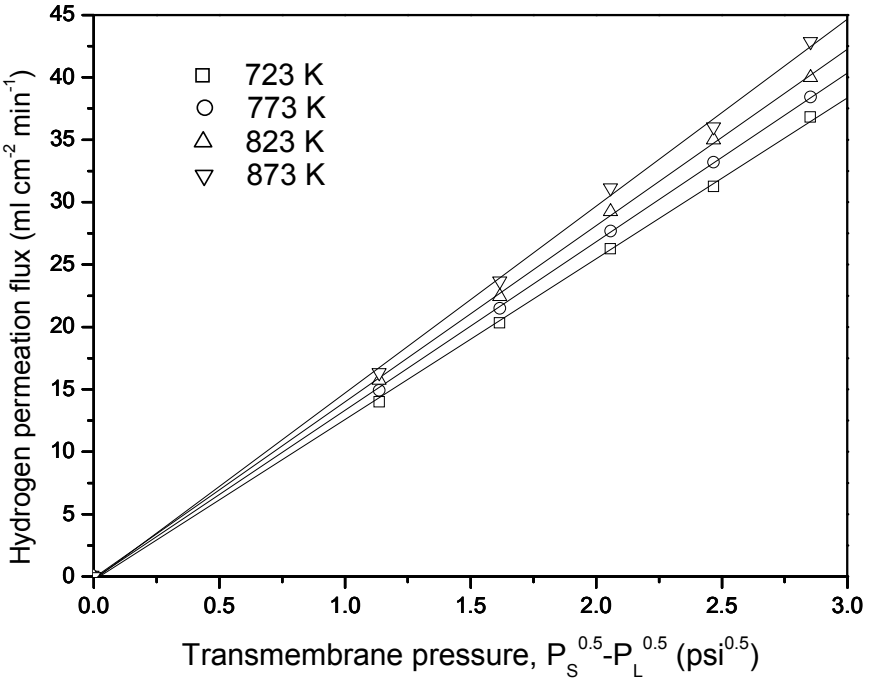


Figure 4-31 Relationship between square root of pressure difference and hydrogen permeation flux through Pd/Ag composite membrane at different temperatures

As can be seen in Figure 4-31, hydrogen permeation flux increased with increasing temperature. The linear relationship between the hydrogen flux and the square root of the pressure difference indicated that the pressure exponent (n) is close to 0.5 in the temperature range of 723-873 K (Appendix B, Table B-2). This n value was determined by taking the sum of the greatest least squares regression value for the all the temperatures. Therefore, bulk diffusion is the controlling step in hydrogen permeation[38]. The apparent activation energy (E_a) of hydrogen permeation, which was calculated according to the Arrhenius plot shown in Figure 4-32, was approximately 5.4 kJ/mol, agreeing well with the reported values of 6.38 [12], 5.73 [149] and 5.7 kJ/mol [150]. However, higher E_a values of 9.8 [88], 11.36 [151] and 15.5 kJ/mol [82] have also been reported, indicating that the E_a value of Pd/Ag membranes is an indication of the net effects of a number of factors. Irrespective to the uniformity of the membrane, the E_a of the Pd/Ag membranes is closely related to the weight ratio between Pd and Ag. For example, Pd/Ag membranes with 20-23 wt.% of Ag possess a relatively low E_a. Also, E_a is dependent on the controlling step of the hydrogen permeation. For instance, the E_a value for the hydrogen permeation process controlled by bulk diffusion is lower than that controlled by surface exchange.

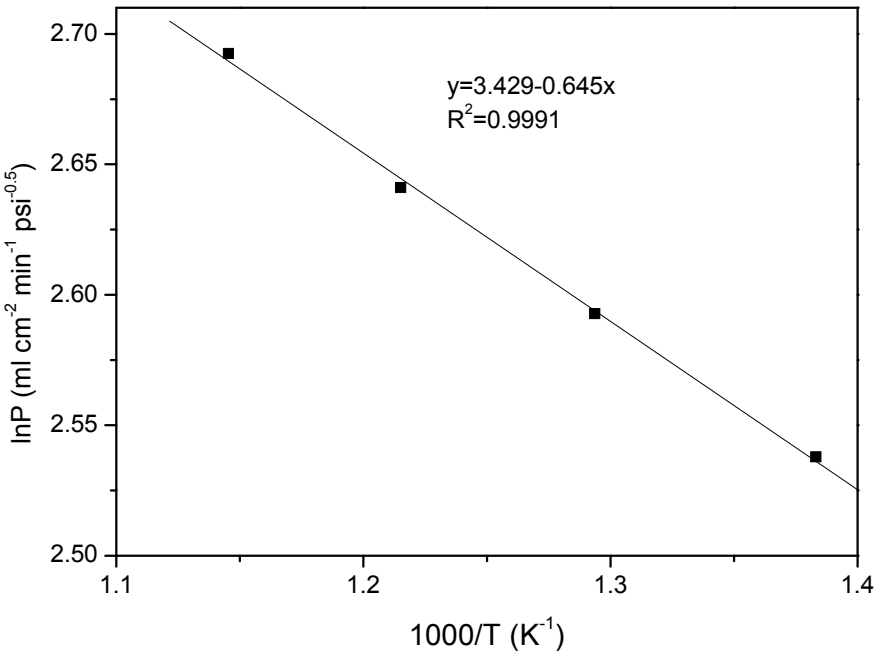


Figure 4-32 Arrhenius plot of hydrogen permeance for Pd/Al_2O_3 hollow fibre composite membrane

4.3.6 Dehydrogenation of propane to propene

The performance of the iHFMR was compared with a fixed bed reactor (FBR), in which 0.1 g of Pt(0.5wt.%)/γ-alumina catalyst was packed into the centre of a dense ceramic tube of 9 mm in diameter. As can be seen in Figure 4-33, the propane conversion in the FBR started at about 22 % and then reduced to about 8 % after 40 min, which is close to the equilibrium conversion of propane at 723 K. In the meantime, the propene selectivity increased from about 34 % to 80 %. This trend agrees well with the work of Lobera [152], in which the coke content increased abruptly in approximately the first 10 min, causing quick catalyst deactivation at the initial stage of the reaction. As the propane conversion was calculated based on the amount of propane reactant left in the product stream in the FBR, the initial propane conversion in Figure 4-33 is above the equilibrium. This further indicates that coke-formation is the dominant reaction at this

stage. In the case of the iHFMRs, the initial propane conversion of the 1st iHFMR was measured to be about 37 %, which is approximately 68 % higher than that of the FBR.

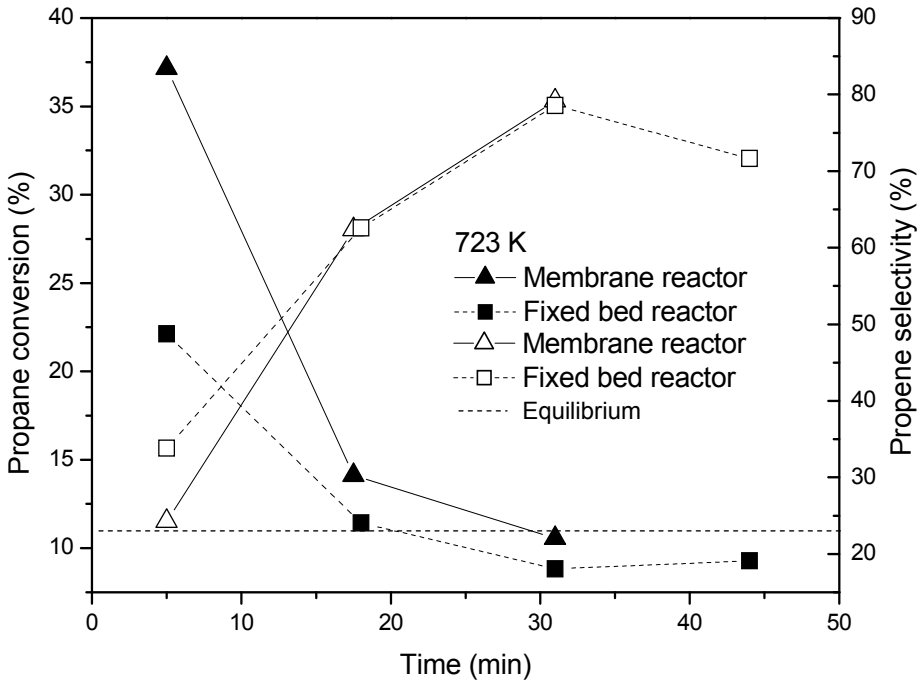


Figure 4-33 Propane conversion (solid symbols), equilibrium conversion (--- dashed lines), propene selectivity (open symbols) of the inorganic hollow fibre membrane reactor (iHFMR) and fixed bed reactor (FBR) at 723 K

Similar results listed in Table 4-9, was also obtained for a 2nd and 3rd iHFMRs. This indicates that although the iHFMR achieved higher conversions during the initial stages of the reaction, it suffered a faster decrease in the conversion possibly due to more serious carbon deposition [141]. As coke formation appears to be also dominant in the FBR during the first several minutes, this suggests that the use of membrane reactor actually promotes more coke formation. This problem may be overcome by using coking-resistant catalysts such as Pt-Sn supported catalyst [153]. In commercial dehydrogenation operations, the generation of hydrogen from the reaction serves to reduce the tendency for carbon formation. Although the removal of generated hydrogen

in a membrane reactor contributes to an increase in conversion and yield of the reaction (Figure 4-34), it aggravates the formation of carbon, which may block the surface of the catalyst, foul the reactor or even accumulate on the membrane surface, blocking further hydrogen permeation [141]. Instead of removing hydrogen as soon as it forms, a certain amount of hydrogen should be deliberately kept in the reaction zone to mitigate catalyst deactivation, although the conversion of the reaction is reduced at the same time.

Table 4-9 Propane conversion and propene selectivity of iHFMRs

	Time (min)	Propane conversion %	Propene selectivity %
1st iHFMR	5	37.2	24.3
	17.5	14.1	62.4
2nd iHFMR	5	35.7	27.9
	16	12.3	75.5
3rd iHFMR	5	42.1	-
	45	6.3	-

Figure 4-33 further illustrates that the difference in performance between the two reactor designs is diminished as a function of time. One of the possible reasons for this result is that due to the relatively low propane conversion at 723 K, the amount of hydrogen produced in the iHFMRs was small. Hence, limited driving force of the hydrogen can be built up for the hydrogen permeation, leading to the similar performances between iHFMR and FBR. For endothermic dehydrogenation reactions, the high demand for heat means that the products of reaction can be trapped within the pores of the catalyst, resulting in fast catalyst deactivation as a consequence of carbon deposition [141]. So it is logical to conclude that hydrogen permeation through the membrane is not the rate limiting process, because the rate of hydrogen production in the catalytic membrane reactor is limited by catalyst productivity [154]. As a result, use of coking-resistant catalysts with enhanced catalytic activity is critically important to

further improve the performance of the membrane reactor. However, because of the high surface area of the asymmetric substrates, comparable propane conversion and propene selectivity were obtained with much less catalyst (around 1.15 mg in the reaction zone) employed in the iHFMR compared to that of FBR.

In order to compare the fixed bed tests to that of the membrane reactor, space-time yields (STY) and propene yield was calculated. The STY measures the amount of propene produced per gram of catalyst per hour. Table 4-10 shows the space-time yields (STY) of the 1st iHFMR and FBR. As can be seen, the STY of the iHFMR is more than 6 times that of the FBR. It should be noted that this value can be further increased to approximately 14 when smaller ceramic substrates (OD = 1.3 mm) with similar asymmetric structures are employed [15]. Moreover, the STY of the iHFMR, in view of the amount of catalyst employed, is more than 60 times that of the FBR, indicating that the iHFMR is more efficient in propene production. This demonstrates another advantage of the iHFMR in propane dehydrogenation. Figure 4-34 shows the propene yields for the FBR and iHFMR tests. The FBR achieved yields of about 4.25 %, while the iHFMRs produced yields reaching 8.30 % after 31 min.

Table 4-10 Space-time yields (STY) of the 1st iHFMR and FBR

Time (min)	STY of iHFMR		Time (min)	STY of FBR	
	(mol propene/ $m^3 \cdot h$)	(g propene/ g catalyst · h)		(mol propene/ $m^3 \cdot h$)	(g propene/ g catalyst · h)
5	2488.6	12.8	5	398.6	0.21
17.5	2431.6	12.5	18	379.6	0.20
31	2298.6	11.8	31	367.0	0.19
			44	352.2	0.18

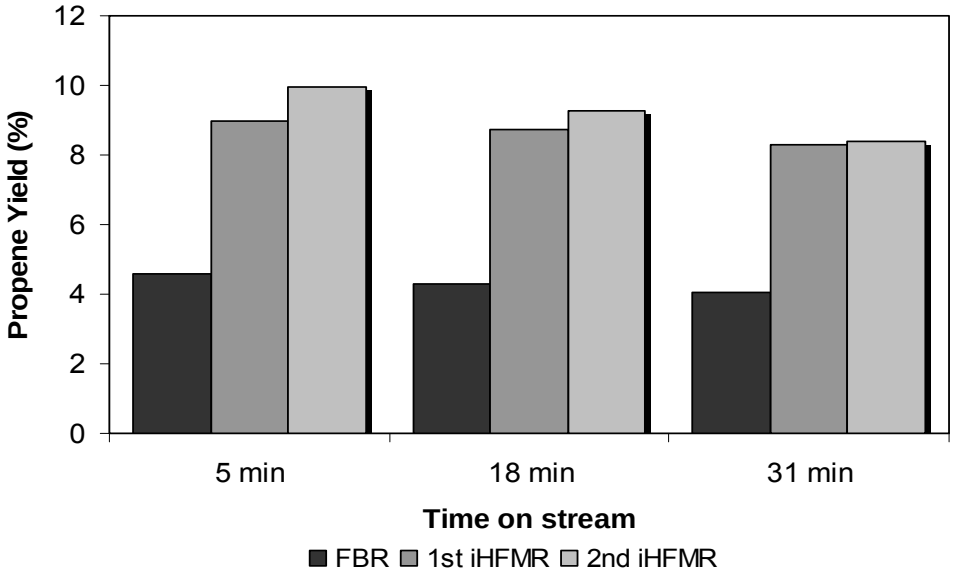


Figure 4-34 Propene yields of FBR and iHFMR

To further assess the performance of the iHFMR, a 3rd iHFMR was employed in propane dehydrogenation using the same operating conditions described previously. As shown in Table 4-9, similar to the other two iHFMRs, the propane conversion of the 3rd iHFMR decreased from 42.07 % at 5 min to 6.29 % after 45 min as a result of catalyst deactivation. The reactor was then regenerated at 773 K for 2 h, using a stream consisting of 40 % O_2 and 60 % Ar. As shown in Figure 4-35, after the regeneration the initial propane conversion was recovered to 38.89 %, which is approximately 8 % lower than that of the fresh iHFMR. In addition, the final propane conversion was about 5.54 %.

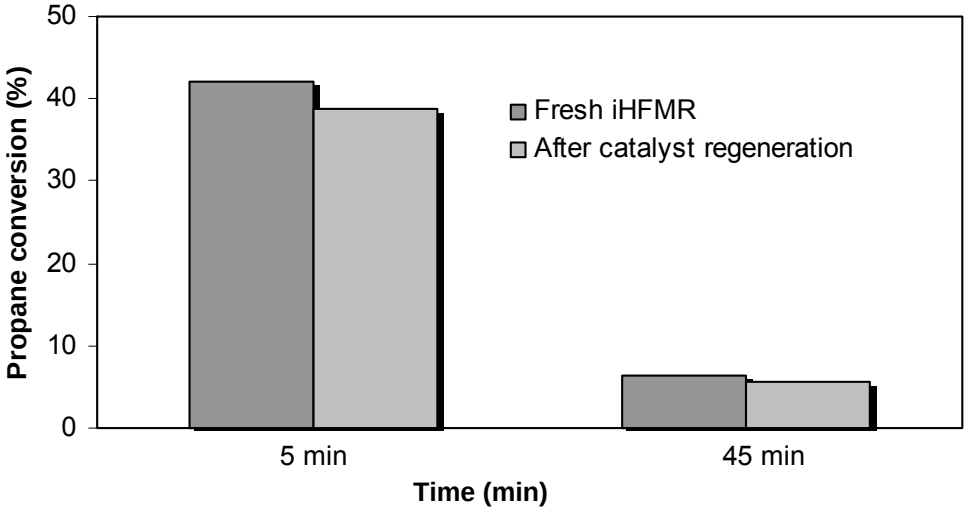


Figure 4-35 The performance comparison of a third iHFMR in the dehydrogenation of propane

Although high initial propane conversions have been achieved in the iHFMRs, quick catalyst deactivation is still a challenge. In order to improve the performance of the iHFMR in dehydrogenation reactions, coking-resistant catalysts such as Pt-Sn catalysts with sufficiently great activity at high operating temperatures should be used. Furthermore, the beneficial effect of the highly compact multifunctional iHFMR developed in this study can be employed in other catalytic reactions with less coking problems such as steam reforming (SR) or water-gas shift (WGS) reactions.

4.4 Conclusions

Al_2O_3 hollow fibre substrates with a unique asymmetric structure were prepared by a combined phase inversion/sintering technique. The asymmetric structure consists of long finger-like voids and a uniform outer sponge-like layer of about 60-70 μm in thickness. Based on this analysis, the outer sponge-like layer of the substrate provides a sufficiently smooth surface for direct coating of thin and dense Pd/Ag membranes for hydrogen separation. After depositing sub-micron sized Pt(0.5wt.%)/γ-alumina catalyst particles in the finger-like voids, a highly compact multifunctional membrane reactor was developed and applied to the dehydrogenation of propane to propene. At an operating temperature of 723 K, propane conversion as high as 42 % was achieved in the iHFMR at the initial stage of the reaction with propene yields almost double that of the FBR. The advantage of using iHFMR compared to FBR is diminished after 40 min of operation due to deactivation of the catalyst and the low equilibrium conversion of propane. However, due to the high surface area of the asymmetric substrates, comparable propane conversion and propene selectivity were obtained with much less catalyst employed in the case of iHFMR, which clearly demonstrated the advantages of the developed iHFMR.

CHAPTER 5

A Multifunctional Pd/Alumina Hollow Fibre Membrane Reactor for Propane Dehydrogenation

Abstract

Following the successful development of a hollow fibre membrane reactor (HFMR-I) in chapter 4, a highly compact multifunctional Pd/alumina hollow fibre membrane reactor (HFMR-II) was further developed and applied to the catalytic dehydrogenation of propane to propene. The developed HFMR-II consists of a thin and defect free Pd membrane coated directly onto the outer surface of an alumina hollow fibre substrate with a unique asymmetric pore structure, i.e. a sponge-like outer layer and a finger-like inner layer where Pt(1 wt.%)/SBA-15 catalyst is deposited. Benefiting from this novel design, the functionalized alumina hollow fibre substrates with a surface area/volume value of up to 1918.4 m^2/m^3 possess a catalyst surface area of 31.8 m^2/g, which is significantly higher than that of the HFMR-I in which Pt (0.5 wt%)/γ-Al_2O_3 catalyst is deposited. In contrast with a conventional fixed-bed reactor (FBR), greater propene selectivity, propene yield and a one order of magnitude higher space-time yield (STY) have been achieved by using the HFMR-II for propane dehydrogenation. Although the process controlling step in the HFMR-II is believed to be the catalytic reaction, as a consequence of catalyst deactivation due to coke-formation, the advantages of HFMR-II, such as easy catalyst deposition and high catalytic surface area for catalytic reactions, are possibly more promising for other catalytic reactions with less coking problems, such as the water-gas shift (WGS) reaction and steam reforming (SR) etc.

5.1 Introduction

In the last several decades, inorganic catalytic membrane reactors (CMR) combining catalytic reaction and separation into a single unit have attracted extensive attention in the research community [121, 141, 155, 156] and can be divided into two major categories of dense CMRs in view of the function of the membranes. The first is the use of a membrane to selectively remove a product from a reaction that is limited by chemical equilibrium [38, 157], shifting the reaction towards the product side and simplifying subsequent product separations. The second is the use of a membrane to simultaneously purify and uniformly distribute a reactant throughout the reactor [1, 158], offering a high level of control over how the reactants interact.

Use of Pd or Pd-alloy membranes in CMRs, where the membrane "extracts" hydrogen - a critically important energy carrier - from a reaction, have been proved experimentally and theoretically to be efficient in enhancing conversions and/or lowering operating temperatures of endothermic, equilibrium-limited reactions [38, 141] such as dehydrogenation of propane ($C_3H_8 \leftrightarrow C_3H_6 + H_2, \Delta H° = 124 kJ/mol$) [12, 13]. Thin and defect-free Pd or Pd-alloy membranes with high hydrogen permeability and selectivity can be supported by porous alumina hollow fibres [19, 78, 85, 86, 132, 144-146] with to date the highest surface area/volume value, demonstrating the advantages of using composite membranes of this type in hydrogen separation. Moreover, in a recent work by Kingsbury et. al., porous alumina hollow fibres with a unique asymmetric pore structure [16], i.e. a sponge-like outer layer and a finger-like inner layer, have been developed by using a one-step dry-wet spinning/sintering technique [144]. Such alumina hollow fibres have also been used for the construction of a highly compact hollow fibre

membrane reactor (HFMR-I) for propane dehydrogenation by directly coating a thin Pd/Ag membrane onto the outer surface of the alumina hollow fibres and depositing Pt (0.5 wt%)/γ-Al_2O_3 catalyst into the finger-like inner layer [135, 159]. The deposition of sub-micron sized catalyst particles was repeated 3 times in order to obtain a reasonable loading of catalyst, offering an increase in the surface area of the reaction zone (5 cm in length) of up to about 0.22 m^2 in the HFMR-I made with a single hollow fibre.

In order to further improve the process of depositing catalyst into the asymmetric alumina hollow fibres and to achieve a higher surface area in the reaction zone, which can be critically important in improving the performance of CMRs in catalytic reactions such as water-gas shift (WGS) and steam reforming (SR) reactions, mesoporous silica (SBA-15) [160] with a surface area as high as about 850 m^2/g [161] and significant thermal stability up to 1473 K [162] has been prepared inside the finger-like structure of the asymmetric alumina hollow fibres in this study, by using an easy and efficient method via liquid-paraffin-medium protected solvent evaporation [163, 164]. After impregnating Pt onto the deposited SBA-15 and coating a Pd hydrogen separation membrane onto the outer surface of the functionalized alumina hollow fibre substrates, a highly compact multifunctional HFMR-II with a surface area/volume ratio of up to 1918.4 m^2/m^3 is developed. Greater propene selectivity as well as a one order of magnitude higher space-time yield (STY) has been achieved when compared with a conventional fixed bed reactor (FBR) for propane dehydrogenation. In contrast with HFMR-I developed in Chapter 4 of this work, a significant increase in the surface area of HFMR-II is achieved by replacing γ-Al_2O_3 with mesoporous SBA-15. Although the performance of two HFMR designs are comparable as a consequence of catalyst deactivation during the dehydrogenation of propane, the advantages of HFMR-II can be applied to other

catalytic reactions of great importance, such as WGS and SR etc. with less catalyst deactivation problems.

5.2 Experimental

5.2.1 Materials

Alumina hollow fibres

Aluminium oxide powders of 1 μm (alpha, 99.9% metals basis, S.A. 6-8 m^2/g), 0.05 μm (gamma-alpha, 99.5% metals basis, S.A. 32-40 m^2/g) and 0.01 μm (gamma-alpha, 99.98% metals basis, S.A. 100 m^2/g) were purchased from Alfa Aesar and were used as supplied. Polyethersulfone, (PESf, Radel A-300, Ameco Performance, USA), N-methyl-2-pyrrolidone (NMP, HPLC grade, Rathbone) and Arlacel P135 (Uniqema, UK) were used as binder, solvent and additive, respectively. DI water and tap water were used as the internal and external coagulants, respectively, for the fabrication of alumina hollow precursor fibres.

Electroless plating of Pd membrane

$Pd(NH_4)_2Cl_4$ (Ammonium tetrachloropalladate, 99.99%, Sigma Aldrich), $SnCl_2 \cdot 2H_2O$, $Na_2EDTA \cdot 2H_2O$, HCl (37%), N_2H_4 and $NH_3 \cdot H_2O$ (28%) (Fisher Sci. Ltd) were used for preparing the Pd hydrogen separation membrane.

Mesoporous silica SBA-15

Tetraethoxysiliane (TEOS) as a silica source and poly-(ethylene oxide)-poly(propylene oxide)-poly(ethylene oxide) (PEO-PPO-PEO) amphiphilic block copolymer $EO_{20}PO_{70}EO_{20}$ (Pluronic P123, MW=5800, Aldrich) as a structure-directing

agent were used for the preparation of mesoporous silica SBA-15. H_2PtCl_6 (99.995%, Aldrich) as a Pt source was used for preparing Pt(1 wt.%)/SBA-15 catalyst.

5.2.2 Fabrication of multifunctional HFMR-II

Asymmetric alumina hollow fibre substrates

Asymmetric alumina hollow fibre substrates were fabricated via by the dry-wet spinning/sintering technique [144]. The preparation of the alumina spinning suspension has been described in the previous chapters [16]. The resultant spinning suspension was degassed under vacuum for 2 h to fully remove air bubbles trapped inside. After degassing, the suspension was transferred to a 200 ml Harvard stainless steel syringe and was extruded through a tube-in-orifice spinneret (ID 1.2 mm, OD 3.0 mm) into a coagulation bath containing 120 litres of water with an air-gap of 15 cm. DI water was used as the internal coagulant and the flow rate ranged from 5 to 15 ml/min. The extrusion rate of the spinning suspension and the flow rate of the internal coagulant were accurately controlled and monitored by two individual Harvard PHD 22/2000 Hpsi syringe pumps, ensuring the uniformity of the prepared precursor fibres. The formed precursor fibres were first heated in a CARBOLITE tube furnace at 873 K for 2 h to remove the organic polymer binder and were then sintered at 1723 K for 4 h with heating and cooling rates of 5 K/min. The outer surfaces of the sintered substrates (about 30 cm in length) were coated with a thin and gas-tight glaze layer with the exception of the central part of the fibre of 5 cm in length, which was left unglazed for the subsequent electroless plating (ELP) of the Pd membrane.

Catalyst preparation and deposition

The synthesis of mesostructured silica monoliths, which were used as the support for the Pt catalyst, has been reported elsewhere [163]. For a typical synthesis, 5

g of P123 was first dissolved fully in a mixture consisting of 25 g of ethanol and 1 g of aqueous HCl (1 mol/L). 10.4 g of TEOS was then slowly added to the solution under stirring, forming a transparent sol. The unglazed outer surface of the alumina hollow fibre substrate was covered by a thin layer of epoxy resin and the fibres were immersed in the resultant sol and were degassed under vacuum for 1 h at room temperature, removing air trapped in the finger-like voids of the substrates and allowing the infiltration of the sol into the substrates. After degassing, the remaining sol in the substrate lumen was expelled using compressed air. The substrates were then placed in a flowing air stream at room temperature for 48 h, during which the sol in the substrates changed to gel. After that, the substrates were heated at 333 K for 20 h in liquid paraffin and sintered at 823 K for 6 h with heating and cooling rates of 0.5 K/min, during which time the gel changed into silica SBA-15 inside the finger-like voids of the substrate, while the thin epoxy resin layer on the outer surface of the substrate was simultaneously removed. The amount of deposited silica SBA-15 was determined by measuring the weight gain of the samples. Pt was subsequently impregnated onto the deposited silica SBA-15 by immersing the resultant samples in an aqueous solution of H_2PtCl_6 at room temperature. After impregnation, the substrates with the Pt (1 wt.%)/SBA-15 catalyst in the finger-like voids were dried at 383 K overnight and calcined at 773 K for 4 h with heating and cooling rates of 2 K/min.

Pd membrane coating

The Pd membranes were coated directly onto the unglazed outer surface of the functionalized alumina hollow fibre substrates by a conventional ELP method [38]. Prior to coating, the substrates were cleaned and activated by the Pd-Sn activation procedure. The activation process consisted of successive immersion of the substrates in tin (II) chloride ($SnCl_2$) solution and palladium chloride ($PdCl_2$) solution at room temperature.

Deionised water and 0.1 M HCl were used to rinse the samples between the immersions. The activation process was repeated 6 times, after which the substrate surface turned brown. The Pd membrane was coated using a plating bath with the same composition described elsewhere [128].

5.2.3 Characterization of HFMR-II

The morphology of the asymmetric alumina hollow fibre substrates, the coated Pd membranes and the mesoporous silica SBA-15 deposited into the finger-like voids were visually observed using a scanning electron microscope (SEM, JEOL JSM-5610LV, Tokyo, Japan). The pore structures of the functionalized asymmetric alumina hollow fibre substrates were characterized by mercury intrusion porosimetry (Autopore IV 9500, Micromeritics) and BET and from the adsorption branch of the isotherms using the BJH method. EDS analysis (INCA Energy by Oxford Instruments) was employed to investigate the elemental distribution across the cross sections of the composite Pd/alumina hollow fibre membranes.

5.2.4 Dehydrogenation of propane to propene using HFMR-II

The apparatus for dehydrogenation of propane to propene has been described in Chapter 4. A gaseous stream containing propane (5 vol.%) and hydrogen (4.5 vol.%) with balanced nitrogen was introduced at 30 ml/min into the lumen of the reactor. Argon with a flow rate of 50 ml/min was used as a sweep gas to carry the permeated hydrogen to a TCD gas chromatograph (Varian-3900) for analysis. The membrane reactor was operated at atmospheric pressure and the effluent gases from the reactor were analyzed on-line using a FID gas chromatograph (Varian-3900).

5.3 Results and Discussion

5.3.1 Microstructure of asymmetric alumina hollow fibre substrates

As a result of instabilities at the interface between the non-solvent (internal coagulant) and the spinning suspension [16], the prepared alumina hollow fibre substrates possess a unique asymmetric pore structure that is characterized by a thin, uniform sponge-like outer layer and a thick finger-like inner layer (Figure 5-36(a) and (b)). Finger-like voids extend across approximately 80 % of the fibre cross section from a highly porous inner surface (Figure 5-36c) with the remaining 20 % consisting of the sponge-like outer layer, forming a smooth and denser outer surface (Figure 5-36d). The entrances of the finger-like voids exist on the highly porous inner surface and open into micro-channels (Figure 5-36e), while no finger-like structures are found in the sponge-like outer layer (Figure 5-36f). The OD and ID of the sintered hollow fibre substrates with uniform wall thickness were measured at approximately 1893 μm and 964 μm, respectively, resulting in a surface area/volume value of up to 1918.4 m^2/m^3. It should be noted here that this value can be further increased to 2789.0 m^2/m^3 when porous YSZ hollow fibres (OD=1300 μm) with similar asymmetric structures [15] are employed, yielding a significantly higher surface area per volume value for HFMRs.

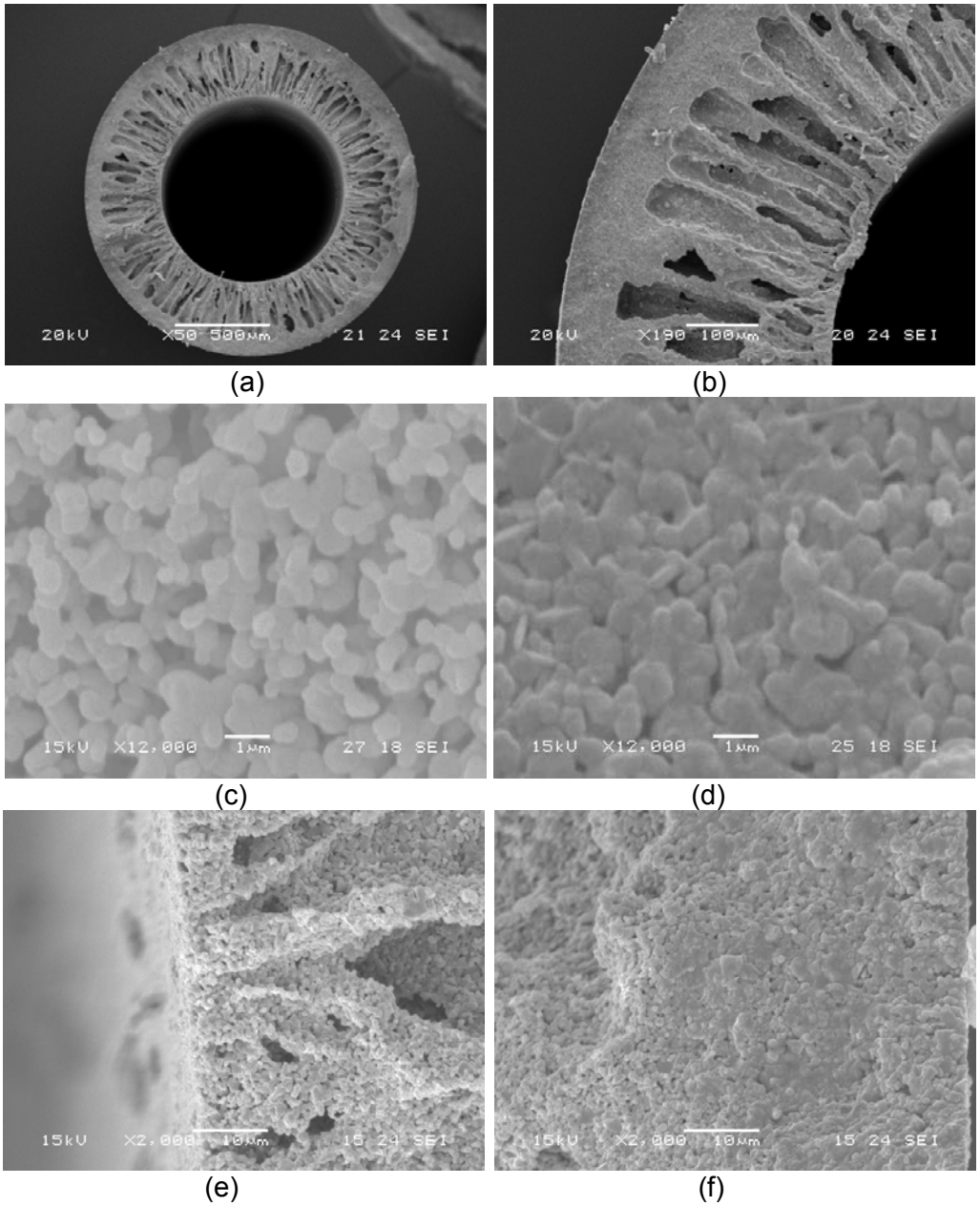


Figure 5-36 SEM images of the asymmetric alumina hollow fibre substrate sintered at 1723 K for 4 h: (a) whole view, (b) cross section, (c) inner surface, (d) outer surface, (e) inner edge and (f) outer edge

The asymmetric pore structures, especially those above 100 nm, of the sintered alumina hollow fibre substrates were then quantified by mercury intrusion porosimetry. As can be seen in Figure 5-37, two distinct peaks, i.e. a narrow, strong peak at 6.03 μm and a wide, weak one at 151.4 nm are observed, indicating the mean pore sizes of the

entrance of the highly porous inner region (Figure 5-36c) and the denser sponge-like outer region (Figure 5-36d), respectively. In contrast with the sponge-like outer layer, the pore volume of the finger-like inner layer is significantly higher, further proving the feasibility of developing a highly compact multifunctional HFMR by depositing catalyst into the finger-like voids through the highly porous inner skin-layer of the substrate.

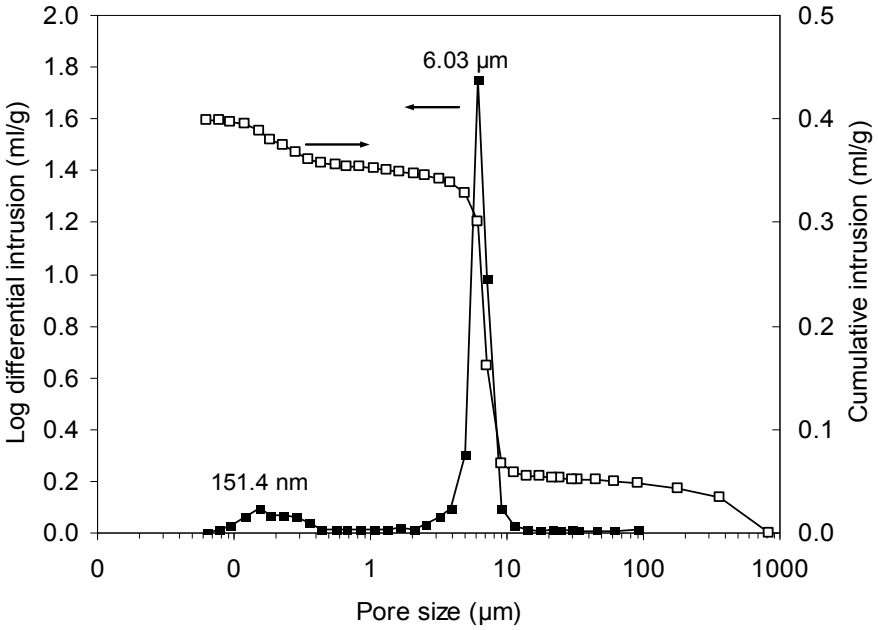


Figure 5-37 Mercury intrusion of asymmetric alumina hollow fibre substrates sintered at 1723 K for 4 h

5.3.2 Microstructure of the functionalized alumina hollow fibre substrates

Prepared mesoporous SBA-15 yields a type IV isotherm with a H1 hysteresis loop (Figure 5-38), which agrees well with a typical adsorption and desorption for mesoporous materials with 2D-hexagonal structures [160]. A well defined step occurs at about p/p^0=0.45-0.55, associated with the filling of the mesopores as a result of capillary condensation. A narrow pore size distribution (inset of Figure 5-38), which was calculated from the adsorption branch based on the BJH model, indicates a uniform pore

structure with a mean pore diameter of approximately 4.74 nm, which is consistent with the reported pore sizes of SBA-15 ranging from 4.6 to 30 nm [160]. The BET surface area and the total pore volume of prepared SBA-15 were measured at 596.58 m^2/g and 0.65 cm^3/g, respectively.

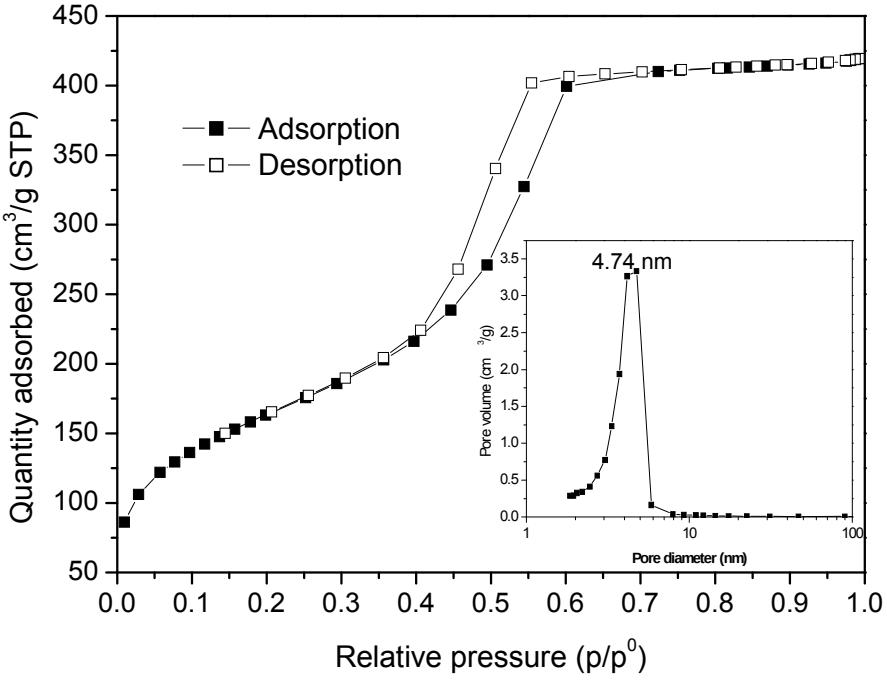


Figure 5-38 Nitrogen adsorption/desorption isotherm plots and pore size distribution curve (inset) of SBA-15 sintered at 823 K for 6 h

The asymmetric alumina hollow fire substrates were then functionalized by preparing SBA-15 inside the finger-like voids followed by impregnation of Pt. As can be seen in Figure 5-39, SBA-15 is successfully deposited into the alumina hollow fibre substrates by using the method described above. Instead of fully blocking the finger-like voids, there is a gap between the deposited SBA-15 and the wall of the finger-like voids after sintering. The pore structures of the inner surface (Figure 5-39c) and the outer surface (Figure 5-39d) are in good agreement with their untreated counterparts, although a small amount of SBA-15 scum is found scattered loosely across the inner surface. The

pore structure of the functionalized substrates, which was further characterized by mercury intrusion and is shown in Figure 5-40, agrees well with that of the untreated substrates (Figure 5-37) except for a new peak at about 62.5 nm, representing one type of pore structure in the deposited SBA-15. A comparison between Figure 5-37 and Figure 5-40 further indicates that the deposition of SBA-15 does not significantly change the pore structure of the hollow fibre substrates, because the pore size distribution representing the entrance of the finger-like voids and the one representing the mean pore size of the outer sponge-like layer are consistent with their untreated counterparts. This further suggests that the deposition of SBA-15 does not create significant additional resistance to gas permeation through the functionalized substrates.

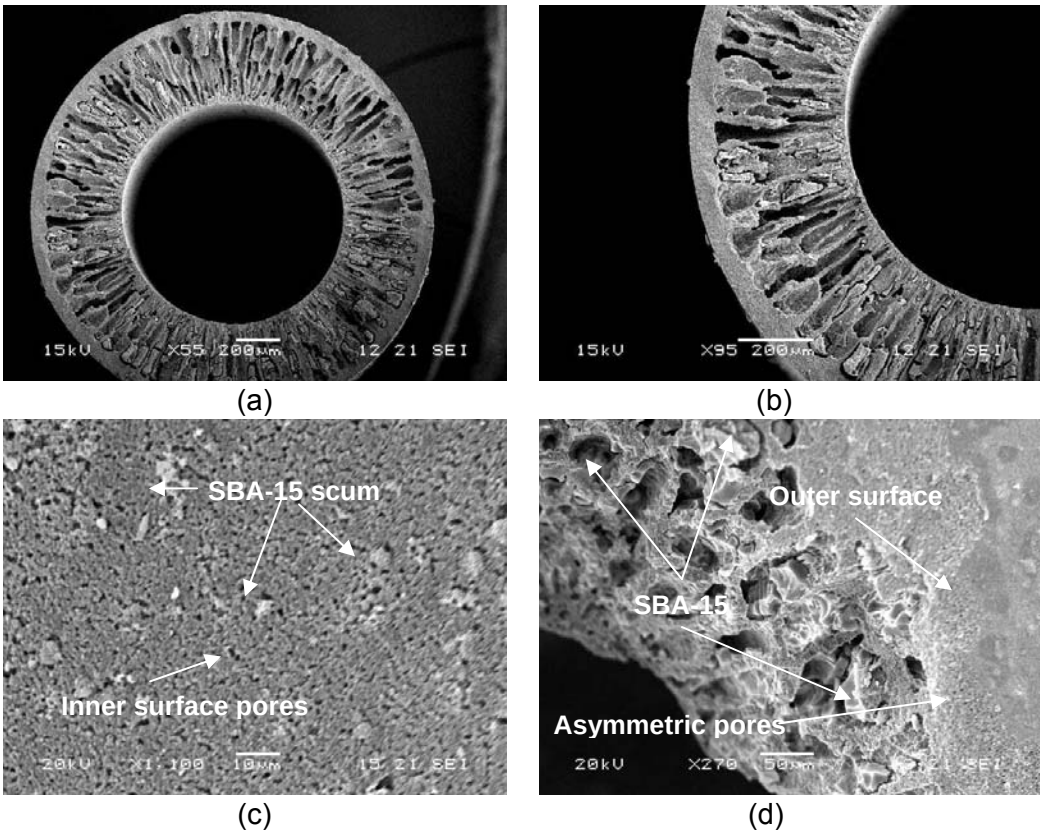


Figure 5-39 SEM images of the functionalized alumina hollow fibre substrate: (a) whole view, (b) cross section, (c) inner surface and (d) top view from outer surface

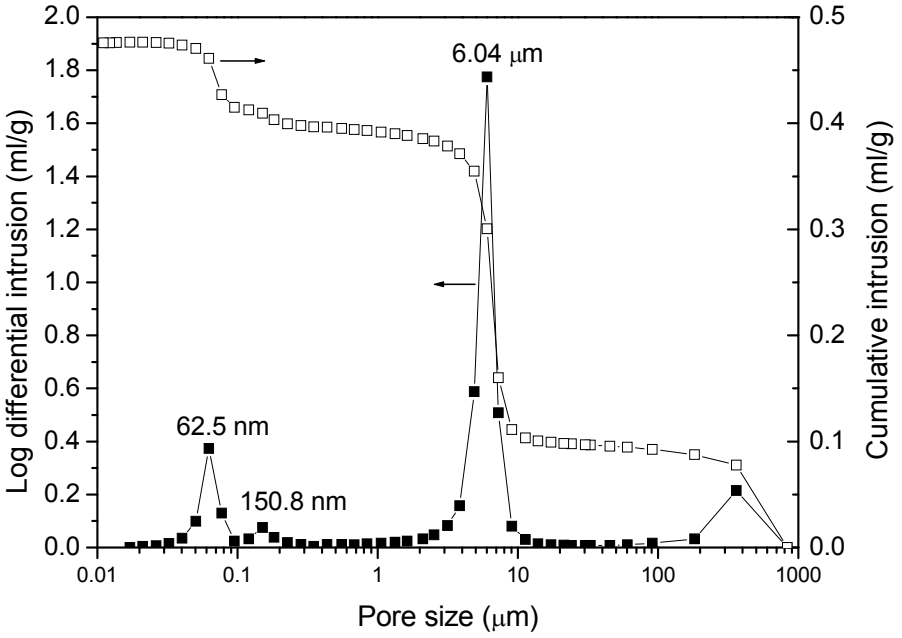


Figure 5-40 Mercury intrusion of the functionalized alumina hollow fibre substrates

The pore structures of the functionalized hollow fibre substrates, especially those less than 100 nm, were characterized by BET. As can be seen in Figure 5-41, the peak at 4.83 nm, which represents the mesoporous structure of the deposited SBA-15, agrees well with that in Figure 5-38, indicating that the major pore structure of the deposited SBA-15 was confined during the deposition. The peak at 44.19 nm should represent the same pore structure as the one at 62.5 nm in Figure 5-40, but differs slightly due to different characterization methods. This indicates that, besides the mesopores in the deposited SBA-15, bigger pores, probably small cracks, were formed during the deposition, which is possibly due to non-uniform shrinking of SBA-15 monoliths in the finger-like voids during the sintering. Furthermore, the functionalized substrates possess a much higher pore volume in contrast with the untreated substrates in view of the pore sizes between 2 and 100 nm, showing the advantages of depositing mesoporous materials of this type into the developed asymmetric hollow fibre substrates in increasing the surface area of the reactor.

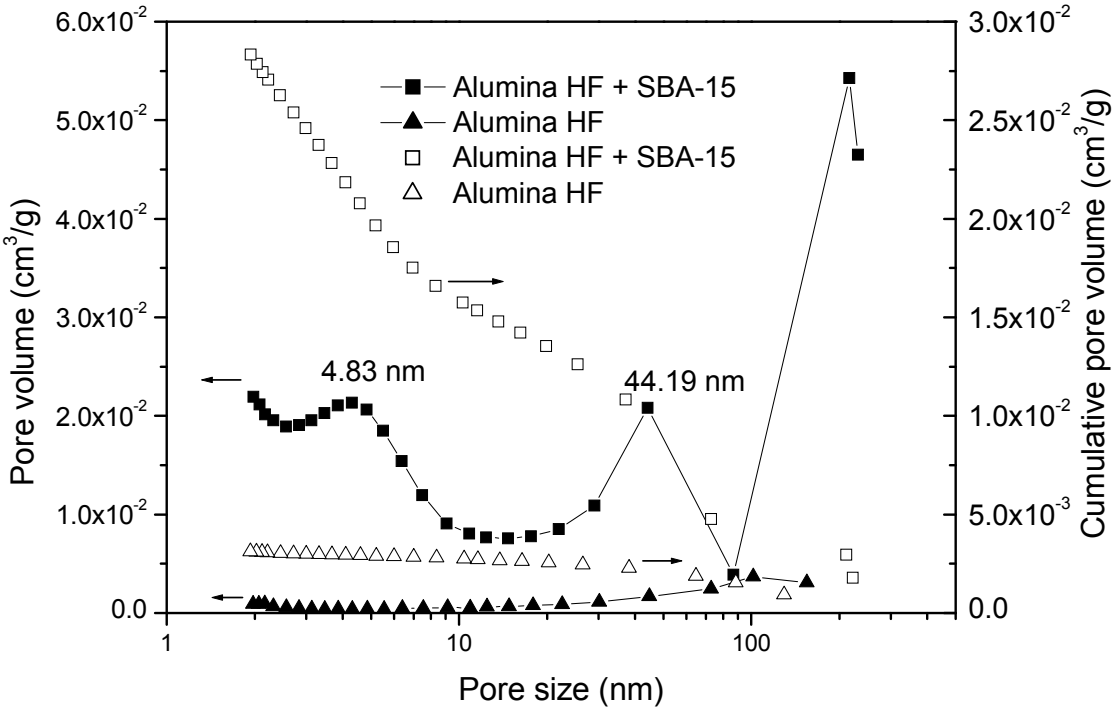


Figure 5-41 Pore size (< 100 nm) distribution and pore volume of functionalized and untreated alumina hollow fibre substrates

The characteristics of the functionalized as well as the untreated substrates are listed in Table 5-11. In comparison with our previous catalyst deposition method [135], in which sub-micron sized catalyst particles were dispersed in solution prior to the deposition, the current method is much more efficient for greater loading of catalyst with a higher surface area, and as a result, yields a significantly higher catalyst surface area in the functionalized substrates. The increase of 5.19 m^2 in the surface area of the reaction zone (5 cm in length) in HFMR-II, which was calculated on the amount of SBA-15 deposited, is much higher than the value of 0.22 m^2 obtained in the previous work for HFMR-I.

Table 5-11: Characteristics of functionalized and untreated alumina hollow fibre substrates

	Deposited material	Weight gain (%)	BET S.A. (m^2/g)	Increase of S.A. in reaction zone (5 cm long) (m^2)
Alumina fibre			0.71	
3rd deposition (HFMR-I) [135]	γ-alumina (180 m^2/g)	0.74	< 2.04	0.22
1st deposition (HFMR-II)	SBA-15 (596.58 m^2/g)	6.96	31.83	5.19

5.3.3 Dehydrogenation of propane to propene

After impregnating Pt into the deposited SBA-15, a multifunctional Pd/alumina HFMR-II was developed by directly coating a Pd membrane of approximately 6 μm in thickness onto the outer surface of the functionalized alumina hollow fibre substrate, using a conventional ELP method [38]. No mechanically weak, intermediate γ-Al_2O_3 layer was employed to modify the substrate surface prior to the coating of the Pd membrane. EDS analysis shown in Figure 5-42 reveals that Pd plating solution penetrated slightly into the substrate (approx. 2 μm beneath the substrate surface) during the ELP process, which also agrees with the previous study [135]. The hydrogen permeation flux through the Pd/alumina hollow fibre composite membrane was investigated and is described elsewhere [128], and is applicable to the composite membranes described here as they were prepared from the same batch using the same preparation conditions.

For comparison, the catalytic activity of the Pt(1 wt.%)/SBA-15 catalyst, which was prepared by a conventional wet impregnation method, was investigated in a fixed bed reactor (FBR) using the same operating conditions as those of the HFMR-II. Approximately 0.1 g of the catalyst was packed into the centre of a dense ceramic tube

of 9 mm in diameter. Initial propane conversion values refer to the analysis of the reaction products after 5 minutes on stream. As can be seen in Figure 5-43, the propane conversion started at 75.3 % at 773 K and then reduced to 9 % after 120 min of the reaction, in agreement with the work of Lobera et al.[152], in which the coke content increased abruptly in approximately the first 10 minutes, causing rapid catalyst deactivation at the initial stage of the reaction. In the meantime, the propene selectivity increased sharply from 2 % to 70 % after around 35 minutes on stream, as a result of deactivation of highly active co-ordinatively unsaturated surface Pt sites by coke [161]. This indicates that, although coke formation is the main reason for catalyst deactivation in the dehydrogenation of propane to propene, the formed coke functioning as a promoter improves the propene selectivity by deactivating the sites that are active for C-C bond activation [161]. Figure 5-43 further illustrates that increasing the operating temperature reduces the propane conversion as well as the propene selectivity due to a higher level of catalyst deactivation, as a consequence of which the operating temperature of the HFMR-II was chosen to be 773 K.

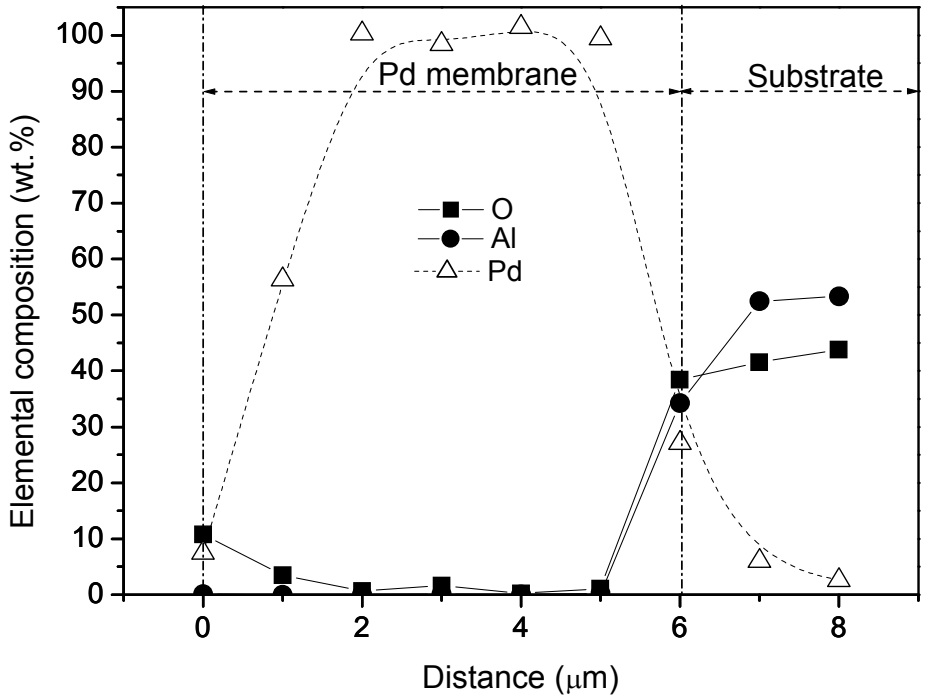


Figure 5-42 EDS analysis of the Pd/alumina composite hollow fibre membrane

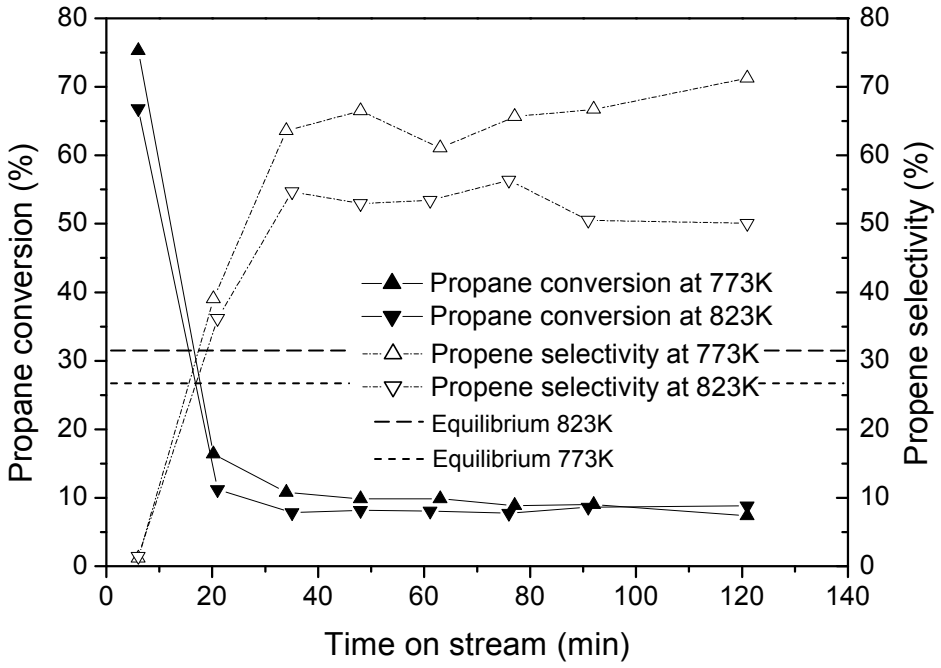


Figure 5-43 Propane conversion (solid symbols), equilibrium conversion (dashed lines) and propene selectivity (open symbols) of the Pt(1 wt.%)/SBA-15 catalysts.

In contrast with the FBR, the initial propane conversion of the HFMR-II was lower and was measured at approximately 48.7%, as shown in Figure 5-44. It has been proved that the use of Pd-based membranes to remove hydrogen as a product from a dehydrogenation reaction enhances the catalyst deactivation in membrane reactors as a consequence of faster coke formation [141]. As a result, in the first several minutes of the reaction, the propane conversion values in the HFMR-II may be significantly higher than 48.7% and drops sharply before the first product sample in Figure 5-44, which was taken 5 minutes after the reaction, was analyzed. As the reaction proceeds, the propane conversions of the HFMR-II and FBR are comparable. For endothermic dehydrogenation reactions, the high demand for heat means that the products of reaction can be trapped within the pores of the catalyst, resulting in rapid catalyst deactivation due to carbon deposition [141]. Therefore, it is logical to conclude that hydrogen permeation through the membrane is not the rate limiting step, because the rate of hydrogen production in a catalytic membrane reactor of this type is limited by the catalyst productivity [154]. Use of coking-resistant catalysts such as Pt-Sn supported catalysts [153] with high catalytic activity and stability is, in this case, critically important to further improve the performance of membrane reactors of this type. However, the propene selectivity of the HFMR-II is higher than that of the FBR, demonstrating the advantages of the developed HFMR-II in view of the amount of the catalyst employed. After 2 h of testing, the HFMR was regenerated at 773 K overnight, using a stream consisting of 5 % of O_2 and 95 % of Ar. As can be seen in Figure 5-44, the propane conversions after the regeneration were slightly lower than that of the fresh HFMR-II, while the propene selectivity was well recovered.

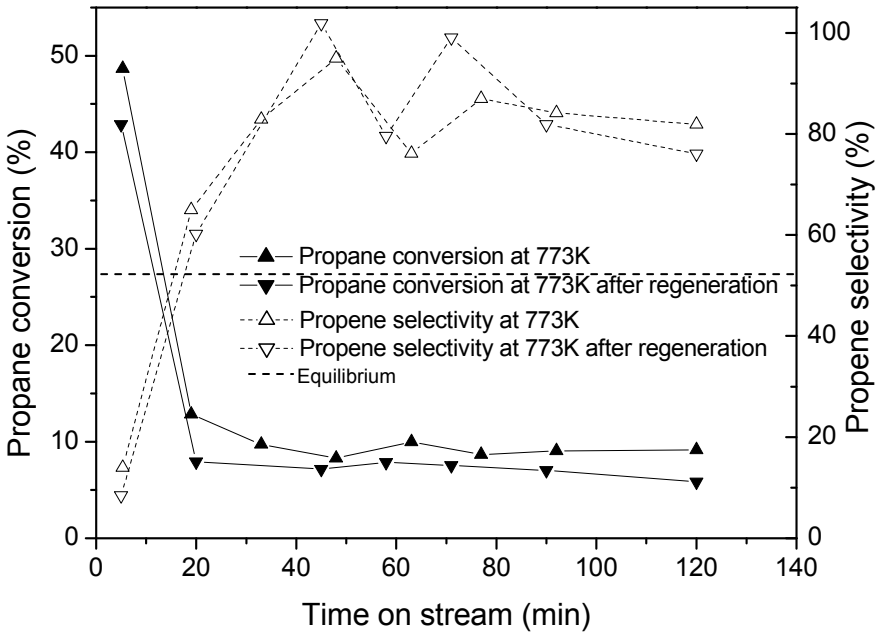


Figure 5-44 Propane conversion (solid symbols), equilibrium conversion (dashed lines) and propene selectivity (open symbols) of the multifunctional HFMR-II.

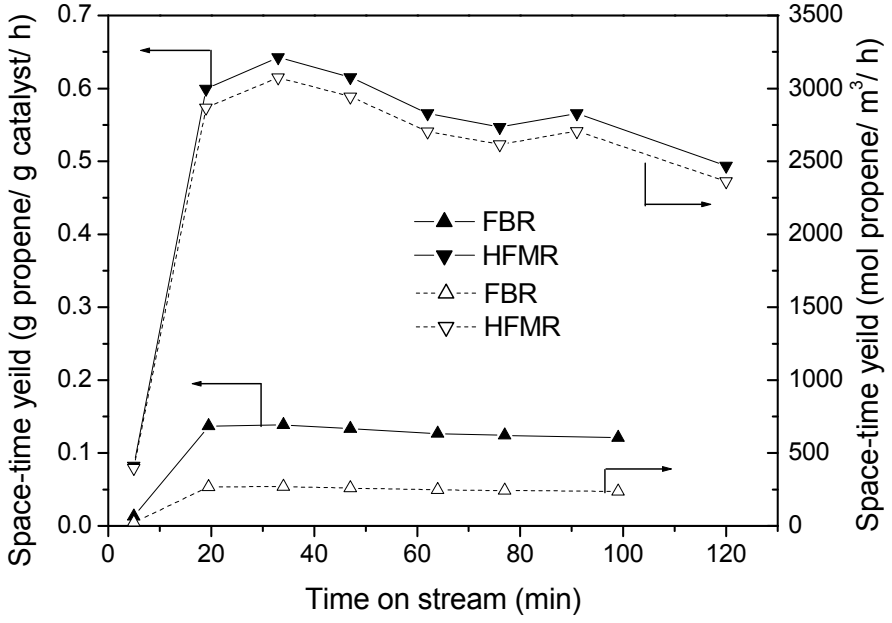


Figure 5-45 The space-time yields (STY) the FBR and the HFMR-II at 773 K

Although the performance of the FBR and the HFMR-II seem to be comparable in view of the propane conversion and the propene selectivity, much less catalyst is required in the HFMR-II because of the greater surface area of the functionalized alumina hollow fibre substrate. As can be seen in Figure 5-45, the volumetric space-time yield (STY) of the HFMR-II is more than 10 times that of the FBR. It should be noted here that this value can be further increased to approximately 20 when smaller ceramic substrates (OD=1.3 mm) with similar asymmetric structures are employed [15]. In addition, the STY of the HFMR-II, in view of the amount of catalyst employed, is more than 4 times that of the FBR, indicating that the HFMR-II is more efficient in propene production. This efficiency in propene production can be seen in Figure 5-46, which shows a comparison of the propene yields of the FBR and HFMR-II. Propene yield increased from 0.9 % in the first few minutes to maximum of 6.9 % in the FBR, and from 6.8 % to a maximum of 8.3 % in the HFMR-II.

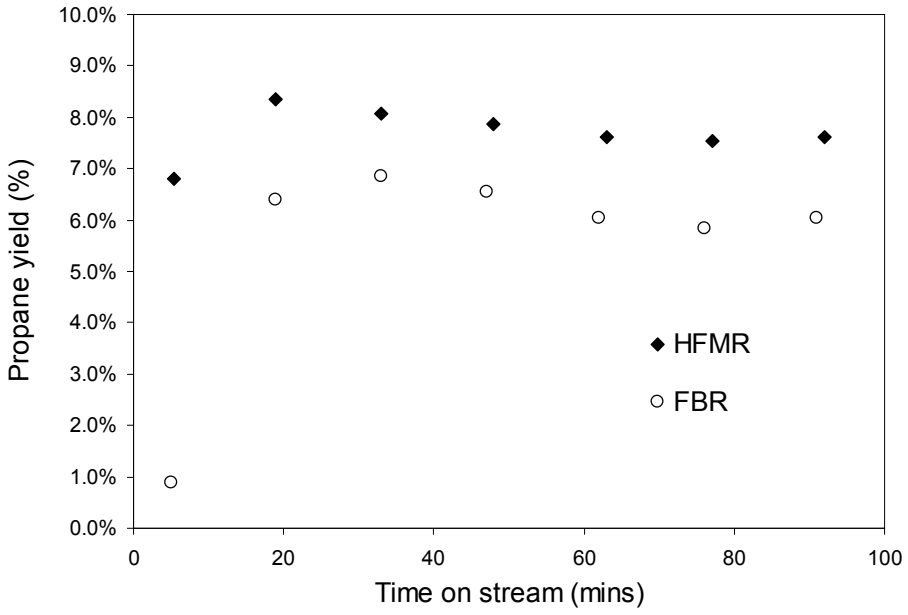


Figure 5-46 Propene yields of FBR and the HFMR-II at 773 K

In comparison with the HFMR-I, described in chapter 4, the performance of the two HFMR designs are comparable in regard to propane conversion as well as propene selectivity, which indicates that higher catalyst loading and surface area in the membrane reactor cannot be appreciated as a consequence of fast catalyst deactivation. However, the advantages of the current HFMR design, which have been demonstrated in this study, can be applied to a number of other catalytic reactions of great importance, such as WGS and SR, with less coke-formation problems.

5.4 Conclusions

Porous alumina hollow fibre substrates with a unique asymmetric pore structure, i.e. a sponge-like outer layer and a finger-like inner layer, and with high surface area/volume ratios of up to 1918.4 m^2/m^3 have been prepared by a one-step dry-wet spinning/sintering method. These substrates are employed to construct a highly compact multifunctional Pd/alumina hollow fibre membrane reactor for dehydrogenation of propane. Prior to the direct coating of Pd membranes onto the outer surface of the developed substrates, the substrates were functionalized by depositing mesoporous SBA-15 with a surface area as high as 596.58 m^2/g into the finger-like inner layer, using an easy and efficient method via liquid-paraffin-medium protected solvent evaporation, followed by the impregnation of Pt. This offers both a high catalyst loading and an increase in the surface area of the reaction zone (5 cm in length) in the HFMR-II of 5.19 m^2. The novel design achieved better propene selectivity and yield in the HFMR-II with less catalyst when compared with a conventional fixed bed reactor (FBR) under the same operating conditions, indicating that the developed HFMR-II is more efficient in propene production. The space-time yield (STY) of the HFMR-II was more than 10 times that of the FBR, demonstrating the advantages of the developed HFMR. In comparison with HFMR-I, similar propane conversion as well as propene selectivity were obtained, indicating that higher catalyst loading and surface area in the membrane reactor cannot be appreciated as a consequence of coke-formation. However, the advantages of HFMR-II can be applied to other catalytic reactions with less coking problems, such as the water-gas shift (WGS) reaction and steam reforming (SR) etc.

CHAPTER 6

A Pd/Alumina Functionalized Hollow Fibre Membrane Reactor for Water-Gas Shift Reaction

Abstract

In this chapter, porous alumina hollow fibres with an asymmetric morphology, i.e. a finger-like structure and sponge-like structure, are prepared and functionalized by depositing Pt/CeO_2/SBA-15 catalyst into the finger-like macro-voids. Such functional alumina hollow fibres are used to develop a highly compact membrane reactor by electroless plating a Pd membrane with a thickness of approximately 2 microns for the water-gas shift (WGS) reaction. The performance of a membrane reactor design of this type is systematically evaluated and compared with a fixed bed reactor (FBR) and porous membrane reactor (PMR). The results indicate that depositing a small amount of catalyst (approximately 30 mg in this study) into the finger-like macro-voids significantly improves the interaction between reactants and catalyst without significantly impacting gas transfer from the reaction zone to the Pd membrane. This leads to a high hydrogen recovery rate of up to nearly 99 % and better hydrogen yields. However, at relatively low reactant flow rates, the efficient hydrogen separation does not significantly “shift” the reaction towards the product side as the access of reactants to the deposited catalyst is the controlling step. This can be improved by the net-effect of hydrogen separation and probably greater turbulence in the lumen as a result of higher reactant flow rates, although elevated operating temperatures and/or higher sweep gas flow rates, in this case, are suggested to promote H_2 separation.

6.1 Introduction

A membrane reactor (MR) is a unit coupling catalytic reaction and membrane separation and has been widely studied in the last several decades [103, 141, 156, 165]. The advantage of a membrane reactor to selectively remove/separate products from or introduce/distribute reactants into a reaction zone while a catalytic reaction is taking place offers the potential for higher conversion/yield by "shifting" the reaction towards the product side or to better control the contact between reactants. It has also been proved that, reduced membrane thickness and enlarged membrane surface area per unit volume of MRs are always beneficial for improving membrane separation, as well as promoting the catalytic reaction. On the other hand, a more active catalyst with a larger surface area and a greater access to reactants are preferred for increasing the processing capability of MRs. As a result, the performance or efficiency of a MR design is always determined by two factors, membrane separation and catalytic reaction.

In conventional MR designs, an excessive amount of catalyst is packed on the membrane surface to enhance its contact with reactants, however, this greatly increases the size of the MR. Moreover, the external mass flow resistance significantly impacts membrane separation, for example hydrogen permeation through a Pd membrane in the water-gas shift (WGS) reaction, unless a substantial reduction of catalyst bed height can be achieved [166]. Another major reason for such "catalyst packing" is that most conventional membranes/membrane substrates are of a symmetric structure. As such, depositing or dispersing a certain amount of catalyst into a membrane/membrane substrate of this type would significantly increase permeation/diffusion resistance and consequently reduce MR performance. However, it has been estimated that a

membrane catalyst could be ten times more active than the powder counterpart, probably because the active surface accessible to the reactants per gram of catalyst deposited/dispersed in membrane/membrane substrate is higher than that in the powder form [92].

As an alternative, in our previous studies, porous alumina hollow fibres with a controllable asymmetric morphology which are composed of a finger-like structure and a sponge-like structure have been successfully prepared by a combined phase-inversion and sintering process [16, 167]. Catalyst can thus be deposited into the finger-like macro-voids without significantly increasing gas permeation resistance. A highly compact MR design, as a result, can be achieved by depositing catalysts for propane dehydrogenation into the finger-like macro-voids of asymmetric alumina hollow fibres followed by electroless plating of Pd-based membranes for hydrogen separation [168, 169]. The advantages of such a hollow fibre membrane reactor (HFMR) design, such as a substantially higher surface area to volume ratio, a reduction in the amount of catalyst required, better product yields etc., have been demonstrated. However, coke-formation during the reaction deactivates the catalyst and lowers propane conversion with reaction time. As a consequence, it is still difficult to comprehensively evaluate the performance of a HFMR design of this type.

As a result, the developed HFMR design is employed in this study for the WGS reaction with little coking related catalyst deactivation, and is compared with a fixed bed reactor (FBR) as well as a porous membrane reactor (PMR) under similar operating conditions. Besides the advantages that have been demonstrated in our previous studies, a high hydrogen recovery rate up to approximately 99 % can be achieved, as a

result of the reduced mass transfer resistance between the deposited catalyst/reaction zone and the Pd membrane. Moreover, promoting hydrogen separation by elevating operating temperatures, using higher sweep gas flow rates or even increasing feed stream pressure, together with accelerating the access of reactants to the deposited catalyst by increasing reactant flow rates are suggested for better performance of the HFMR design for the WGS reaction.

6.2 Experimental

6.2.1 Materials

Asymmetric alumina hollow fibres: Aluminium oxide powders of 1 μm (alpha, 99.9% metals basis, S.A. 6-8 m^2/g), 0.05 μm (gamma-alpha, 99.5% metals basis, S.A. 32-40 m^2/g) and 0.01 μm (gamma-alpha, 99.98% metals basis, S.A. 100 m^2/g) were purchased from Alfa Aesar and were used as supplied. Polyethersulfone, (PESf, Radel A-300, Ameco Performance, USA), N-methyl-2-pyrrolidone (NMP, HPLC grade, Rathbone) and Arlacel P135 (Uniqema, UK) were used as binder, solvent and additive, respectively. DI water and tap water were used as the internal and external coagulants, respectively, for the fabrication of alumina hollow precursor fibres.

Pt/CeO_2/SBA-15 catalyst: Tetraethoxysiliane (TEOS) as a silica source and poly-(ethylene oxide)-poly(propylene oxide)-poly(ethylene oxide)(PEO-PPO-PEO) amphiphilic block copolymer $EO_{20}PO_{70}EO_{20}$ (Pluronic P123, M_W=5800, Aldrich) as a structure-directing agent were used for the preparation of mesoporous silica SBA-15. H_2PtCl_6 (99.995%, Aldrich) as a Pt source, C_2H_5OH (Aldrich) and Cerium (III) nitrate hexahydrate ($Ce(NO_3)_3.6H_2O$) (99%) were used for preparing Pt/CeO_2/SBA-15 catalyst.

Electroless plating of Palladium membrane: $Pd(NH_4)_2Cl_4$ (Ammonium tetrachloropalladate, 99.99%, Aldrich), $SnCl_2 \cdot 2H_2O$, $Na_2EDTA \cdot 2H_2O$, HCl (37%), N_2H_4 and $NH_3 \cdot H_2O$ (28%) (Fisher Sci. Ltd) were used for preparing the Pd hydrogen separation membrane.

6.2.2 Fabrication of Pd/functionalized HFMR

Details of fabricating the compact HFMR, including a combined phase inversion /sintering process for preparing asymmetric alumina hollow fibres, functionalization of these fibres with SBA-15 followed by catalyst impregnation, as well as electroless plating of the Pd membrane on the functionalized hollow fibre substrates, have been described in Chapter 5. The only difference is that, during catalyst impregnation, CeO_2 is impregnated onto SBA-15 followed by a sintering at 773 K for 4 h, prior to the impregnation of Pt.

6.2.3 Characterization

The morphology of the asymmetric alumina hollow fibre substrates, the coated Pd membranes and the mesoporous silica SBA-15 deposited into the finger-like voids were visually observed using a scanning electron microscope (SEM, JEOL JSM-5610LV, Tokyo, Japan). The pore structures of fabricated SBA-15 and Pt/CeO2/SBA-15 catalyst were characterized by BET and from the adsorption branch of the isotherms using the BJH method. EDS analysis (INCA Energy by Oxford Instruments) was employed to investigate the elemental distribution across the cross sections of the functionalized alumina hollow fibres.

6.2.4 WGS reaction using HFMR

The experimental apparatus for the WGS reaction is schematically shown in Figure 6-47. The developed HFMR was mounted in a dense alumina tube of 9 mm in diameter forming a tube-in-tube reactor configuration, and was inserted into a tubular furnace with a constant heating zone of approximately 10 cm. The feed stream flowing through the lumen of the HFMR was composed of CO(10 %)/Ar and an Ar stream passing through a vapour-saturator containing DI water, the flow rates of which were both controlled by mass flow controllers. While a second Ar stream with controlled flow rates passed through the shell of the reactor. Thermocouples (not shown in Figure 6-47) were positioned at the vapour-saturator, in the centre of the HFMR, as well as at the inlets of the reactor to monitor the actual temperatures of the system. During the operation, CO and H_2O in the feed stream made contact with the catalyst deposited into the finger-like macro-voids and converted to H_2 and CO_2 products. H_2 permeating through the Pd membrane supported on the sponge-like structure of the alumina hollow fibre was carried away by the Ar sweep gas flowing in counter-current mode. Both of the streams coming out from the shell and lumen of the reactor were directed to a GC (Varian-3900) equipped with a TCD detector for analysis. It should be noted that the above operation is only used for lab-scale apparatus. For a commercial unit, it would be logical to use vacuum instead of using Ar as a sweep gas. Also, the HFMR would be constructed with a bundle of the fibres instead of a single fibre to obtain a surface area/volume ratio suitable for commercial applications. The WGS reaction activity of the catalyst and performance of the MR were evaluated according to CO conversion (X_{CO}), CH_4 selectivity (S_{CH4}), H_2 recovery rate (R_{H2}) and H_2 yield (Y_{H2}) equations:

$$X_{CO}(\%) = \frac{[CO]_{in} - [CO]_{out}}{[CO]_{in}} \times 100 \quad (1)$$

$$S_{CH_4}(\%) = \frac{[CH_4]_{out}}{[CO]_{in} - [CO]_{out}} \times 100 \quad (2)$$

$$R_{H_2}(\%) = \frac{[H_2]_{permeate}}{[H_2]_{permeate} + [H_2]_{retentate}} \times 100 \quad (3)$$

$$Y_{H_2}(\%) = \frac{[H_2]_{permeate} + [H_2]_{retentate}}{[CO]_{in}} \times 100 \quad (4)$$

Where CO_{in} is the molar concentration of CO at the reactor inlet and CO_{out} and $CH_{4\,out}$ are molar concentrations of CO and CH_4 at reactor outlet. $H_{2\,permeate}$ and $H_{2\,retentate}$ are the permeate and retentate hydrogen fluxes.

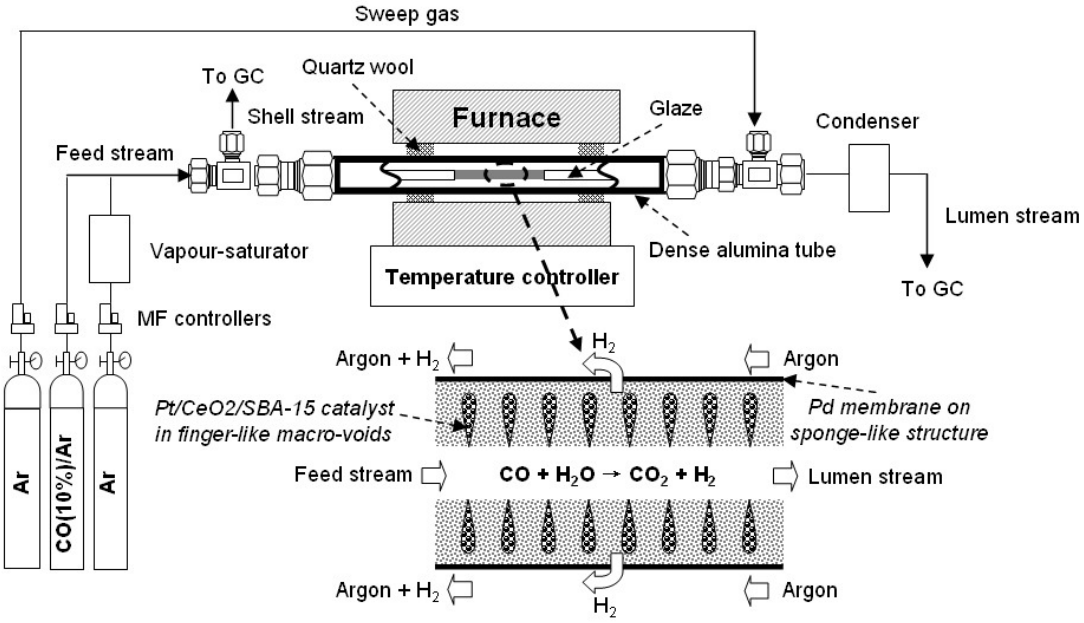


Figure 6-47 Schematic diagram of the experimental set-up for the WGS reaction using HFMR

6.3 Results and Discussion

6.3.1 Pt/CeO_2/SBA-15 catalyst for WGS reaction

Catalyst consisting of 1 wt.% Pt supported on CeO_2 modified SBA-15, an ordered mesoporous silica (OMS), has been reported to have a high level of activity for the WGS reaction, especially when nanocrystalline CeO_2 can be embedded into the mesopores of SBA-15 [120]. Moreover, the extremely high surface area of SBA-15 substantially enlarges the effective reaction area in a HFMR [169] and as a result, Pt/CeO_2/SBA-15 was chosen as the catalyst in this study.

Figure 6-48 shows pore size distributions of the prepared SBA-15 and Pt/CeO_2/SBA-15 catalyst. As can be seen, the BET surface area of the prepared SBA-15 is 522.02 m^2/g, with a pore volume of 0.78 cm^3/g. After impregnation of Pt and CeO_2, a significant reduction of the surface area to 393.14 m^2/g was observed, together with a decrease of pore volume to 0.54 cm^3/g, which indicates that CeO_2 particles promoting catalytic activity of Pt are too big to be embedded into the mesopores of SBA-15. As a result of the conventional impregnation process, segregation occurs on the surface of SBA-15, causing the blocking of mesopores. This is in agreement with the limited change in the pore size distribution but the significant drop in peak intensity observed after impregnation, as shown in Figure 6-48.

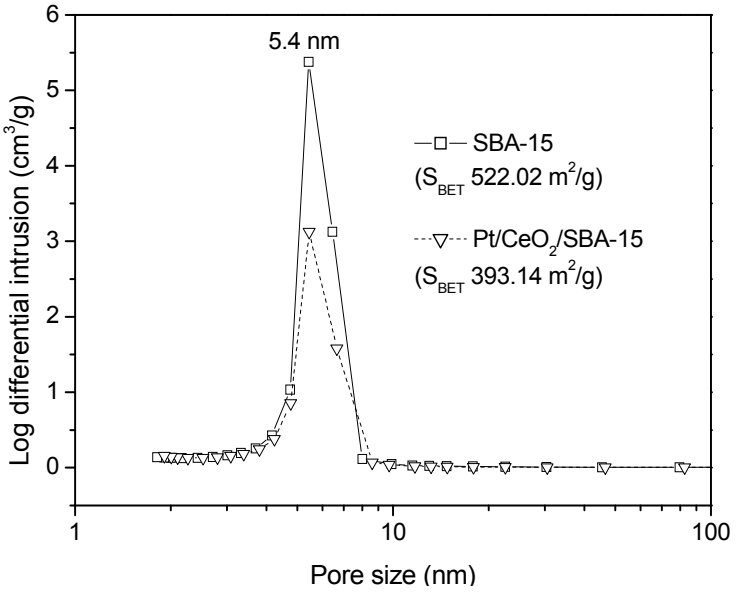


Figure 6-48 Pore size distribution (PSD) of SBA-15 and Pt/CeO_2/SBA-15 calculated from the adsorption branch of the isotherms using the BJH method

The catalytic activity of the prepared Pt/CeO_2/SBA-15 catalyst for the WGS reaction was investigated in a fixed bed reactor (FBR) between 673 and 823 K. 50 mg of catalyst was packed inside the reactor with gas hourly space velocity GHSV of 14088 $cm^3/(g \cdot h)$ and the steam to carbon (S/C) ratio of 1. As can be seen in Figure 6-49, CO conversion slightly decreases from approximately 67.34 to 61.73 % and gets closer to the equilibrium conversion with elevating temperatures. In the meantime, CH_4 selectivity reduces to 0.45 %, indicating a high level of selectivity for CO and H_2. Figure 6-50 shows the impact of the GSHV on Pt/CeO_2/SBA-15 catalyst for the WGS reaction at 723 K, in which the same amount of catalyst was employed with the S/C ratio at 1. CO conversion gradually deviates away from the equilibrium line with a reduction in CH_4 selectivity with the GHSV increasing from 13800 to 67800 $cm^3/(g \cdot h)$.

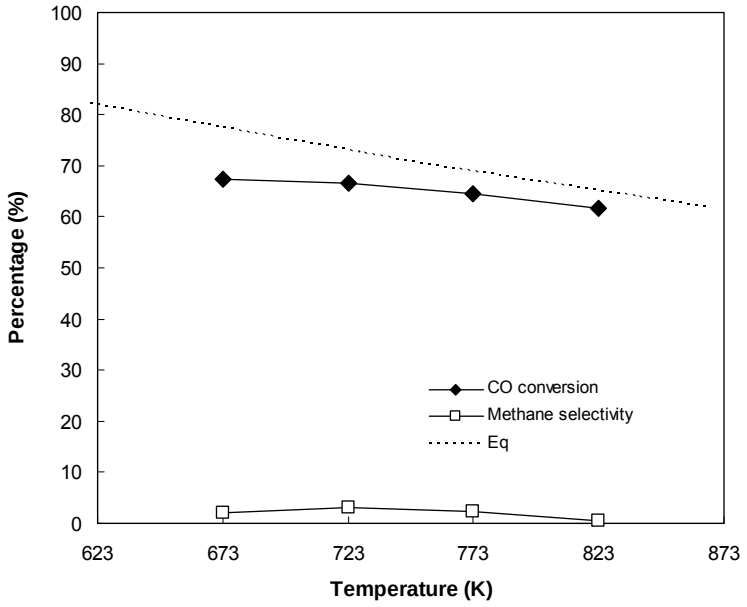


Figure 6-49 Effect of temperature on CO conversion and CH_4 selectivity over 50 mg of Pt/CeO_2/SBA-15 catalyst in a fixed bed reactor (atm pressure, S/C = 1, GHSV= 14,088 $cm^3/(g \cdot h)$, CO concentration = 4.2%)

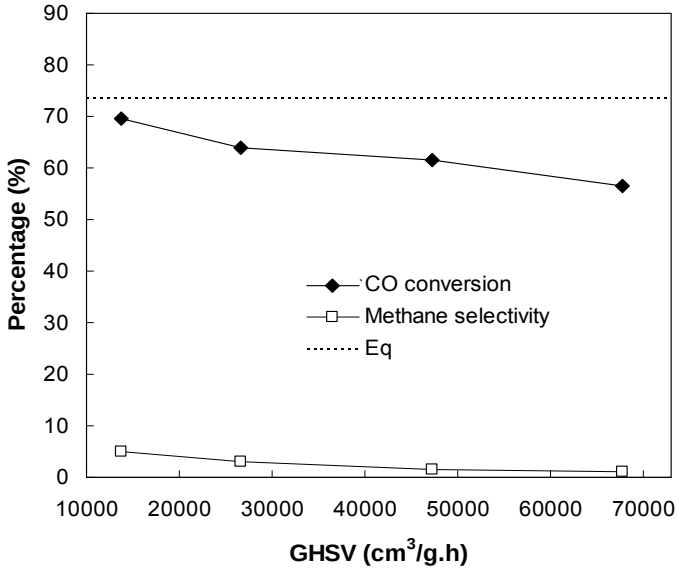


Figure 6-50 Influence of GHSV on CO conversion and CH_4 selectivity over 50 mg of Pt/CeO_2/SBA-15 catalyst in a fixed bed reactor (atmospheric pressure, S/C= 1, feed flow rate 10-60 ml/min, CO concentration = 4.2%)

6.3.2 Functionalized asymmetric alumina hollow fibres for WGS reaction

The morphology of the asymmetric alumina hollow fibres employed in this study can be characterized by a thin, uniform sponge-like outer layer supported on a thick finger-like inner layer, the formation mechanism and structural features of which have been systematically investigated in our previous studies [16, 167-169]. Finger-like voids extend across approximately 90 % of the fibre cross section from a highly porous inner surface with the remaining 10 % consisting of the sponge-like outer layer, forming a smooth and denser outer surface. The asymmetric morphology of this type possesses a number of unique and important advantages over conventional symmetric counterparts, especially in view of MRs. For example, catalyst can be deposited into the finger-like macro-voids of such fibres without significantly increasing permeation resistance, while the thin uniform sponge-like layer, besides facilitating permeation, can be used for the direct coating of a Pd membrane.

Functionalization of such fibres is achieved by depositing materials with high surface areas, i.e. SBA-15, into the finger-like voids followed by impregnation with CeO_2 and Pt. Figure 6-51 shows SEM images of alumina hollow fibres with deposited SBA-15. A large amount of finger-like macro-voids can be found in the cross section of the fibre (Figure 6-51(a)), which allows deposition of a considerable amount of catalyst [169]. SBA-15 is observed in the finger-like voids (Figure 6-51(b) and (c)), which substantially increases catalytic surface area within the fibre. The inner surface of the fibre is maintained highly porous even if a small amount of SBA-15 scum is present (Figure 6-51(d)).

After impregnating CeO_2 and Pt, an “active” alumina hollow fibre can be obtained. EDS analysis indicates that Ce and Pt are actually distributed across the whole fibre, as shown in Figure 6-52, as a consequence of the nature of the wet impregnation process. However, the majority of catalyst taking part in the following WGS reactions is still considered to be inside the finger-like macro-voids where SBA-15 is deposited. This assumption is made because of the dominating pore volume from the finger-like voids and the extremely high surface area of the deposited SBA-15.

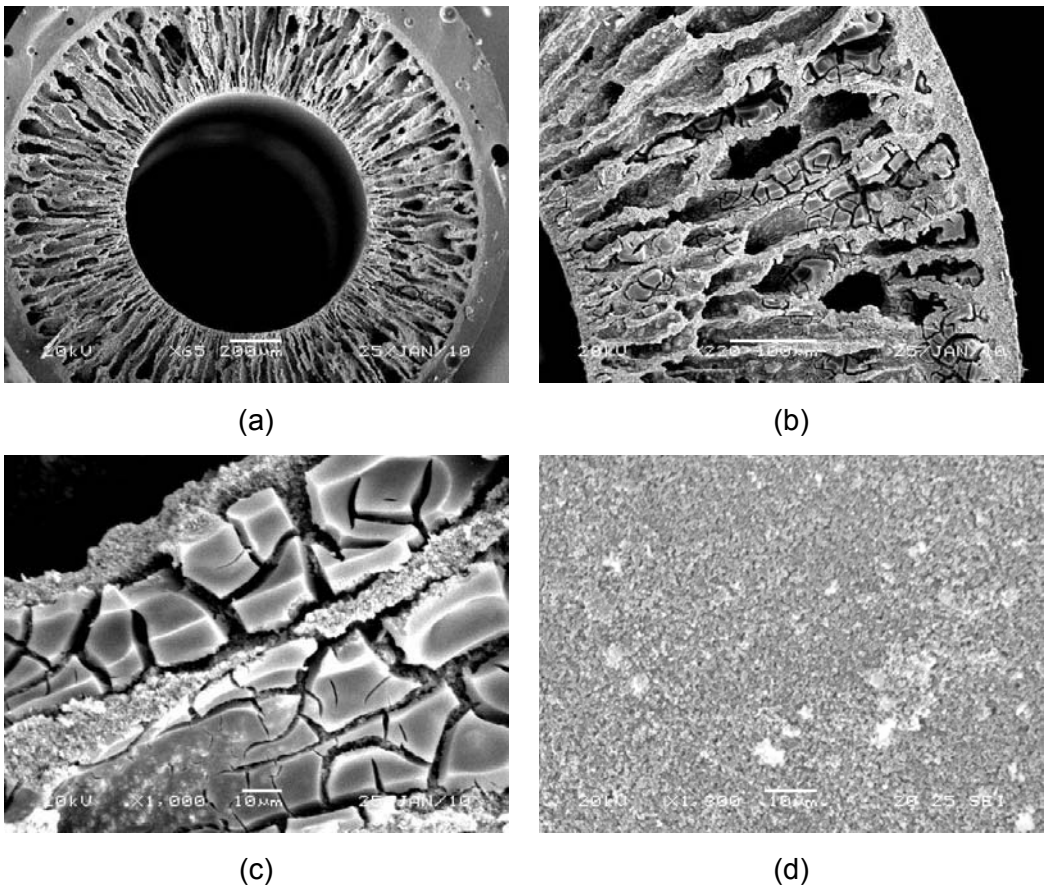


Figure 6-51 SEM images of asymmetric alumina hollow fibre with deposited SBA-15, (a) whole view, (b) cross section, (c) deposited SBA-15 and (d) inner surface

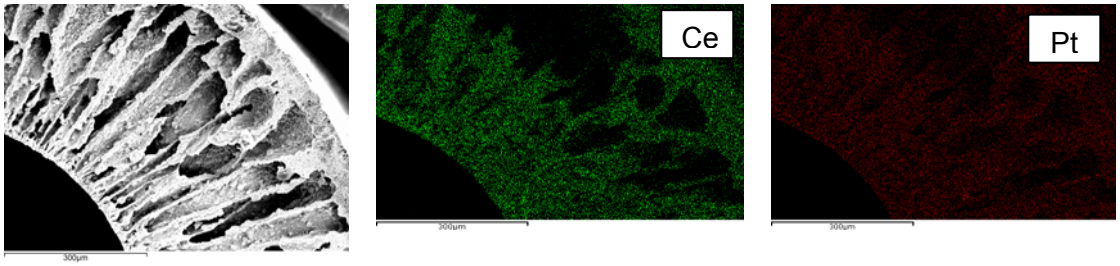


Figure 6-52 SEM-EDS analysis of functionalized an alumina hollow fibre

The functionalized alumina hollow fibres, in which approximately 30 mg of $Pt/CeO_2/SBA-15$ catalyst was deposited, were used as a porous membrane reactor (PMR) for the WGS reaction, using the same experimental set-up shown in Figure 6-47 except without a Pd membrane. The feed stream through the lumen was the same as for the FBR, while an Ar sweep gas of 50 ml/min was directed through the shell side of the reactor. As can be seen in Figure 6-53, CO conversion increases and gets closer to the equilibrium line as the temperature increases from 673 to 823 K. In the meantime, CH_4 selectivity is maintained at a lower level, i.e. less than 1 %, in comparison with the FBR (Figure 6-49), indicating a higher selectivity for CO and H_2. As the way that reactants gain access to the catalyst in the PMR, in which CO and H_2O in the hollow fibre lumen must diffuse axially into the finger-like macro-voids to make contact with the deposited catalyst, is quite different from the FBR, a direct comparison of these two reactor designs using GSHV cannot be made. As a result, space-time-yield which is a parameter based on the amount of products, for example H_2 in this study, produced on per unit weight of catalyst employed per unit time is used to evaluate the efficiency of the catalyst in different reactor designs. These results are discussed in the following section.

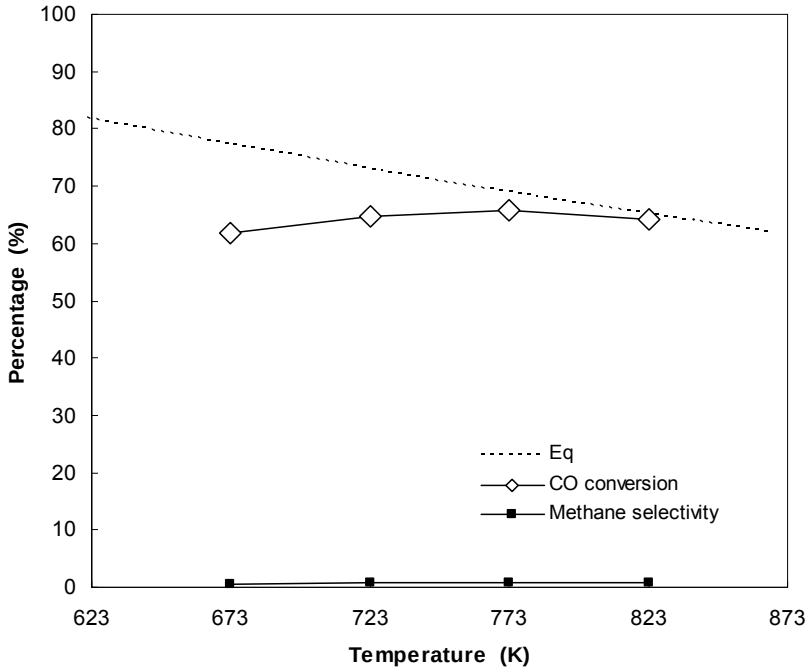


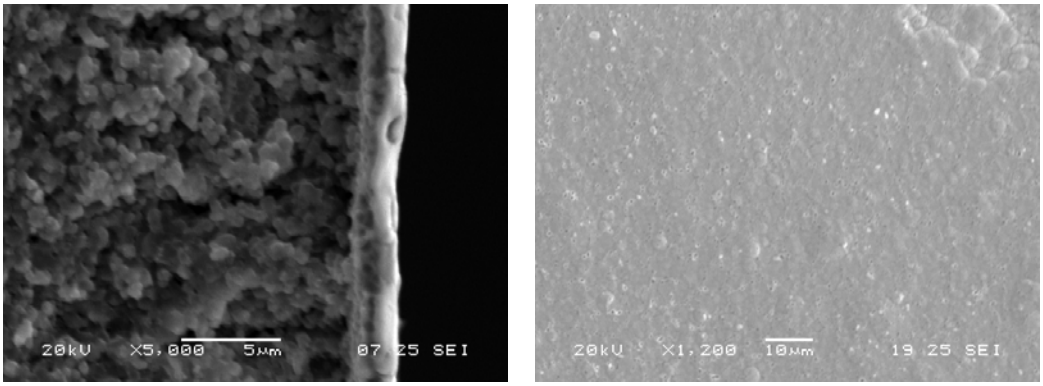
Figure 6-53 CO conversion and CH_4 selectivity as a function of temperature in a porous membrane reactor (PMR) with approximately 30 mg of deposited catalyst. (Ar sweep gas = 50 ml/min, S/C = 1, feed flow rate = 10 ml/min, CO concentration = 4.2 %)

6.3.3 Pd/alumina functionalized hollow fibre membrane reactor for WGSR

After electroless plating of a Pd membrane of approximately 2 micron in thickness directly onto the outer surface of the functionalized alumina hollow fibre, as shown in Figure 6-54(a), a HFMR can be obtained for the WGS reaction. Benefiting from the uniform sponge-like structure, thin and high quality Pd membranes can be coated conveniently on the surface without observable defects or pinholes (Figure 6-54(b)).

An investigation on the performance of HFMR for the WGS reaction was carried out using the same conditions as for the PMR. Product streams from shell and lumen sides of the reactor were simultaneously separately and directed to GC for analysis. It

should be noted here that, no CO or CO_2 was detected on the shell side of the reactor for all of the following results, which indicates great integrity of the coated Pd membranes and agrees well with the SEM images shown in Figure 6-54.



(a) (b)

Figure 6-54 SEM images of the Pd membrane coated on the functionalized alumina hollow fibre, (a) cross section and (b) Pd membrane surface

Figure 6-55 presents CO conversion, CH_4 selectivity, H_2 recovery rate and the ratio between the amounts of hydrogen permeated through the Pd membrane and hydrogen produced during the reaction of the HFMR between 673 and 823 K. As can be seen, CO conversion increases first when the temperature is elevated from 673 to 723 K, and then slowly decreases with increasing temperature up to 823 K, reaching and slightly exceeding the equilibrium line when the temperature is above 773 K. CH_4 selectivity shows a similar trend as in the PMR with no CH_4 detected above 773 K. In the meantime, a high H_2 recovery rate above 90 % is achieved, which is impacted little by the elevating temperatures.

In contrast with the PMR, CO conversion is only slightly “shifted” to a greater value considering the high level of removal of H_2 from the reaction zone. This seems to be quite different from conventional membrane reactors where catalyst is packed inside,

because a certain level of H_2 removal always leads to a significant promotion of CO conversion above the equilibrium line [111, 116, 170] despite the fact that achieving a good H_2 recovery rate is still challenging, due to the external mass flow resistance from the catalyst bed [166]. As a result, the flow rates of sweep gas to the shell side and reactants to the lumen side were varied to systematically investigate the performance of the HFMR design for the WGS reaction at 673 K, the results of which are shown in Figure 6-56 and Figure 6-57.

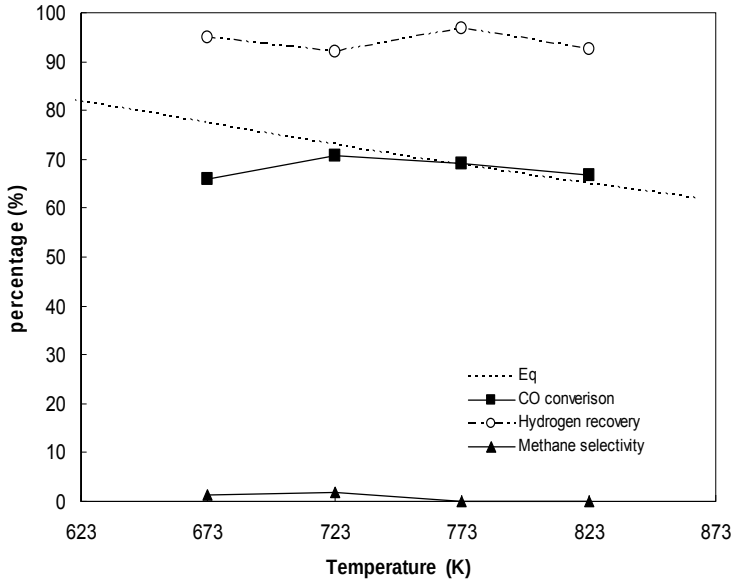
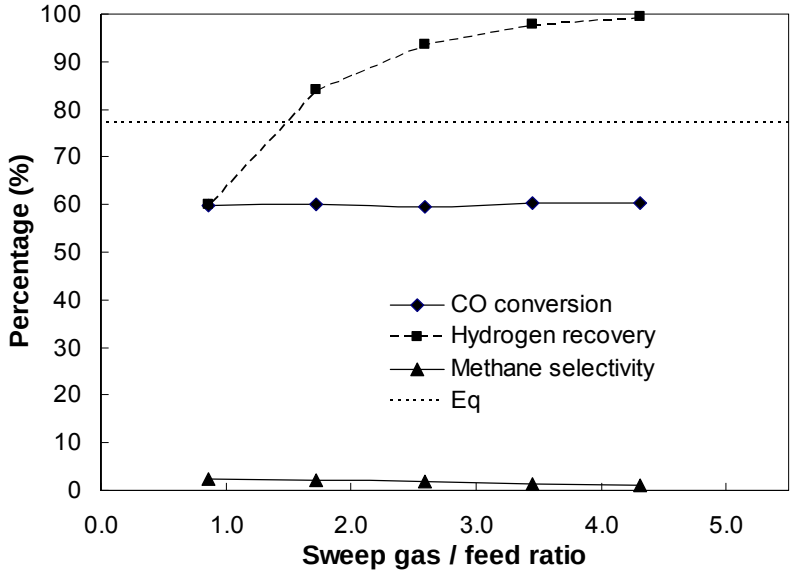
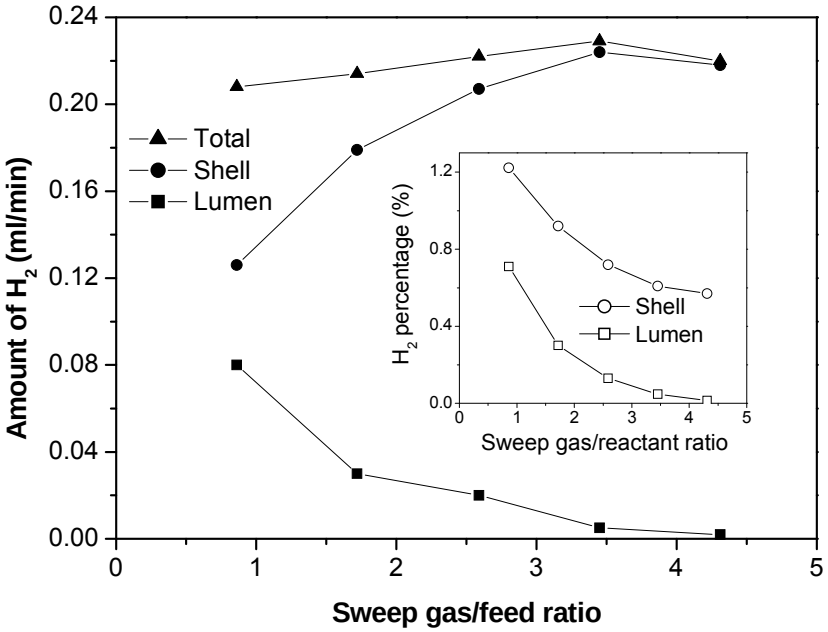


Figure 6-55 CO conversion, CH_4 selectivity and H_2 recovery rate as a function of temperature in HFMR with approximately 30 mg of deposited catalyst. (Ar sweep gas = 50 ml/min, S/C = 1, feed flow rate = 10 ml/min CO concentration = 4.2 %).



(a)



(b)

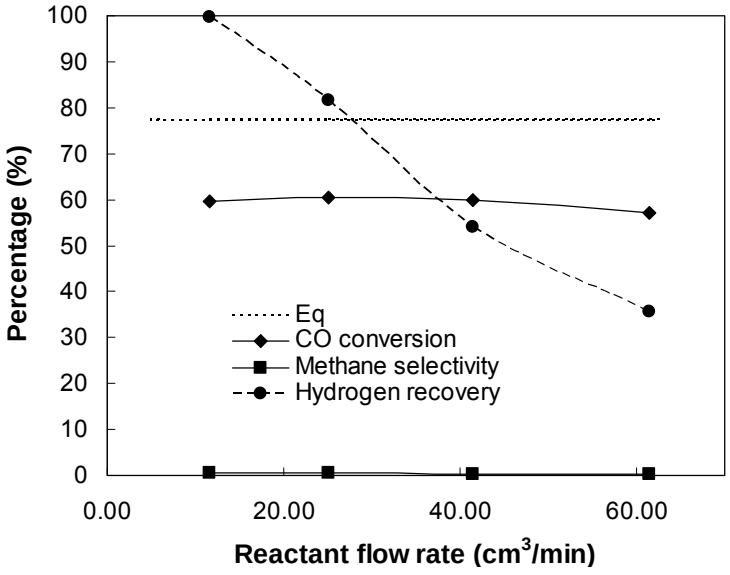
Figure 6-56 Effect of sweep gas to feed ratio on (a) CO conversion, CH_4 selectivity and H_2 recovery and (b) amount and concentration of H_2 produced, separated and retained of HFMR with approximately 30 mg of deposited catalyst (Ar sweep gas = 10-50 ml/min, S/C = 1, feed flow rate = 10 ml/min, 673 K)

As can be seen in Figure 6-56, in which the reactant stream was kept at approximately 10 ml/min and was same as the one in Figure 6-55, while the sweep gas flow rate was varied from approximately 10 to 50 ml/min, resulting in a sweep gas/reactant ratio from approximately 0.9 to 5.0. Interestingly, CO conversion varied very little (Figure 6-56(a)), although H_2 can be efficiently separated from the reaction zone with the increasing sweep gas flow rate as a result of a lower H_2 partial pressure on the permeate side of the Pd membrane (inserted plot in Figure 6-56(b)). This indicates that, at a low reactant flow rate, the access of reactants from the hollow fibre lumen to the deposited catalyst is the controlling step. The extremely high H_2 recovery rate of up to approximately 99 % demonstrates one of the advantages of the HFMR design over the conventional membrane reactor with packed catalyst, that is, minimized gas permeation resistance between the deposited catalyst (or reaction zone) and the Pd membrane. Figure 6-56(b) shows the amount of H_2 produced as well as H_2 detected in the shell and lumen of the reactor. A higher sweep gas flow rate, although contributing to improve H_2 separation, only slightly promotes the total amount of H_2 produced, indicating a very limited improvement in facilitating the mass transfer of reactant towards the deposited catalyst. This is in agreement with the results in Figure 6-56(a), showing that efficient separation of H_2 does not significantly increase CO conversion.

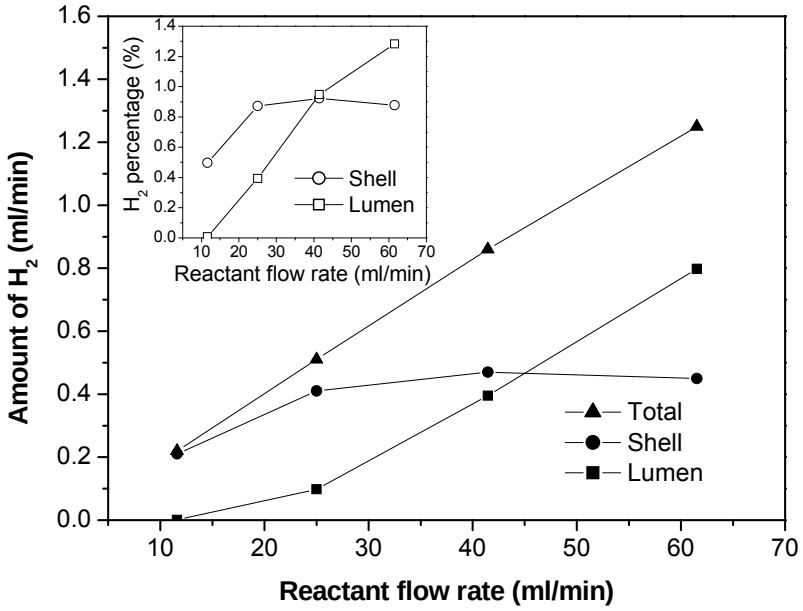
When the flow rate of the sweep gas was kept at approximately 50 ml/min while the reactant flow rate was increased from approximately 10 to 60 ml/min with a constant S/C ratio of 1, as shown in Figure 6-57(a), H_2 recovery rate kept decreasing from approximately 99 to 36 % while CO conversion, interestingly, was affected little. The amount of H_2 produced increased linearly with the increasing reactant flow rate (Figure 6-57(b)), which indicates that H_2 separation and probably greater turbulence in the hollow fibre lumen, due to the higher reactant flow rate, contribute to improve the access

of reactant to the deposited catalyst. However, permeated H_2 slightly increased and reached a constant value while more and more H_2 was detected remaining in the lumen (Figure 6-57(b)). This means that under current conditions H_2 separation through the Pd membrane becomes the controlling step unless further elevated operating temperatures and/or higher sweep gas flow rates can be employed.

Furthermore, when comparing the H_2 yields of the different reactor designs shown in Figure 6-58, the deposited catalyst in the PMR and HFMR are clearly more efficient in the reaction in contrast with the FBR, demonstrating another advantage of the membrane reactor design. The H_2 yield of the HFMR is slightly lower than that of the PMR, because it is less "permeable" to CO and H_2O due to the existence of the Pd membrane. This further addresses the importance of an efficient contact between reactants and the deposited catalyst in the current HFMR design.



(a)



(b)

Figure 6-57 Effect of reactant flow rate on (a) CO conversion, CH_4 selectivity and H_2 recovery and (b) amount and concentration of H_2 produced, separated and retained in an HFMR with approximately 30 mg of deposited catalyst (Ar sweep gas = 50 ml/min, S/C = 1, feed flow rate = 10-60 ml/min, 673 K)

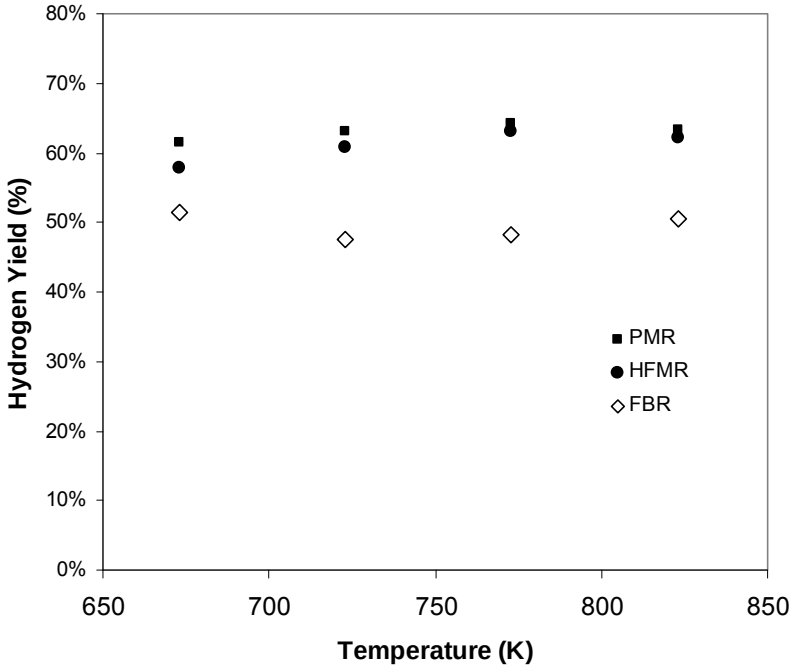


Figure 6-58 Hydrogen yields of FBR, PMR and HFMR

A comparison of the performance the three reactor designs in this study, i.e. FBR (Figure 6-49 and Figure 6-50), PMR (Figure 6-53) and HFMR (Figure 6-55, Figure 6-56, Figure 6-57), clearly indicates that depositing catalyst into the finger-like macro-voids of asymmetric alumina hollow fibres enhances the efficiency of the reaction. This is thought to result from improving the interaction between reactants and the catalyst without significantly impacting efficient gas transfer from the deposited catalyst/reaction zone to the Pd membrane. As a result, a higher H_2 recovery rate compared to a conventional membrane reactor with packed catalyst can be achieved. However, the access of reactants to the deposited catalyst is the controlling step at low reactant flow rate, which counteracts the contribution of H_2 separation for “shifting” CO conversion to a higher value or above the equilibrium line. The net-effect of H_2 removal from the system and greater turbulent flow in the lumen due to increasing reactant flow rates is to improve the access of reactants to the deposited catalyst. Therefore, higher operating temperatures, higher sweep gas flow rates and even higher feed side pressures are suggested to promote H_2 separation and higher CO conversion. Moreover, depositing more catalyst into the finger-like macro-voids and a better distribution of catalyst along the reactor are also considered helpful in further improving the performance of the HFMR design.

6.4 Conclusions

A highly compact hollow fibre membrane reactor design, which consists of a thin and defect-free Pd membrane deposited directly onto a functionalized asymmetric alumina hollow fibre by electroless plating, has been achieved and used for the water-gas shift (WGS) reaction. Deposition of Pt/CeO_2/SBA-15 catalyst into the finger-like macro-voids significantly improves the interaction between the reactants and the catalyst, resulting in a higher hydrogen yield in contrast with the counterpart in powder form. In addition, it does not significantly impact gas transfer from the deposited catalyst/reaction zone to the Pd membrane, leading to a high hydrogen recovery rate. At low reactant flow rate, the efficient hydrogen separation does not significantly “shift” the reaction towards the product side, because the controlling step is the access of reactant to the deposited catalyst. This can be improved by increasing reactant flow rate in the lumen, in conjunction with hydrogen separation. However, higher operating temperatures and/or sweep gas flow rates are, in this case, suggested to further promote hydrogen separation.

CHAPTER 7

Conclusions and Recommendations

This work investigated the application of multifunctional inorganic membranes for chemical reactions. The focus was on fabrication and functionalization of Pd/asymmetric alumina hollow fibre composite membranes and their potential for dehydrogenation of propane and water-gas shift reactions. Inorganic hollow fibre membranes can withstand harsh thermal and chemical conditions compared with polymeric membranes and their hollow fibre geometry also gives them superior surface area to volume ratios in comparison to commercial tubular and disk configurations. The permselectivity and durability of inorganic membranes means that they are also suitable for a range of membrane-based reactive separation processes. In this work, the finger-like voids present in asymmetric hollow fibre membrane supports were functionalised using different catalyst deposition techniques followed by coating of thin palladium-based hydrogen separation films on the outer surface of the supports to form catalytic membrane reactors for chemical reactions.

The major findings in the study are summarised below:

7.1 Asymmetric hollow fibre support

Porous alumina hollow fibre supports with an asymmetric structure have been successfully prepared by a combined phase inversion and sintering method. The asymmetric structure is characterized by a very porous inner surface from which finger-like voids extend across approximately 80 % of the fibre cross section with the remaining 20 % consisting of a denser sponge-like outer layer of about 60-70 μm in thickness. It is

believed that finger-like void formation is initiated by hydrodynamically unstable viscous fingering developed when a less viscous fluid (non-solvent) is in contact with a higher viscosity fluid (ceramic suspension containing invertible polymer binder).

Based on SEM analysis, the outer sponge-like layer of the substrate provides a sufficiently smooth surface for direct coating of thin palladium or palladium-silver membranes for hydrogen separation without the need for modifications. The finger-like voids also offer the possibility of depositing sub-micron sized catalyst particles or catalyst supports within the fibre structure to develop highly compact membrane reactors.

7.2 Palladium-based composite membrane

Thin (3-10 μm) and defect-free palladium and palladium-silver films have been successfully deposited on the outer surface of asymmetric supports using an electroless plating coating technique. The films possess high stability under high temperature and pressure conditions over 4-5 thermal cycles. The H_2/N_2 permselectivity were infinite at room temperatures and up to 823 K and 4 bar transmembrane pressure.

The Pd membrane achieved a high hydrogen flux of 60 $ml/cm^2.min^1$ at 723 K and 4 bar transmembrane pressure and an activation energy of 14.62 kJ/mol whilst a 5 μm Pd-Ag membrane achieved a similar hydrogen flux with an activation energy of 5.4 kJ/mol.

Three types of membrane/catalyst arrangements were investigated in this work. In hollow fibre membrane reactor (HFMR-I) sub-micron sized Pt(0.5 wt.%)/γ-alumina

catalyst particles were impregnated in the finger-like voids of the alumina support, followed by electroless plating of a Pd-Ag film via a coating-diffusion method. HFMR-II was constructed by depositing mesoporous SBA-15 - with a surface area as high as 596.58 m^2/g - into the finger-like voids using a sol-gel method, followed by impregnation with platinum catalyst. A palladium membrane was then electroless plated on the outer surface of the functionalized support to develop the catalytic membrane reactor. HFMR-III is a variation of HFMR-II but with platinum catalyst supported on both ceria and SBA-15 material.

7.3 Palladium-based membrane reactor

In the propane dehydrogenation tests, HFMR-I achieved a conversion as high as 42 % at 723 K in the initial stage. However, the advantage of using HFMR-I compared to a fixed bed reactor (FBR) is diminished after 40 min of operation due to deactivation of the catalyst and the low equilibrium conversion of propane. Because of the high surface area of the asymmetric substrates used, comparable propane conversion and propene selectivity were obtained with much less catalyst employed in the membrane reactor.

HFMR-II also achieved better propene selectivity and yield with less catalyst compared with a conventional FBR under the same operating conditions. This showed that the developed HFMR-II is more efficient in propene production. Furthermore, the HFMR-II achieved better H_2 yields compared to FBR, demonstrating the advantages of the developed membrane reactor. In comparison with HFMR-I, similar propane conversions as well as propene selectivity were obtained, indicating that higher catalyst loading and surface area in the membrane reactor cannot be appreciated as a consequence of coke-formation.

In the water-gas shift reaction test, the prepared HFMR-III demonstrated how deposition of Pt/CeO_2/SBA-15 catalyst into the finger-like macro-voids significantly improved the interaction between the reactants and the catalyst, and resulted in a higher space-time-yield (STY) and hydrogen yield in contrast with the counterpart in powder form. The HFMR-III design did not significantly impact gas transfer from the deposited catalyst/reaction zone to the Pd membrane; this led to a high hydrogen recovery rate. At low reactant flow rates, efficient hydrogen separation did not significantly "shift" the reaction towards the product side. This is a as a result of a controlling step involving the access of reactants to the deposited catalyst. The limiting step could be improved by increasing the reactant flow rate to produce greater turbulence in the lumen in conjunction with hydrogen separation. However, higher operation temperatures and/or sweep gas flow rates are suggested to further promote hydrogen separation.

7.4 Recommendations for future work

7.4.1 Membrane support and catalyst deposition

In this work, porous alumina hollow fibre supports with a unique morphology were successfully fabricated reproducibly using a spinning process by adjusting the starting materials and spinning parameters. However, other factors such as the viscosity of the starting dope and additives etc. can be further studied with the specific aim of increasing the porosity of the inner finger-like voids to accommodate more catalyst material. Controlled deposition of catalysts in the membrane is necessary because it influences the performance of a membrane reactor. Therefore, it is recommended that a systematic study of various deposition techniques is carried out to initially attain some

level of consistency and reproducibility, and then to determine optimal deposition conditions.

7.4.2 Catalyst activity

A major limitation with the use of catalytic membrane reactors encountered in this study was catalyst deactivation. As a result, further work should be directed at improving the stability and activity of catalysts that are, for example, less susceptible to coking during dehydrogenation reactions. Bimetallic or trimetallic catalysts made from noble metals can be explored as possible candidates for future studies.

7.4.3 Membrane reactor design and long term stability studies

The fluid dynamics of the reactant and catalyst was shown to be rate-limiting in certain conditions i.e. low reactant flow rates. Therefore, it is recommended that further experimental work is carried out to investigate the flow pattern and access of reactants to deposited catalysts in the hollow fibre lumen.

To successfully integrate membrane reactor technologies with existing processes, long-term stability tests under ideal process conditions need to be investigated. For example, a feed mixture of H_2S and syngas can simulate placing a Pd-based membrane reactor to perform the WGS reaction downstream of a coal gasifier in a coal-to-hydrogen production scheme. Integration of a membrane reactor at the exit of a gasifier benefits from high temperature kinetics and increased hydrogen permeance at elevated temperatures.

7.4.4 Reactor modelling

To gain a better understanding of the permeation behaviour of composite hollow fibre membranes, gas transport models should be developed and verified with experimental data. The model should account for simultaneous transport through the pores of the support using a generalized diffusion model and a solution-diffusion model through the Pd or Pd-Ag membrane. Hydrogen fluxes can be investigated as a function of membrane separation layer type, thickness, temperature and gas partial pressures.

List of Publications

1. Ejiro Gbenedio, Zhentao Wu and K. Li., A Pd/Functionalized Alumina Hollow Fibre Membrane Reactor for Water-Gas Shift Reaction, to be submitted

2. Ejiro Gbenedio, Zhentao Wu, Irfan M. D. Hatim, B.F.K Kingsbury and K. Li., A Multifunctional Pd/Alumina Hollow Fibre Membrane Reactor for Propane Dehydrogenation, Catalysis Today, **2010**, 156, 93

3. Zhentao Wu, Irfan M. D. Hatim, B.F.K Kingsbury, Ejiro Gbenedio and K. Li., A Novel Inorganic Hollow Fibre Membrane Reactor for Catalytic Dehydrogenation of Propane, AiChE Journal, **2009**, 55, 9

REFERENCES

1. Li, K., *Ceramic Membranes for Separation and Reaction*. 2007: Wiley.
2. Saracco, G., G.F. Vesteeg, and W.P.M. van Swaaij, *Current hurdles to the success of high-temperature membrane reactors.* Journal of Membrane Science, 1994. **95**(2): p. 105-123.
3. Capannelli, G., E. Carosini, F. Cavani, O. Monticelli, and F. Trifiro, *Comparison of the catalytic performance of V2O5/[gamma]-Al2O3 in the oxidehydrogenation of propane to propylene in different reactor configurations: i) packed-bed reactor, ii) monolith-like reactor and iii) Catalytic Membrane Reactor.* Chemical Engineering Science, 1996. **51**(10): p. 1817-1826.
4. Ferreira-Aparicio, P., I. Rodriguez-Ramos, and A. Guerrero-Ruiz, *Pure hydrogen production from methylcyclohexane using a new high performance membrane reactor.* Chemical Communications, 2002(18): p. 2082-2083.
5. Michaels, A.S., Chem. Eng. Prog., 1968(64): p. 31.
6. Gobina, E. and R. Hughes, *Reaction coupling in catalytic membrane reactors.* Chemical Engineering Science, 1996. **51**(11): p. 3045-3050.
7. Guo, Y., G. Lu, Y. Wang, and R. Wang, *Preparation and characterization of Pd-Ag/ceramic composite membrane and application to enhancement of catalytic dehydrogenation of isobutane.* Separation and Purification Technology, 2003. **32**(1-3): p. 271-279.
8. Kiwi-Minsker, L., O. Wolfrath, and A. Renken, *Membrane reactor microstructured by filamentous catalyst.* Chemical Engineering Science, 2002. **57**(22-23): p. 4947-4953.
9. Giessler, S., L. Jordan, J.C. Diniz da Costa, and G.Q. Lu, *Performance of hydrophobic and hydrophilic silica membrane reactors for the water gas shift reaction.* Separation and Purification Technology, 2003. **32**(1-3): p. 255-264.
10. Quicker, P., V. Höllein, and R. Dittmeyer, *Catalytic dehydrogenation of hydrocarbons in palladium composite membrane reactors.* Catalysis Today, 2000. **56**(1-3): p. 21-34.
11. Shu, J., B.P.A. Grandjean, E. Ghali, and S. Kaliaguine, *Simultaneous deposition of Pd and Ag on porous stainless steel by electroless plating.* Journal of Membrane Science, 1993. **77**(2-3): p. 181-195.

12. Yildirim, Y., E. Gobina, and R. Hughes, *An experimental evaluation of high-temperature composite membrane systems for propane dehydrogenation.* Journal of Membrane Science, 1997. **135**(1): p. 107-115.
13. Luyten, J., A. Buekenhoudt, W. Adriansens, J. Cooymans, H. Weyten, F. Servaes, and R. Leysen, *Preparation of LaSrCoFeO3-x membranes.* Solid State Ionics, 2000. **135**(1-4): p. 637-642.
14. Tan, X., S. Liu, and K. Li, *Preparation and characterization of inorganic hollow fiber membranes.* Journal of Membrane Science, 2001. **188**(1): p. 87-95.
15. Wei, C.C., O.Y. Chen, Y. Liu, and K. Li, *Ceramic asymmetric hollow fibre membranes--One step fabrication process.* Journal of Membrane Science, 2008. **320**(1-2): p. 191-197.
16. Kingsbury, B.F.K. and K. Li, *A morphological study of ceramic hollow fibre membranes.* Journal of Membrane Science, 2009. **328**(1-2): p. 134-140.
17. Li, A., W. Liang, and R. Hughes, *Characterisation and permeation of palladium/stainless steel composite membranes.* Journal of Membrane Science, 1998. **149**(2): p. 259-268.
18. Pan, X.L., N. Stroh, H. Brunner, G.X. Xiong, and S.S. Sheng, *Pd/ceramic hollow fibers for H2 separation.* Separation and Purification Technology, 2003. **32**(1-3): p. 265-270.
19. Pan, X.L., G.X. Xiong, S.S. Sheng, N. Stroh, and H. Brunner, *Thin dense Pd membranes supported on [small alpha]-Al2O3 hollow fibers.* Chemical Communications, 2001(24): p. 2536-2537
20. Gobina, E., K. Hou, and R. Hughes, *Equilibrium-shift in alkane dehydrogenation using a high-temperature catalytic membrane reactor.* Catalysis Today, 1995. **25**(3-4): p. 365-370.
21. Sanchez Marcano, J.G. and T.T. Tsotsis, *Catalytic Membranes and Membrane Reactors*. 2002, Weinheim: Wiley-VCH Verlag GmbH.
22. Uemiya, S., T. Matsuda, and E. Kikuchi, *Hydrogen permeable palladium-silver alloy membrane supported on porous ceramics.* Journal of Membrane Science, 1991. **56**(3): p. 315-325.
23. Tan, X., Y. Liu, and K. Li, *Mixed conducting ceramic hollow-fiber membranes for air separation.* AIChE Journal, 2005. **51**(7): p. 1991-2000.
24. Li, K., X. Tan, and Y. Liu, *Single-step fabrication of ceramic hollow fibers for oxygen permeation.* Journal of Membrane Science, 2006. **272**(1-2): p. 1-5.

25. Hsieh, H.P., *Inorganic Membranes for Separation and Reaction*. 1996, Amsterdam: Elsevier Science.
26. Liu, S. and G.R. Gavalas, *Oxygen selective ceramic hollow fiber membranes.* Journal of Membrane Science, 2005. **246**(1): p. 103-108.
27. Zydorczak, B., Z. Wu, and K. Li, *Fabrication of ultrathin La0.6Sr0.4Co0.2Fe0.8O3-hollow fibre membranes for oxygen permeation.* Chemical Engineering Science, 2009. **64**(21): p. 4383-4388.
28. Koonaphapdeelert, S., X. Tan, Z. Wu, and K. Li, *Solvent distillation by ceramic hollow fibre membrane contactors.* Journal of Membrane Science, 2008. **314**(1-2): p. 58-66.
29. Othman, M.H.D., Z. Wu, N. Droushiotis, G. Kelsall, and K. Li, *Morphological studies of macrostructure of Ni-CGO anode hollow fibres for intermediate temperature solid oxide fuel cells.* Journal of Membrane Science, 2010. **360**(1-2): p. 410-417
30. Droushiotis, N., M.H.D. Othman, U. Doraswami, Z. Wu, G. Kelsall, and K. Li, *Novel co-extruded electrolyte-anode hollow fibres for solid oxide fuel cells.* Electrochemistry Communications, 2009. **11**(9): p. 1799-1802.
31. Wu, Z., B. Wang, and K. Li, *A novel dual-layer ceramic hollow fibre membrane reactor for methane conversion.* Journal of Membrane Science. **352**(1-2): p. 63-70.
32. Gbenedio, E., Z. Wu, I. Hatim, B.F.K. Kingsbury, and K. Li, *A multifunctional Pd/alumina hollow fibre membrane reactor for propane dehydrogenation.* Catalysis Today, 2010. **156**(3-4): p. 93-99.
33. Liu, S., W.K. Teo, X. Tan, and K. Li, *Preparation of PDMSvi-Al2O3 composite hollow fibre membranes for VOC recovery from waste gas streams.* Separation and Purification Technology, 2005. **46**(1-2): p. 110-117.
34. Burggraaf, A.J. and L. Cot, *Fundamentals of Inorganic Membranes*. Science and Technology Series 4. 1996, Amsterdam: Elsevier Science B.V.
35. *Materials Research for Separations Technologies: Energy and Emission Reduction Opportunities*. 2005, BCS, Inc, and Oak Ridge National Laboratory. p. 103.
36. zur Megede, D., *Fuel processors for fuel cell vehicles.* Journal of Power Sources, 2002. **106**(1-2): p. 35-41.

37. Hughes, R., *Composite palladium membranes for catalytic membrane reactors.* Membr. Technol., 2001. **131**(3): p. 9-13.
38. Paglieri, S.N., and Way, J. D, *Review - Innovations in Palladium Membrane Research.* Separation and Purification Methods 2002. **31**: p. 1-169.
39. Buevich, Y.A. and A.K. Ivonin, *Diffusion-kinetic theory of the gas permeability of membranes.* Russ.J.Phys.Chem, 1987. **61**(10): p. 1482.
40. Athayde, A.L., R.W. Baker, and P. Nguyen, *Metal composite membranes for hydrogen separation.* Journal of Membrane Science, 1994. **94**(1): p. 299-311.
41. Hurlbert, R.C. and J.O. Konency, *Diffusion of hydrogen through palladium.* J. Chem. Phys, 1961. **34**(2): p. 655.
42. Cussler, E.L., *Diffusion: Mass Transfer in Fluid Systems*. 2nd ed. 1997, New York: Cambridge University Press.
43. Kompaniets, T.N. and A.A. Kurdyumov, *Surface processes in hydrogen permeation through metal membranes.* Progress in Surface Science, 1984. **17**(2): p. 75-151.
44. Huang, T.-C., M.-C. Wei, and H.-I. Chen, *Permeation of Hydrogen through Palladium/alumina composite membranes.* Separation Science and Technology, 2001. **36**(2): p. 199 - 222.
45. Mardilovich, P.P., Y. She, Y.H. Ma, and M.H. Rei, *Defect-free palladium membranes on porous stainless-steel support.* AIChE Journal, 1998. **44**(2): p. 310-322.
46. Datta, R., S. Dechapanichkul, J.S. Kim, L.Y. Fang, and U. H, *A generalized model for the transport of gases in porous, non-porous, and leaky membranes. I. Application to single gases.* Journal of Membrane Science, 1992. **75**(3): p. 245-263
47. Tosti, S., L. Bettinali, S. Castelli, F. Sarto, S. Scaglione, and V. Violante, *Sputtered, electroless, and rolled palladium-ceramic membranes.* Journal of Membrane Science, 2002. **196**(2): p. 241-249.
48. Jayaraman, V., Y.S. Lin, M. Pakala, and R.Y. Lin, *Fabrication of ultrathin metallic membranes on ceramic supports by sputter deposition.* Journal of Membrane Science, 1995. **99**(1): p. 89-100.
49. Shu, J., A. Adnot, B.P.A. Grandjean, and S. Kaliaguine, *Structurally stable composite Pd---Ag alloy membranes: Introduction of a diffusion barrier.* Thin Solid Films, 1996. **286**(1-2): p. 72-79.

50. Nam, S.-E., S.-H. Lee, and K.-H. Lee, *Preparation of a palladium alloy composite membrane supported in a porous stainless steel by vacuum electrodeposition.* Journal of Membrane Science, 1999. **153**(2): p. 163-173.
51. Jun, C.-S. and K.-H. Lee, *Preparation of palladium membranes from the reaction of Pd(C3H3)(C5H5) with H2: wet-impregnated deposition.* Journal of Membrane Science, 1999. **157**(1): p. 107-115.
52. Liu, S., X. Tan, K. Li, and R. Hughes, *Preparation and characterisation of SrCe0.95Yb0.05O2.975 hollow fibre membranes.* Journal of Membrane Science, 2001. **193**(2): p. 249-260.
53. de Jong, J., N.E. Benes, G.H. Koops, and M. Wessling, *Towards single step production of multi-layer inorganic hollow fibers.* Journal of Membrane Science, 2004. **239**(2): p. 265-269.
54. Wang, B., Z. Wu, A.G. Livingston, and K. Li, *A novel phase transition technique for fabrication of mesopore sized ceramic membranes.* Journal of Membrane Science, 2009. **339**(1-2): p. 5-9.
55. Baker, R.W., *Membrane technology and applications*. 2004, West Sussex: John Wiley and Sons.
56. Rautenbach, R. and R. Albrecht, *Membrane processes*. 1990, New York: John Wiley & Sons Ltd.
57. Liu, S. and K. Li, *Preparation TiO2/Al2O3 composite hollow fibre membranes.* Journal of Membrane Science, 2003. **218**(1-2): p. 269-277.
58. Rice, R.W., *Porosity of ceramics*. 1998: Marcel Dekker Inc, New York.
59. Amano, M., M. Komaki, and C. Nishimura, *Hydrogen permeation characteristics of palladium-plated V---Ni alloy membranes.* Journal of the Less Common Metals, 1991. **172-174**(Part 2): p. 727-731.
60. Franz, A.J., K.F. Jensen, and M.A. Schmidt. *"Palladium Based Micromembranes for Hydrogen Separation and Hydrogenation/Dehydrogenation Reactions"*. in *12th Intl.Workshop on Micro ElectroMechanical Systems-MEMS*. 1999. Orlando, Florida,.
61. Xomeritakis, G. and Y.S. Lin, *Fabrication of a thin palladium membrane supported in a porous ceramic substrate by chemical vapor deposition.* Journal of Membrane Science, 1996. **120**(2): p. 261-272.

62. Huang, L., C.S. Chen, Z.D. He, D.K. Peng, and G.Y. Meng, *Palladium membranes supported on porous ceramics prepared by chemical vapor deposition.* Thin Solid Films, 1997. **302**(1-2): p. 98-101.
63. Deshpande, A.J., T. Toops, J.P. Collins, and T.L. Ward. *"In Fabrication of Metal Membranes by Aerosol-Particle and Chemical-Vapor-Deposition Routes"*. in *N.American Membr.Soc.7th Annual Mtg*. 1995.
64. Charbonnier, M., M. Romand, E. Harry, and M. Alami, *Surface plasma functionalization of polycarbonate: Application to electroless nickel and copper plating.* Journal of Applied Electrochemistry, 2001. **31**(1): p. 57-63.
65. Paglieri, S.N., K.Y. Foo, J.D. Way, J.P. Collins, and D.L. Harper-Nixon, *A New Preparation Technique for Pd/Alumina Membranes with Enhanced High-Temperature Stability.* Industrial & Engineering Chemistry Research, 1999. **38**(5): p. 1925-1936
66. Li, A., G. Xiong, J. Gu, and L. Zheng, *Preparation of Pd/ceramic composite membrane 1. Improvement of the conventional preparation technique.* Journal of Membrane Science, 1996. **110**(2): p. 257-260.
67. Wu, L.-Q., N. Xu, and J. Shi, *Preparation of a Palladium Composite Membrane by an Improved Electroless Plating Technique.* Industrial & Engineering Chemistry Research, 2000. **39**(2): p. 342-348.
68. Schwartz, R.W., J. Collins, M.F. Ng, C.J. Brinker, T.L. Ward, R. Sehgal, C. Xia, C.A. Udovich, J. Masin, and G.P. Hagen, *"Inorganic Membrane Reactor Technology CRADA #1176"*, in *In Final Report and Assessment of Membrane Technology, SAND97-0949*. 1997, Sandia National Laboratory.
69. Zhao, H.B., K. Pflanz, J.H. Gu, A.W. Li, N. Stroh, H. Brunner, and G.X. Xiong, *Preparation of palladium composite membranes by modified electroless plating procedure.* Journal of Membrane Science, 1998. **142**(2): p. 147-157.
70. Cheng, Y.S. and K.L. Yeung, *Effects of electroless plating chemistry on the synthesis of palladium membranes.* Journal of Membrane Science, 2001. **182**(1-2): p. 195-203.
71. Kikuchi, H., *Preparation of Hydrogen Separating Medium* 1987.
72. Konno, M., M. Shindo, S. Sugawara, and S. Saito, *A composite palladium and porous aluminum oxide membrane for hydrogen gas separation.* Journal of Membrane Science, 1988. **37**(2): p. 193-197

73. Uemiya, S., Y. Kude, K. Sugino, N. Sato, T. Matsuda, and E. Kikuchi, *A palladium/porous-glass composite membrane for hydrogen separation* Chem. Lett., , 1988: p. 1687.
74. Collins, J.P. and J.D. Way, *Preparation and characterization of a composite palladium-ceramic membrane.* Industrial & Engineering Chemistry Research, 1993. **32**(12): p. 3006-3013.
75. Zheng, W. and L. Wu, *Preparation and pore size shrinkage of palladium-ceramic composite membrane by electroless plating under hydrothermal conditions.* Materials Science and Engineering A, 2000. **283**(1-2): p. 122-125.
76. Souleimanova, R.S., A.S. Mukasyan, and A. Varma, *Effects of osmosis on microstructure of Pd-composite membranes synthesized by electroless plating technique.* Journal of Membrane Science, 2000. **166**(2): p. 249-257.
77. Souleimanova, R.S., A.S. Mukasyan, and A. Varma, *Pd-composite membranes prepared by electroless plating and osmosis: synthesis, characterization and properties.* Separation and Purification Technology, 2001. **25**(1-3): p. 79-86.
78. Sun, G.B., K. Hidajat, and S. Kawi, *Ultra thin Pd membrane on [alpha]-Al2O3 hollow fiber by electroless plating: High permeance and selectivity.* Journal of Membrane Science, 2006. **284**(1-2): p. 110-119.
79. Pugachev, V.A., F.I. Busol, E.I. Nikolaev, and B.P. Nam, *Penetration and diffusion of hydrogen in palladium–silver alloys.* Russ.J.Phys.Chem, 1975. **49**: p. 1045.
80. Shu, J., B.P.A. Grandjean, A.V. Neste, and S. Kaliaguine, *Catalytic palladium-based membrane reactors: A review.* The Canadian Journal of Chemical Engineering, 1991. **69**(5): p. 1036-1060.
81. Keuler, J.N., L. Lorenzen, R.D. Sanderson, V. Prozesky, and W.J. Przybylowicz, *Characterization of electroless plated palladium-silver alloy membranes.* Thin Solid Films, 1999. **347**(1-2): p. 91-98.
82. Uemiya, S., N. Sato, H. Ando, Y. Kude, T. Matsuda, and E. Kikuchi, *Separation of hydrogen through palladium thin film supported on a porous glass tube.* Journal of Membrane Science, 1991. **56**(3): p. 303-313.
83. Li, A., W. Liang, and R. Hughes, *Fabrication of defect-free Pd/[alpha]-Al2O3 composite membranes for hydrogen separation.* Thin Solid Films, 1999. **350**(1-2): p. 106-112.

84. Pan, X.L., N. Stroh, H. Brunner, G.X. Xiong, and S.S. Sheng, *Deposition of sol-gel derived membranes on [alpha]-Al2O3 hollow fibers by a vacuum-assisted dip-coating process.* Journal of Membrane Science, 2003. **226**(1-2): p. 111-118.
85. Nair, B.K.R., J. Choi, and M.P. Harold, *Electroless plating and permeation features of Pd and Pd/Ag hollow fiber composite membranes.* Journal of Membrane Science, 2007. **288**(1-2): p. 67-84.
86. Tong, J., L. Su, K. Haraya, and H. Suda, *Thin and defect-free Pd-based composite membrane without any interlayer and substrate penetration by a combined organic and inorganic process.* Chemical Communications, 2006(10): p. 1142-1144.
87. Kikuchi, E. and S. Uemiya, *Preparation of supported thin palladium-silver alloy membranes and their characteristics for hydrogen separation.* Gas Separation & Purification, 1991. **5**(4): p. 261-266.
88. Hou, K. and R. Hughes, *Preparation of thin and highly stable Pd/Ag composite membranes and simulative analysis of transfer resistance for hydrogen separation.* Journal of Membrane Science, 2003. **214**(1): p. 43-55.
89. Pacheco Tanaka, D.A., M.A. Llosa Tanco, S.-i. Niwa, Y. Wakui, F. Mizukami, T. Namba, and T.M. Suzuki, *Preparation of palladium and silver alloy membrane on a porous [alpha]-alumina tube via simultaneous electroless plating.* Journal of Membrane Science, 2005. **247**(1-2): p. 21-27.
90. Tong, J., L. Su, Y. Kashima, R. Shirai, H. Suda, and Y. Matsumura, *Simultaneously Depositing Pd-Ag Thin Membrane on Asymmetric Porous Stainless Steel Tube and Application To Produce Hydrogen from Steam Reforming of Methane.* Industrial & Engineering Chemistry Research, 2005. **45**(2): p. 648-655.
91. Pizzi, D., R. Worth, M. Giacinti Baschetti, G.C. Sarti, and K.-i. Noda, *Hydrogen permeability of 2.5 [mu]m palladium-silver membranes deposited on ceramic supports.* Journal of Membrane Science, 2008. **325**(1): p. 446-453.
92. Zaspalis, V.T., W. van Praag, K. Keizer, J.G. van Ommen, J.R.H. Ross, and A.J. Burggraaf, *Reactions of methanol over catalytically active alumina membranes.* Applied Catalysis B: Environmental, 1991. **74**: p. 205-222.
93. Gonzalez, R.D., T. Lopez, and R. Gomez, *Sol--Gel preparation of supported metal catalysts.* Catalysis Today, 1997. **35**(3): p. 293-317.

94. Meille, V., *Review on methods to deposit catalysts on structured surfaces.* Applied Catalysis A: General, 2006. **315**: p. 1-17.
95. Zhao, H., D.J. Draelants, and G.V. Baron, *Preparation and characterisation of nickel-modified ceramic filters.* Catalysis Today, 2000. **56**(1-3): p. 229-237.
96. Belochapkine, S., J. Shaw, D. Wenn, and J.R.H. Ross, *The synthesis by deposition-precipitation of porous [gamma]-alumina catalyst supports on glass substrates compatible with microreactor geometries.* Catalysis Today, 2005. **110**(1-2): p. 53-57.
97. Yeong, K.K., A. Gavriilidis, R. Zapf, and V. Hessel, *Catalyst preparation and deactivation issues for nitrobenzene hydrogenation in a microstructured falling film reactor.* Catalysis Today, 2003. **81**(4): p. 641-651.
98. VrÃlstad, T.r., W.R. Glomm, G. Ã˜ye, J. SjÃblom, and M. StÃcker, *Cobalt Functionalization of Mesoporous Silica by Incipient Wetness Impregnation and Co-precipitation.* Journal of Dispersion Science and Technology, 2005. **26**(1): p. 87 - 94.
99. Pina, M.P., M. Menéndez, and J. Santamaría, *The Knudsen-diffusion catalytic membrane reactor: An efficient contactor for the combustion of volatile organic compounds.* Applied Catalysis B: Environmental, 1996. **11**(1): p. L19-L27.
100. Perez, V., S. Miachon, J.-A. Dalmon, R. Bredesen, G. Pettersen, H. Ræder, and C. Simon, *Preparation and characterisation of a Pt/ceramic catalytic membrane.* Separation and Purification Technology, 2001. **25**(1-3): p. 33-38.
101. Klein, L.C., Ann. Rev. Mar. Sci. , 1985. **15**: p. 227.
102. Saracco, G. and V. Specchia, *Studies on sol-gel derived catalytic filters.* Chemical Engineering Science, 1995. **50**(21): p. 3385-3394.
103. Alfonso, M.J., A. Julbe, D. Farrusseng, M. Menéndez, and J. Santamarla, *Oxidative dehydrogenation of propane on V/Al2O3 catalytic membranes. Effect of the type of membrane and reactant feed configuration.* Chemical Engineering Science, 1999. **54**(9): p. 1265-1272.
104. Meille, V., S. Pallier, G.V. Santa Cruz Bustamante, M. Roumanie, and J.-P. Reymond, *Deposition of gamma-Al2O3 layers on structured supports for the design of new catalytic reactors.* Applied Catalysis A: General, 2005. **286**(2): p. 232-238.

105. Roumanie, M., C. Pijolat, V. Meille, C. De Bellefon, P. Pouteau, and C. Delattre, *Deposition of Pt-catalyst in a micro-channel of a silicon reactor: Application to gas micro-TAS working at high temperature.* Sensors and Actuators B: Chemical, 2006. **118**(1-2): p. 297-304.
106. Uzio, D., J. Peureux, A. Giroir-Fendler, M. Torres, J. Ramsay, and J.A. Dalmon, *Platinum/[gamma]-Al2O3 catalytic membrane: preparation,morphological and catalytic characterizations.* Applied Catalysis A: General, 1993. **96**(1): p. 83-97.
107. Schimpf, S., M. Lucas, C. Mohr, U. Rodemerck, A. Brückner, J. Radnik, H. Hofmeister, and P. Claus, *Supported gold nanoparticles: in-depth catalyst characterization and application in hydrogenation and oxidation reactions.* Catalysis Today, 2002. **72**(1-2): p. 63-78.
108. Janicke, M.T., H. Kestenbaum, U. Hagendorf, F. Schüth, M. Fichtner, and K. Schubert, *The Controlled Oxidation of Hydrogen from an Explosive Mixture of Gases Using a Microstructured Reactor/Heat Exchanger and Pt/Al2O3 Catalyst.* Journal of Catalysis, 2000. **191**(2): p. 282-293.
109. Choy, K.L. and H.-K. Seh, *Fabrication of Ni-Al2O3-based reforming catalyst using flame-assisted vapour deposition.* Materials Science and Engineering A, 2000. **281**(1-2): p. 253-258.
110. Ladebeck, J.R. and J.P. Wagner, *Catalyst development for water-gas shift*, in *Handbook of Fuel Cells - Fundamentals, Technology and Applications*. 2003, John Wiley & Sons, Ltd: Chichester. p. 190-231.
111. Uemiya, S., N. Sato, H. Ando, and E. Kikuchi, *The water gas shift reaction assisted by a palladium membrane reactor.* Industrial & Engineering Chemistry Research, 1991. **30**(3): p. 585-589.
112. Basile, A., A. Criscuoli, F. Santella, and E. Drioli, *Membrane reactor for water gas shift reaction.* Gas Separation & Purification, 1996. **10**(4): p. 243-254.
113. Xue, E., M. O'Keeffe, and J.R.H. Ross, *Water-gas shift conversion using a feed with a low steam to carbon monoxide ratio and containing sulphur.* Catalysis Today, 1996. **30**(1-3): p. 107-118.
114. Criscuoli, A., A. Basile, and E. Drioli, *An analysis of the performance of membrane reactors for the water-gas shift reaction using gas feed mixtures.* Catalysis Today, 2000. **56**(1-3): p. 53-64.

115. Criscuoli, A., A. Basile, E. Drioli, and O. Loiacono, *An economic feasibility study for water gas shift membrane reactor.* Journal of Membrane Science, 2001. **181**(1): p. 21-27.
116. Tosti, S., A. Basile, G. Chiappetta, C. Rizzello, and V. Violante, *Pd-Ag membrane reactors for water gas shift reaction.* Chemical Engineering Journal, 2003. **93**(1): p. 23-30.
117. Barbieri, G., A. Brunetti, G. Tricoli, and E. Drioli, *An innovative configuration of a Pd-based membrane reactor for the production of pure hydrogen: Experimental analysis of water gas shift.* Journal of Power Sources, 2008. **182**(1): p. 160-167.
118. Brunetti, A., G. Barbieri, and E. Drioli, *Upgrading of a syngas mixture for pure hydrogen production in a Pd-Ag membrane reactor.* Chemical Engineering Science, 2009. **64**(15): p. 3448-3454.
119. Bi, Y., H. Xu, W. Li, and A. Goldbach, *Water-gas shift reaction in a Pd membrane reactor over Pt/Ce0.6Zr0.4O2 catalyst.* International Journal of Hydrogen Energy, 2009. **34**(7): p. 2965-2971.
120. Bi, Y., W. Zhang, H. Xu, and W. Li, *Nanocrystalline CeO2; in SBA-15: Performance of Pt/CeO2/SBA-15 Catalyst for Water-gas-shift Reaction.* Catalysis Letters, 2007. **119**(1): p. 126-133.
121. Sammells, A.F. and M.V. Mundschau, *Economics Associated with Implementation of Membrane Reactors*, in *Nonporous Inorganic Membranes*. 2006, WILEY-VCH Verlag GmbH & Co.: KGaA, Weinheim.
122. Moparthi, A., R. Uppaluri, and B.S. Gill, *Economic feasibility of silica and palladium composite membranes for industrial dehydrogenation reactions.* Chemical Engineering Research and Design, 2010. **88**(8): p. 1088-1101.
123. Dixon, A.G., *Recent Research in Catalytic Inorganic Membrane Reactors.* International Journal of Chemical Reactor Engineering, 2003. **3**(1): p. 1-35.
124. Jong-San Chang, Hyun-Seog Roh, Min Seok Park, and S.-E. Park, *Propane Dehydrogenation over a Hydrogen Permselective Membrane Reactor.* Bull. Korean Chem. Soc., 2002. **23**(5).
125. Liang, W. and R. Hughes, *The catalytic dehydrogenation of isobutane to isobutene in a palladium/silver composite membrane reactor.* Catalysis Today, 2005. **104**(2-4): p. 238-243.

126. Yamamoto, S., T. Hanaoka, S. Hamakawa, K. Sato, and F. Mizukami, *Application of a microchannel to catalytic dehydrogenation of cyclohexane on Pd membrane.* Catalysis Today, 2006. **118**(1-2): p. 2-6.
127. Sato, T., H. Yokoyama, H. Miki, and N. Itoh, *Selective dehydrogenation of unsaturated alcohols and hydrogen separation with a palladium membrane reactor.* Journal of Membrane Science, 2007. **289**(1-2): p. 97-105.
128. Gimeno, M.P., Z.T. Wu, J. Soler, J. Herguido, K. Li, and M. Menéndez, *Combination of a Two-Zone Fluidized Bed Reactor with a Pd hollow fibre membrane for catalytic alkane dehydrogenation.* Chemical Engineering Journal, 2009. **155**(1-2): p. 298-303.
129. Barbir, F. and T. Gómez, *Efficiency and economics of proton exchange membrane (PEM) fuel cells.* International Journal of Hydrogen Energy, 1996. **21**(10): p. 891-901.
130. Dunn, S., *Hydrogen futures: toward a sustainable energy system.* International Journal of Hydrogen Energy, 2002. **27**(3): p. 235-264.
131. Gao, H., Y.S. Lin, Y. Li, and B. Zhang, *Chemical Stability and Its Improvement of Palladium-Based Metallic Membranes.* Industrial & Engineering Chemistry Research, 2004. **43**(22): p. 6920-6930.
132. Wang, W.P., S. Thomas, X.L. Zhang, X.L. Pan, W.S. Yang, and G.X. Xiong, *H2/N2 gaseous mixture separation in dense Pd/[alpha]-Al2O3 hollow fiber membranes: Experimental and simulation studies.* Separation and Purification Technology, 2006. **52**(1): p. 177-185.
133. Mallory, G.O.H., J.B. *Electroless Plating,*. in *American Electroplaters and Surface Finishers Society*. 1990. Orlando, Florida.
134. Kingsbury, B.F.K., Z. Wu, and K. Li, *A morphological study of ceramic hollow fibre membranes: A perspective on multifunctional catalytic membrane reactors.* Catalysis Today, 2010.
135. Wu, Z., I.M. Hatim, B.F. Kingsbury, E. Gbenedio, and K. Li, *A novel inorganic hollow fiber membrane reactor for catalytic dehydrogenation of propane.* AIChE Journal, 2009. **55**(9): p. 2389-2398.
136. Yang, H., Q. Shi, B. Tian, S. Xie, F. Zhang, Yan, B. Tu, and D. Zhao, *A Fast Way for Preparing Crack-Free Mesostructured Silica Monolith.* Chemistry of Materials, 2003. **15**(2): p. 536-541.

137. Kulprathipanja, A., G.O. Alptekin, J.L. Falconer, and J.D. Way, *Pd and Pd-Cu membranes: inhibition of H2 permeation by H2S.* Journal of Membrane Science, 2005. **254**(1-2): p. 49-62.
138. Souleimanova, R.S., A.S. Mukasyan, and A. Varma, *Study of structure formation during electroless plating of thin metal-composite membranes.* Chemical Engineering Science, 1999. **54**(15-16): p. 3369-3377.
139. Bhasin, M.M., J.H. McCain, B.V. Vora, T. Imai, and P.R. Pujadó, *Dehydrogenation and oxydehydrogenation of paraffins to olefins.* Applied Catalysis A: General, 2001. **221**(1-2): p. 397-419.
140. Ertl, G., H. Knözinger, and J. Weitkamp, *Handbook of Heterogeneous Catalysis.* VCH, Weinhem, 1997: p. 2140ff.
141. Armor, J.N., *Applications of catalytic inorganic membrane reactors to refinery products.* Journal of Membrane Science, 1998. **147**(2): p. 217-233.
142. Collins, J.P., R.W. Schwartz, R. Sehgal, T.L. Ward, C.J. Brinker, G.P. Hagen, and C.A. Udovich, *Catalytic Dehydrogenation of Propane in Hydrogen Permselective Membrane Reactors.* Industrial & Engineering Chemistry Research, 1996. **35**(12): p. 4398-4405.
143. Uemiya, S., *State-of-the-art of supported metal membranes for gas separation.* Separation and Purification Methods, 1999. **28**(1): p. 51-85.
144. Tan, X.Y., S.M. Liu, and K. Li, *Preparation and characterization of inorganic hollow fiber membranes.* Journal of Membrane Science, 2001. **188**(1): p. 87-95.
145. Pan, X.L., N. Stroh, H. Brunner, G.X. Xiong, and S.S. Sheng, *Pd/ceramic hollow fibers for H2 separation.* Separation and Purification Technology, 2003. **32**(1-3): p. 265-270.
146. Tong, J., L. Su, K. Haraya, and H. Suda, *Thin Pd membrane on [alpha]-Al2O3 hollow fiber substrate without any interlayer by electroless plating combined with embedding Pd catalyst in polymer template.* Journal of Membrane Science, 2008. **310**(1-2): p. 93-101.
147. Jiansheng, L., W. Lianjun, H. Yanxia, L. Xiaodong, and S. Xiuyun, *Preparation and characterization of Al2O3 hollow fiber membranes.* Journal of Membrane Science, 2005. **256**(1-2): p. 1-6.
148. Xiaoyao Tan, Y.L.K.L., *Mixed conducting ceramic hollow-fiber membranes for air separation.* AIChE Journal, 2005. **51**(7): p. 1991-2000.

149. Yoshida, H., S. Konishi, and Y. Naruse, *Effects of Impurities on Hydrogen Permeability through Palladium Alloy Membranes at Comparatively High-Pressures and Temperatures.* Journal of the Less-Common Metals, 1983. **89**(2): p. 429-436.
150. Kikuchi, E. and S. Jemiya, *Preparation of supported thin palladium-silver alloy membranes and their characteristics for hydrogen separation.* Gas separation & Purification, 1991. **5**(4): p. 261-266.
151. Cheng, Y.S., M.A. Peña, J.L. Fierro, D.C.W. Hui, and K.L. Yeung, *Performance of alumina, zeolite, palladium, Pd-Ag alloy membranes for hydrogen separation from Towngas mixture.* Journal of Membrane Science, 2002. **204**(1-2): p. 329-340.
152. Lobera, M.P., C. Téllez, J. Herguido, and M. Menéndez, *Transient kinetic modelling of propane dehydrogenation over a Pt-Sn-K/Al2O3 catalyst.* Applied Catalysis A: General, 2008. **349**(1-2): p. 156-164.
153. de Miguel, S.R., E.L. Jablonski, A.A. Castro, and O.A. Scelza, *Highly selective and stable multimetallic catalysts for propane dehydrogenation.* Journal of Chemical Technology & Biotechnology, 2000. **75**(7): p. 596-600.
154. Matsuda, T., I. Koike, N. Kubo, and E. Kikuchi, *Dehydrogenation of isobutane to isobutene in a palladium membrane reactor.* Applied Catalysis A: General, 1993. **96**(1): p. 3-13.
155. Lin, Y.S., *Microporous and dense inorganic membranes: current status and prospective.* Separation and Purification Technology, 2001. **25**(1-3): p. 39-55.
156. Ritter, J.A. and A.D. Ebner, *State-of-the-art adsorption and membrane separation processes for hydrogen production in the chemical and petrochemical industries.* Separation Science and Technology, 2007. **42**(6): p. 1123-1193.
157. Kikuchi, E., *Membrane reactor application to hydrogen production.* Catalysis Today, 2000. **56**(1-3): p. 97-101.
158. Liu, Y.Y., X.Y. Tan, and K. Li, *Mixed conducting ceramics for catalytic membrane processing.* Catalysis Reviews-Science and Engineering, 2006. **48**(2): p. 145-198.
159. Wu, Z., I.M. Hatim, B.F. Kingsbury, E. Gbenedio, and K. Li, *A novel inorganic hollow fiber membrane reactor for catalytic dehydrogenation of propane.* AIChE Journal, 2009. **55**(9): p. 2389-2398.

160. Zhao, D., J. Feng, Q. Huo, N. Melosh, G.H. Fredrickson, B.F. Chmelka, and G.D. Stucky, *Triblock Copolymer Syntheses of Mesoporous Silica with Periodic 50 to 300 Angstrom Pores.* Science, 1998. **279**(5350): p. 548-552.
161. Santhosh Kumar, M., D. Chen, J.C. Walmsley, and A. Holmen, *Dehydrogenation of propane over Pt-SBA-15: Effect of Pt particle size.* Catalysis Communications, 2008. **9**(5): p. 747-750.
162. Shah, P. and V. Ramaswamy, *Thermal stability of Mesoporous SBA-15 and Sn-SBA-15 Molecular Sieves: An in situ HTXRD study.* Microporous and Mesoporous Materials, 2008. **114**(1-3): p. 270-280.
163. Yang, H., Q. Shi, B. Tian, S. Xie, F. Zhang, Yan, B. Tu, and D. Zhao, *A Fast Way for Preparing Crack-Free Mesostructured Silica Monolith.* Chemistry of Materials, 2003. **15**(2): p. 536-541.
164. Lu, Q., F. Gao, S. Komarneni, and T.E. Mallouk, *Ordered SBA-15 Nanorod Arrays Inside a Porous Alumina Membrane.* Journal of the American Chemical Society, 2004. **126**(28): p. 8650-8651.
165. Coronas, J. and J. Santamaria, *Catalytic reactors based on porous ceramic membranes.* Catalysis Today, 1999. **51**(3-4): p. 377-389.
166. Bi, Y., H. Xu, W. Li, and A. Goldbach, *Water-gas shift reaction in a Pd membrane reactor over Pt/Ce0.6Zr0.4O2 catalyst.* International Journal of Hydrogen Energy, 2009. **34**(7): p. 2965-2971.
167. Kingsbury, B.F.K., Z. Wu, and K. Li, *A morphological study of ceramic hollow fibre membranes: A perspective on multifunctional catalytic membrane reactors.* Catalysis Today, 2010.
168. Wu, Z., I.M. Hatim, B.F. Kingsbury, E. Gbenedio, and K. Li, *A novel inorganic hollow fiber membrane reactor for catalytic dehydrogenation of propane.* AIChE Journal, 2009. **55**(9): p. 2389-2398.
169. Gbenedio, E., Z. Wu, I. Hatim, B.F.K. Kingsbury, and K. Li, *A multifunctional Pd/alumina hollow fibre membrane reactor for propane dehydrogenation.* Catalysis Today, 2010. **156**(3-4): p. 93-99.
170. Kikuchi, E., S. Uemiya, N. Sato, H. Inoue, H. Ando, and T. Matsuda, *Membrane Reactor Using Microporous Glass-supported Thin Film of Palladium. Application to the Water Gas Shift Reaction.* Chemistry Letters, 1989. **18**(3): p. 489-492.

Appendix A

The following is a description of the GC settings used to analyse product streams described in this work.

GC Program

Varian-3900 (FID)

Column: GS-GASPRO
60 m x 0.32mm I.D.
Carrier gas: Argon (10 ml/min)
Make up gas Argon (10 ml/min)

Oven: 170 ^{o}C
Injector: 120 ^{o}C
Detector: 180 ^{o}C

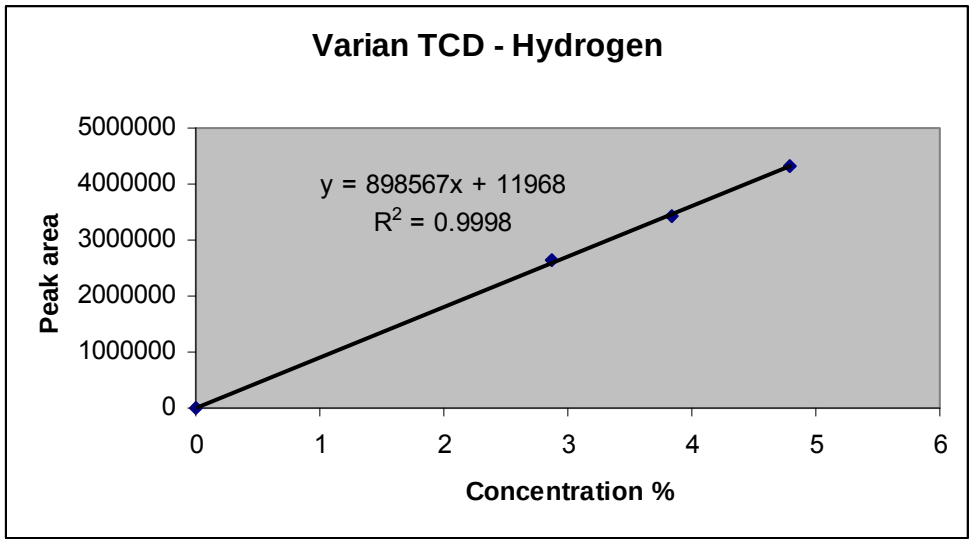
Varian-3900 (TCD)

Column: ShinCarbon ST Micropacked ST 100/120
2 m x 1 mm (ID) x 1.6 mm
Carrier gas: Argon (8 ml/min)
Make up gas: Argon (11 ml/min)

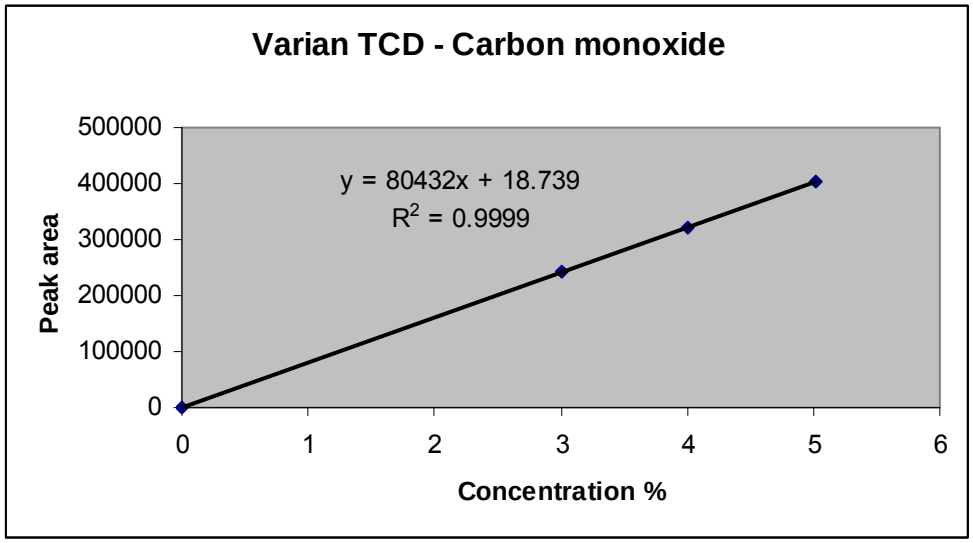
Oven: 120 ^{o}C
Injector: 140 ^{o}C
Detector: 140 ^{o}C

GC Calibrations

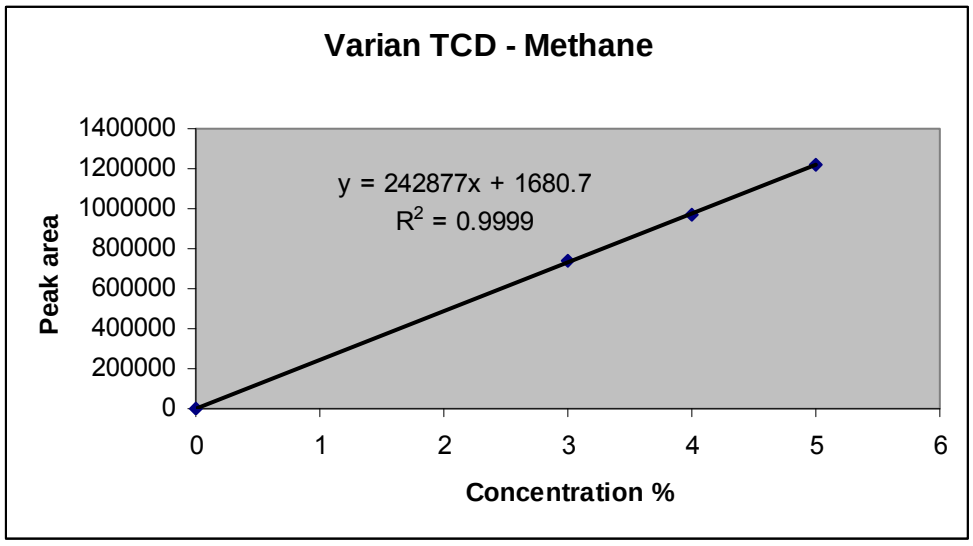
Retention time: 1.103



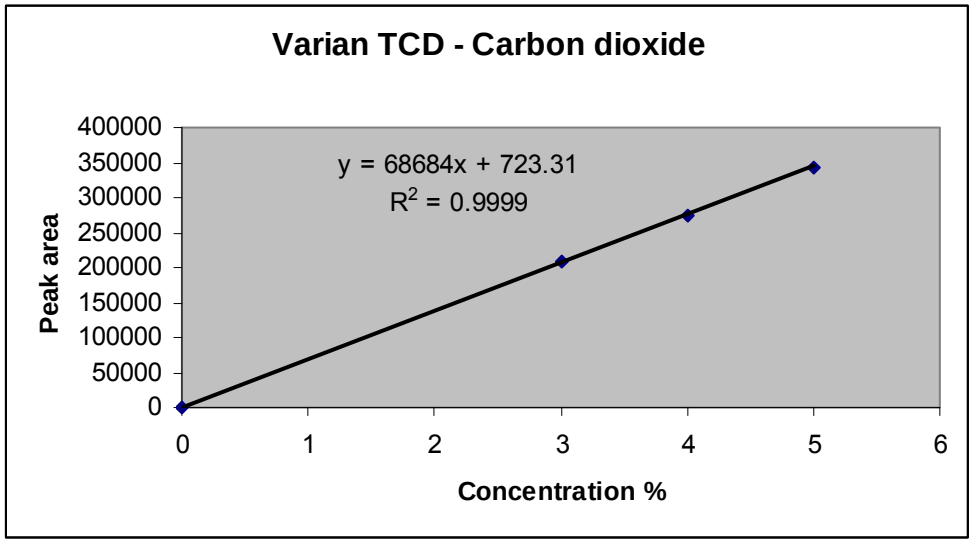
Retention time: 1.608



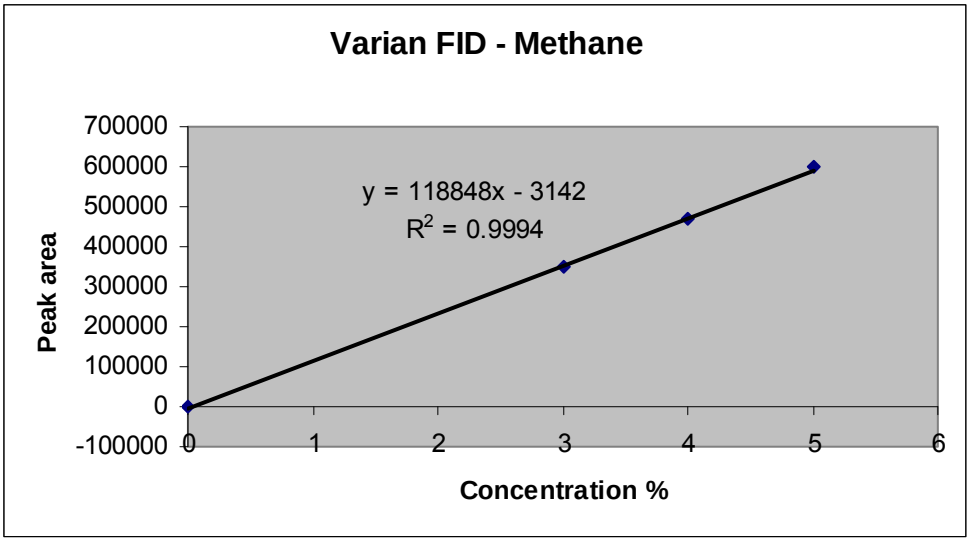
Retention time: 2.165



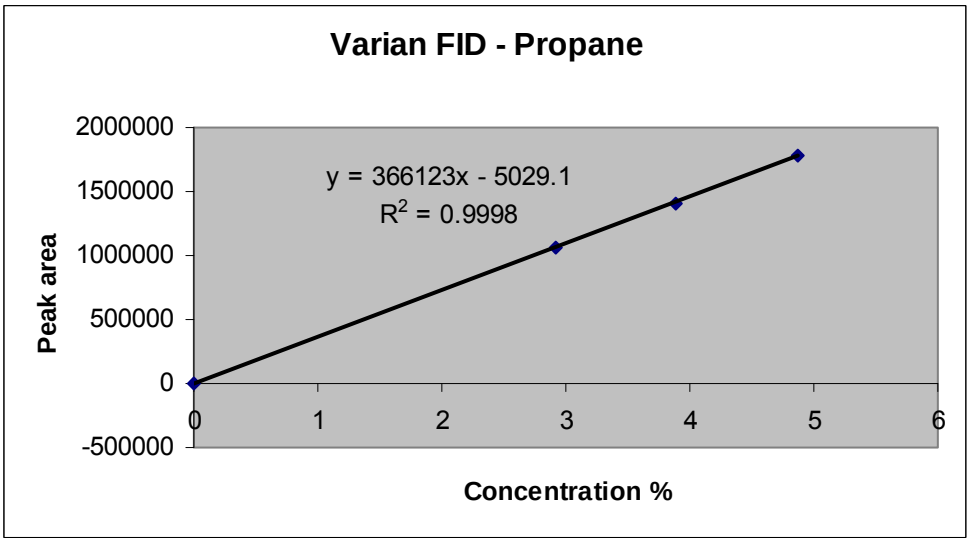
Retention time: 3.148



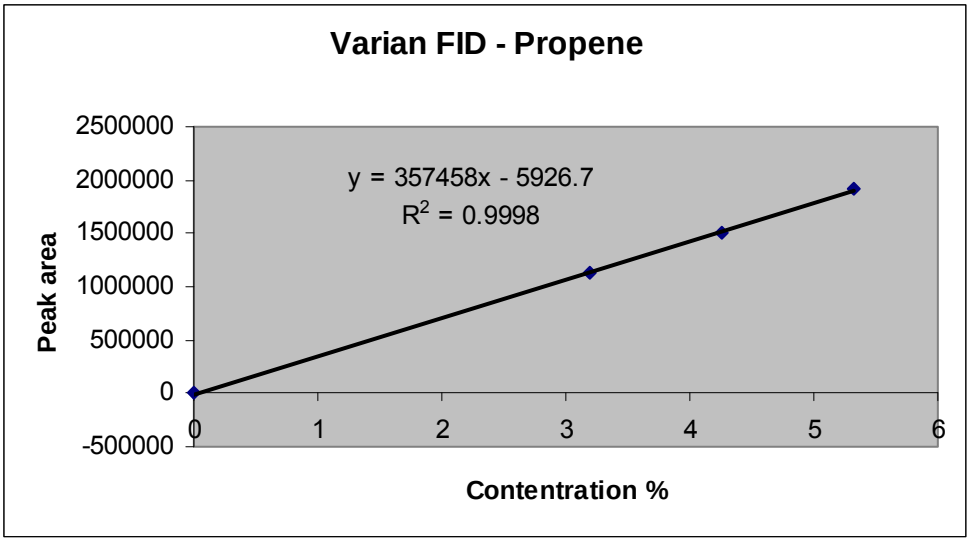
Retention time: 8.623



Retention time: 10.012



Retention time: 10.843



Appendix B

Finding n by minimising the Least Squares Regression Value

Table B-1 and B-2 show that the value of n with the greatest least squares regression value for all temperatures (the sum) is close to 1 (Ch. 3) and 0.5 (Ch. 4) respectively.

Table B-1: Least squares regression values of H_2 gas permeation graph lines for different n values (Fig. 3-22)

	Least Squares Regression Value (R^2)												
	n												
Temperature (K)	0.40	0.45	0.50	0.55	0.60	0.65	0.70	0.75	0.80	0.85	0.90	0.95	1.0
573	0.98831	0.99068	0.99278	0.99460	0.99615	0.99742	0.99844	0.99919	0.99922	0.99969	0.99968	0.99993	0.99992
623	0.98971	0.99194	0.99389	0.99556	0.99696	0.99808	0.99894	0.99954	0.99877	0.99940	0.99987	0.99980	0.99996
673	0.98846	0.99083	0.99291	0.99472	0.99625	0.99752	0.99852	0.99925	0.99921	0.99969	0.99973	0.99995	0.99996
723	0.98904	0.99135	0.99337	0.99512	0.99660	0.99780	0.99874	0.99941	0.99903	0.99958	0.99982	0.99990	0.99999
Sum of R^2	3.95551	3.96479	3.97296	3.98001	3.98596	3.99083	3.99463	3.99738	3.99623	3.99836	3.99911	3.99957	3.99983

Table B-2: Least squares regression values of H_2 gas permeation graph lines for different n values (Fig. 4-31)

	Least Squares Regression Value (R^2)												
	n												
Temperature (K)	0.40	0.45	0.50	0.55	0.60	0.65	0.70	0.75	0.80	0.85	0.90	0.95	1.0
723	0.99854	0.99909	0.99949	0.99974	0.99983	0.99979	0.99959	0.99925	0.99876	0.99813	0.99735	0.99644	0.99539
773	0.99923	0.99962	0.99986	0.99995	0.99986	0.99968	0.99932	0.99882	0.99817	0.99737	0.99644	0.99536	0.99415
823	0.99927	0.99956	0.99970	0.99969	0.99943	0.99922	0.99876	0.99815	0.99739	0.99650	0.99546	0.99428	0.99296
873	0.99819	0.99866	0.99957	0.99906	0.99900	0.99890	0.99859	0.99814	0.99755	0.99681	0.99592	0.99490	0.99374
Sum of R^2	3.99523	3.99693	3.99862	3.99844	3.99812	3.99758	3.99626	3.99436	3.99187	3.98880	3.98517	3.98098	3.97623